Universidade do Minho
Escola de Engenharia

Sílvia Marlene Almeida Santos Pedrosa

Hyaluronic Acid Nanogels

setembro de 2016

Universidade do Minho
Escola de Engenharia

Sílvia Marlene Almeida Santos Pedrosa

Hyaluronic Acid Nanogels

Tese de Doutoramento em Engenharia Biomédica

Trabalho efetuado sob a orientação do
Professor Francisco Miguel Gama
e do
Professor Gil Castro

setembro de 2016

STATEMENT OF INTEGRITY

I hereby declare having conducted my thesis with integrity. I confirm that I have not used plagiarism or any form of falsification of results in the process of the thesis elaboration. I further declare that I have fully acknowledged the Code of Ethical Conduct of the University of Minho.

University of Minho, 5th September 2018

Full name:

Sílvia Marlene Almeida Santos Pedrosa

Signature:

Sílvia Santos Pedrosa

Agradecimentos

O culminar deste projeto de doutoramento e a concretização desta dissertação tem um significado muito especial para mim. Durante este período muita coisa mudou quer a nível profissional, quer pessoal. A todos os que colaboraram na execução deste trabalho queria deixar a minha gratidão. Gostaria no entanto, de realçar algumas pessoas pela sua contribuição:

Ao Professor Miguel Gama, quero agradecer-lhe pela sua orientação, pela enorme disponibilidade, pela compreensão e por nunca ter desistido de acreditar.

Ao Professor Gil Castro, gostaria de lhe agradecer por ter estado disponível sempre que precisei.

Aos meus colegas de laboratório, do FUNCARB e CEB/UM gostaria de agradecer por terem contribuído, de alguma maneira para o sucesso deste trabalho. Gostaria, no entanto, de nomear a Catarina Gonçalves, uma vez que tem uma contribuição efetiva neste trabalho.

Aos amigos que fiz neste período – Paula Pereira, Dina Silva, Alexandre Leitão e Thalita Calado – muito obrigada por terem aligeirado esta etapa por vezes tão dura. Muito obrigada pela vossa amizade e pela vossa ajuda efectiva para a concretização deste trabalho.

Não quero esquecer também os colegas que encontrei em outras Instituições. Muito obrigada à Alexandra Correia pela enorme contribuição e a sua imensa disponibilidade e dedicação. À Dra. Dolores Bonaparte, Dra. Joana Marques, Dr. António Temudo e Dr. José Rino muito obrigada pela vossa disponibilidade e acolhimento na vossa instituição.

Aos Professores José Alberto Martins, Paulo Coutinho, Manuel Vilanova, Arwyn Jones, Laurent David e África Gonzáles, muito obrigada pela vossa contribuição.

Aos meus familiares, quero agradecer o apoio, a compreensão e principalmente a vossa confiança.

De um modo muito especial quero agradecer ao Nuno - o meu porto seguro – a confiança, o companheirismo a compreensão e o apoio em todos os momentos, principalmente nos mais difíceis. Sem ti, este trabalho não seria possível.

Por fim, mas sem duvida mais importante, quero agradecer aos meus filhos, por trazerem luz à minha vida. Vocês são a razão da minha existência.

Muito obrigada a todos.

Aos meus filhos e

ao meu marido

Resumo

“Nanogéis de Àcido Hialurónico”

Nanogéis poliméricos são nanopartículas que possuem uma estrutura tridimensional constituida por um polímero hidrofílico conjugado ou reticulado. O ácido hialurónico é um polissacarídeo aniónico, biodegradável, biocompatível e não-imunogénico, abundante no corpo humano. Neste trabalho descrevemos a produção de um nanogel de ácido hyalurónico através da conjugação de uma molécula hidrofóbica tiolada à cadeia hidrofílica de ácido hyalurónico. O conjugado resultante é capaz de se auto-organizar em estruturas nanométricas, em meio aquoso, de um modo versátil, fácil e reprodutível. Adicionalmente, o nanogel foi reticulado através de uma ligação dissulfito, recorrendo a um agente reticulante reativo com grupos sulfídrilo. O nanogel foi caracterizado quanto à sua estrutura, tamanho, forma, potencial zeta, estabilidade e capacidade de aprisionar moléculas hidrofóbicas. O sucesso da reticulação do nanogel foi confirmado por espectroscopia de ressonância magnética nuclear ^{1}H, microscopia crio-eletrónica de varrimento e dispersão dinâmica de luz e comportamento em ambiente redox. O nanogel desenvolvido foi ainda estudado quanto à sua biocompatibilidade, imuno-compatibilidade e hemato-compatibilidade. Com esse intuito, o nanogel foi incubado com uma série de linhas celulares representativas de órgãos e tecido humanos, relevantes - 3T3, HMEC, A549 e RAW 264.7. O nanogel provou não afectar a atividade metabólica e proliferação celular, ou a integridade da membrana celular. Do mesmo modo, também não observamos nenhum efeito apoptótico em nenhuma das concentrações e linhas celulares testadas. Para além disso, o nanogel provou não ativar a cascata do complemento através da clivagem da proteína C3 e provou também não possuir atividade hemolítica de acordo com o Procedimento Padrão para a Avaliação da Atividade

Hemolítica em Materiais, da Sociedade Americana de Testes em Materiais. Uma das características relevantes do ácido hialurónico aplicada à nano-medicina é o seu potencial de direcionamento para receptores celulares, nomeadamente receptores CD44 e Receptores de Mobilidade para o Ácido Hialurónico. Deste modo, investigamos o direcionamento do nanogel para células que sobreexpressam receptores CD44 – Cancro do pulmão das não-pequenas células. O direcionamento *in vitro* foi avaliado por citometria de fluxo e microscopia confocal e a biodistribuição in vivo foi avaliada por imagiologia em tempo real não-invasiva de infravermelho próximo (NIR). Resultados demostraram uma elevada internalização celular em células que sobreexpressam receptores CD44, *in vitro,* e uma seletividade *in vivo* para o tecido tumoral. Também quisemos estudar a influência das sondas NIR usadas nos estudos de biodistribuição. Portanto, desenvolvemos um estudo comparativo da farmacocinética *in vivo*, de duas sondas de NIR diferentes – Cy5.5 e Alexa Fluor 680. Por fim, estudamos o mecanismo de endocitose através do qual o nanogel interage com as células recorrendo à tecnologia de siRNA para regular a expressão de proteínas alvo envolvidas no processo de endocitose. Os resultados revelaram que, o nanogel é internalizado por um mecanismo dependente de energia que parece ser mediada pela Caveolina e também pela Claterina.

Finalmente, o nanogel foi usado como veículo para o transporte de rifampicina ou outros péptidos antimicrobianos, no tratamento de macrofagos infectados com *Mycobacterium*.

Em resumo, o nanogel apresenta características promissoras como sistema reticulado, no direcionamento de fármacos via endocitose mediada por receptors para o ácido hialurónico.

Nesta dissertação optamos por manter a formatação original de cada artigo que dá origem a cada um dos capitulos.

Abstract

"Hyaluronic Acid Nanogels"

Polymeric nanogels are hydrogel nanoparticles with a tridimensional structure that consist in a conjugated or crosslinked hydrophilic polymer. An exquisite representative of this group of polymers is, hyaluronic acid. Hyaluronic acid is an anionic polysaccharide biodegradable, biocompatible and non-imunogenic, ubiquitous of the human body. The present work comprehends the production of a hyaluronic acid nanogel by the conjugation of a thiolated hydrophobic molecule to the hydrophilic backbone of hyaluronic acid. The resulting conjugate is able to self-assemble in aqueous environment into nanosized structures in a versatile, easy and reproducible manner. Further, nanogel was crosslinked by dissulfide bond, resourcing to a sulfhydryl reactive homobifunctional crosslinker. Nanogel were characterized as to its -structure, size, shape, zeta potential, stability and ability to entrap small hydrophobic molecules. Also, reticulation was confirmed by 1HNMR, UV–Vis spectroscopy, cryo-field-emission scanning electron microscopy, dynamic light scattering characterization and redox-sensitive performance. Engineered nanogel was further studied as to its biocompatibility, immunocompatibility and hemocomptability. For that purpose, nanogel was incubated with a collection of cell lines representative of relevant human tissues - 3T3, HMEC, and RAW 264.7 cells. Nanogel proved to not affect cells metabolic activity and proliferation, or cellular membrane integrity. Also, we didn't observe any apoptotic effect at any nanogel concentration and cell lines tested, using the Annexin V-FITC test. Moreover, nanogel proved to not activate the complement cascade by C3 cleavage and to be non-haemolytic

according to Standard Practice for Assessment of Haemolytic Properties of Materials from the American Society for Testing Materials.

Among the exciting features of hyaluronic acid in nanomedicine applications is the potential of active targeting for cell surface receptors, namely CD44 and Receptor for Hyaluronan Mediated Motility. Thus, we investigated nanogel targetability, towards CD44 over-expressing cells – Non-small cancer lung cells. *In vitro* and *in vivo* targeting was assessed by flow cytometry and confocal fluorescence microscopy and non-invasive real time near-infrared (NIR) imaging in healthy and tumour bearing mice. Results revealed high *in vitro* cellular uptake by CD44 overexpressing cells and *in vivo* selective targeting towards tumour tissue. We also investigated the influence of the NIR probe used in biodistribution studies. For that reason, we performed a comparative study of *in vivo* pharmacokinetics of two different NIR probes - Cy5.5 and Alexa Fluor 680. We further studied the endocytic mechanism through which nanogel interacted with cells interface resourcing to siRNA machinery to regulate expression of key endocytic proteins. Results revealed that nanogel endocytosis occurs through an energy dependent pathway and seems to occur predominantly through caveolae-mediated endocytosis and also, clatherin-mediated endocytosis.

Finally, the HyA-AT nanogel was subsequently tested as drug carrier for the intracellular delivery of Rifampicin or an antimicrobial peptide to *Mycobacterium* infected macrophages.

Our data collectively suggest that HyA-AT nanogel may have potential as intracellular delivery system of therapeutic cargo via endocytosis mediated by hyaluronic acid receptors.

In this thesis we chose to maintain the original formatting of the published articles and corresponding chapters.

List of Publications

This thesis is based in the following book chapter and research articles:

CHAPTER I

Pedrosa, SS., Gama, M. "**Hyaluronic acid and its application in nanomedicine**", Carbohydrates Applications in Medicine, 2013, ISBN: 978-81-308-0523-8

CHAPTER II

Sílvia Santos Pedrosa, Catarina Gonçalves, Laurent David and Miguel Gama, **A Novel Crosslinked Hyaluronic Acid Nanogel for Drug Delivery,** Macromolecular Bioscience, Published August 2014, DOI: 10.1002/mabi.201400135

CHAPTER III

Pedrosa, S.S., Moreira, S., Correia, A. Vilanova, M. and Gama, FM, **Biocompatibility and in vivo biodistribution of a self-assembled crosslinkable hyaluronic acid nanogel**, Macromolecular Biosciences, DOI: 10.1002/mabi.201600221

CHAPTER IV

Pedrosa, S. S., Pereira, P., Correia, A. and Gama, F.M., **Targetability of hyaluronic acid nanogel to cancer cells: in vitro and in vivo studies**, Submitted to Acta Biomaterialia in January 2016

CHAPTER V

Pedrosa, SS, Pereira, P. Correia, A., Jones, A. Gama, FM, **Hyaluronic acid nanogel: cell uptake and exploratory intracellular drug delivery**, Work in progress

Table of contents

List of Figures

CHAPTER I

CHAPTER II

CHAPTER III

CHAPTER IV

List of Tables

List of schemes

CHAPTER II

Abbreviations

^{1}HNMR	^{1}H Nuclear magnetic resonance analysis
3T3	Mouse embryonic fibroblast cell line
A549	Human lung adenocarcinoma epithelial cell line
ACN	Acetonitrile
ADH	Adipic acid dihydrazide
Alexa488	Alexa Fluor 488
Alexa680	Alexa Fluor 680
ANOVA	Analysis of variance
AOT	Sodium bis(2-ethylhexyl) sulfosuccinate
AT	11-amino-undecanethiol
ATP	Adenosine triphosphate
BcL-xL	B-cell lymphoma-extra large
BMDM	Bone marrow derived macrophages
CAC	Critical aggregation concentration
CAV-1	Caveolin 1
CCD	Charged coupled device
CD44	Cluster domain 44
Cdc42	Cell division control protein 42
CDI	1-[3-(dimethylamino)propyl]-3-ethylcarbodiimide methiodide
CDots	Carbon Dots
CHC	Clathrin
CME	Clathrin mediated endocytosis
COX-2	Cyclooxygenase-2
CPT	Camptothecin
Cryo-FESEM	Cryo-Field Emission Scanning Electron Microscopy
CvME	Caveolin mediated endocytosis
Cy5.5	Cyanine Dye 5.5
DA	diethoxyethyl amine
DAPI	4',6-diamidino-2-phenylindole
DCC	1, 3-dicyclohexyl carbodiimide
DCT	Docetaxel
DEA	Diethylamine
DIC	Differential interference contrast
DIPEA	N,N-diisopropyl ethylamine
DLS	Dynamic Light scattering

DMAP	4-Dimethylaminopyridine
DMEM	Dulbecco's Modified Eagle Medium
DMF	Dimethylformamide
DMSO	Dimethyl sulfoxide
DMTMM	4-(4,6-Dimethoxy-1,3,5-triazin-2-yl)-4-methylmorpholinium chloride
DNA	Deoxyribonucleic acid
DOX	Doxorubicin
DPDPB	4-Di-(3'-[2'-pyridyldithio]-propionamido)butane
DS	Degree of substitution
DTPA	Diethylenetriaminepentaacetic dianhydride
EDA	Ethylenediamine
EDC	1-Ethyl-3-(3-dimethylaminopropyl)carbodiimide
EDTA	Ethylenediamine tetraacetic acid
EGF	Epidermal growth factor
EPR	Enhanced permeability and retention
ER	Endoplasmic Reticulum
FBS	Foetal Bovie Serum
FITC	Fluorescein isothiocyanate
Flot-1	Flotilin 1
GFP	Green fluorescent protein
HBSS	Hank's buffered salt solution buffer
HCT 116	colon carcinoma
HeLa	Human cervix adenocarcinoma epithelial cell line
HEPES	4-(2-hydroxyethyl)-1-piperazineethanesulfonic acid buffer
hGH	Human growth hormone
HMEC	Human dermal microvascular endothelial cells
HOBT	Hydroxybenzotriazole
HyA	Hyaluronic acid
IFNα	Interferon alpha
IL	Interleukin
IONs	Iron Oxide Nanoparticles
IRT	Irinoteca
L929	Mouse fibroblast cell line
LCCM	L929 cell conditioned medium
LDH	Lactate dehydrogenase
MDA-MB-231	human breast adenocarcinoma
MES	2-(N-morpholino)ethanesulfonic acid buffer
MFI	Mean fluorescence intensity

mRNA	Messenger RNA
MTT	3-(4,5-dimethylthiazol-2-yl)-2,5-diphenyl tetrazolium bromide
MTX	Methotrexate
MW	Molecular weight
NADH	Nicotinamide adenine dinucleotide
NHS	N-hydroxysuccinimide
NIR	Near infrared
NP	Nanoparticle
NR	Nile red
OptiMEM	Reduced Serum Media
p53	Tumor suppressor protein
PAH	Poly (allylamine)
Pak-1	p21-activated kinase 1
PBS	Phosphate buffered saline
PBST	PBS Tween 20 (0.025%, v/v)
PDGF-BB	Platelet derived growth factor
pDNA	Plasmid DNA
PEG	Polyethylene glycol
PI	Propidium Iodide
PLA	Poly(D,L-lactic acid)
PLGA	Poly(lactic-co-glycolic acid)
PLI	Poly-L-lysine-graft-imidazole
PLL	Poly(ʟ-lysine)
PMDETA	N,N,N′,N′,N″-pentamethyldiethylenetriamine
PTX	Paclitaxel
PUMPT	Polymer-masked UnMasked Protein Therapy
QDots	Quantum dots
RAW	Mouse leukaemic monocyte macrophage cell line
RHAMM	Hyaluronan-mediated motility receptor
Rhoa	Ras homolog gene family, member A
RNAi	RNA-interference
RPMI	Roswell Park Memorial Institute 1640 Medium
SCC7	Squamous cell carcinoma
SD	Standard deviation
SDS-PAGE	Sodium dodecyl sulfate polyacrylamide gel electrophoresis
shRNA	short hairpin RNA
siRNA	Small interference RNA
SPIONs	Super-paramagnetic iron oxide nanoparticles

Sulfo-NHS	N-hydroxysulfosuccinimide
TDI	2,4-toluene diisocyanate
TEA	Triethylamine
THF	Tetrahydrofuran
TMP	2,2,6,6-tetramethylpiperidine
TOS	D-α-tocopheryl succinate
TPP	Tripolyphosphate
UV	Ultraviolet
UV-Vis	Ultraviolet-visible
VEGF	Vascular endothelial growth factor
W/O	Water in oil emulsion
γPGA	gamma-Polyglutamic acid

Aims and Outline

Polymeric nanogels are a class of nanocarrier systems based on biodegradable polymers that can be applied to sustained drug release. Possibly the most noteworthy polyssacharide used in biomedical applications is hyaluronic acid. Hyaluronic acid is a highly hydrophilic polysaccharide with great potential as a drug carrier due to its physicochemical and biological properties, such as biocompatibility, biodegradability and non-immunogenicity. Therefore, major motivation of this work was to develop a hyaluronic acid nanogel as a drug delivery system towards CD44 expressing cells.

Chapter I comprehends an up-to date review of hyaluronic acid based nanocarriers applied to biomedicine, as drug, peptide/proteins or gene delivery systems.

In chapter II, we discusse synthesis and physical-chemical characterization of a hyaluronic acid nanogel and its crosslinking through redox sensitive bond. Also, we address nanogels applicability as drug delivery system.

In chapter III we provide a comprehensive study of nanogels cytocompatibility, immunocompatibility and hemocompatibility in vitro.

Chapter IV comprises in vivo biodistribution and tumour targetability of hyaluronic acid nanogel using a non-invasive in vivo real-time near infrared imaging system.

In chapter V we addresses nanogels cellular uptake mechanism and endocytic pathway by siRNA inhibition and is application as drug carrier for the intracellular delivery of antimicrobials to mycobacteria-infected macrophages

Finally, in chapter VI we synthetise major breakthroughs of this work and set some future perspectives and goals.

CHAPTER I

HYALURONIC ACID AND ITS APPLICATION IN NANOMEDICINE

Adapted and updated from

Carbohydrates Applications in Medicine, 2014: 55-89 ISBN: 978-81-308-0523-8 Editor: M. H. Gil

1. Introduction

The use of hyaluronic acid (HyA) in the biomedical field has been subject of interest for many researchers over the years. Many reviews are available on the use of HyA for tumour targeting [1-5], drug delivery [6-8] and tissue engineering [9]. Chemical modifications of HyA have also been extensily reviewed [10], namely on the conjugation with cytotoxic drugs [2], an also the chemical grafting of hydrophobic molecules to obtain amphiphilic micelles [11] and stimuli responsive materials [12]. Herein, we address some of the most recent works, focusing on the HyA based nanoparticulate systems aimed for biomedical applications.

Hyaluronic acid or hyaluronan is a polyanionic polysaccharide composed of disaccharide units of D-glucuronic acid and N-acetyl-D-glucosamine with β(1,4) and β(1,3) glucosidic bonds (figure 1). Among the natural polymers, HyA is the most abundant in the human body, being present in the extracellular matrix (ECM), connective tissues and body fluids [13, 14]. In physiological conditions, HyA is in the form of a sodium salt, therefore negatively charged and referred to as sodium hyaluronate. HyA is highly hydrophilic and thus in the physiological environment it is shielded by a sphere of water molecules linked by hydrogen bonds. HyA is available in a wide range of molecular weight (MW), from 4000 Da - 10MDa, which influences its biological functions [15]. In the human body, HyA can be cleaved leading to low molecular weight (LMW) polymers (10 kDa <MW < 500 kDa) as well as oligosaccharides (MW < 2000Da) [16]. High molecular weight (HMW) HyA is considered antiangiogenic and non-immunogenic, whereas the LMW polymer is considered inflammatory, immuno-stimulatory and angiogenic [15]. Due to the high molecular weight and strong intermolecular interactions, HyA aqueous solutions are highly viscous and shear-thinning [10].

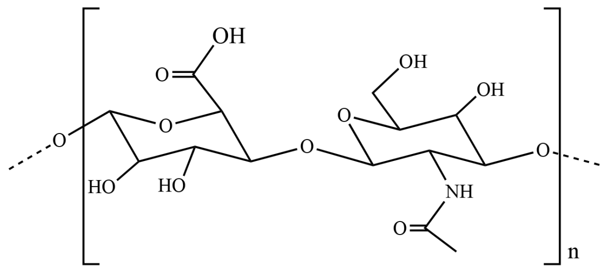

Figure 1: Hyaluronic acid disaccharide composed by D-glucuronic acid and N-acetyl-D-glucosamine units.

Hyaluronic acid is highly hydrophilic and water-soluble and insoluble in organic solvents. Several modifications of HyA have been reported with the goal of altering its solubility, mainly by acetylation [14, 17], ionic exchange with a lipophilic cationic salt [10, 18-22] and nano-complexation with dimethoxy polyethylene glycol [23].
The attention given to HyA as a potential drug carrier is due to its: i) suitability for the development of nanostructures when chemically modified ii) stability in blood flow – stealth properties - that allows passive tumour targeting by the enhanced permeability and retention (EPR) effect; iii) specific affinity for various cancer cells that overexpress HyA receptors and, iv) ability to release drugs in targeted cells with enhanced therapeutic efficacy. Moreover, HyA gathers highly desirable physicochemical and biological properties, such as biocompatibility, biodegradability and non-immunogenicity [2, 24].

2. Synthesis of Hyaluronic acid

Endogenously, HyA is synthesized in the inner face of the plasma membrane by the HyA synthases (HyASs): HyAS-1, HyAS-2 and HyAS-3, which are transmembrane proteins. During the synthetic process, HyA is secreted onto the cell surface, or into the ECM. In addition, HyA can be found inside the cells [2].

Formerly, the HyA was obtained from bovine vitreous humour, rooster combs and human umbilical cord [10]. Nowadays the industrial production is achieved using genetically modified bacteria, avoiding contaminations by animal pathogens, in a more cost effective and high-yield method [9, 10]. The majority of the commercial products are obtained by fermentation from *Bacillus sp.*, *Lactococcus lactis*, *Agrobacterium sp.*, *Escherichia coli*, *Streptococcis equi* and *Bacillus subtilis* [9].

3. Catabolism and degradation of HyA

HyA is quickly degraded and removed from the human body. About 30% is renewed every day [2]. The half-life of HyA after injection into skin and joints is no longer than 24 h and by intravenous administration it is mainly catabolized in the liver sinusoidal endothelial cells after internalized by a HyA receptor – HARE receptor. HyA turnover occurs within the lymph node following internalization into the lymphatic cells by a lymphatic vessel endothelial receptor-1 (LYVE-1) [10] [2]. The degradation of HyA can occur by enzymatic or non-enzymatic reactions. Three types of enzyme (hyaluronidase, b-D-glucuronidase and b-N-acetyl-hexosaminidase) are involved in the enzymatic degradation of HyA. These enzymes can be found in the intercellular space and in serum [25]. The non-enzymatic mechanisms of degradation include thermal or shear stress, and chemical reactions such as, acidic/alkaline hydrolysis, and degradation by oxidants [25].

There are six hyaluronidase genes - HYAL1, HYAL2, HYAL3, HYAL4, HSPAM1 and HYALP1 - identified in the human genome. Hyal-1 is widely expressed in various somatic tissues and is known as lysosomal enzymes due to its sharp optimum pH around 3.7. It degrades HyA oligomers into small fragments. A significant portion of HyA degradation outcome is followed by receptor-mediated internalization by Cluster determinant 44 (CD44) positive cells [2].

4. HyA and Hyaladherins

Hyaladherins are a group of heterogeneous proteins linked by their ability to bind HyA. These include diverse proteoglycans, HyA receptors and link proteins. The proteoglycan molecules bind to the HyA and form complexes that act as structural components of cartilage, blood vessels, skin and brain [2, 7, 25].

HyA receptors include CD44, receptor for hyaluronan-mediated motility (RHAMM), tumour necrosis factor-stimulated gene-6 (TSG-6), glial hyaluronate-binding protein (GHAP), Intercellular Adhesion Molecule 1 (ICAM-1) and Lymphatic Vessel Endothelial Receptor 1 (LYVE-1). Among these, CD44 and RHAMM seem to have received more attention, since they have been found to be involved in cancer metastases [25]. CD44 is responsible for tissue structuring by cell-cell and cell-matrix adhesion, cell proliferation and differentiation, cell migration during morphogenesis, angiogenesis, arrangement of cytokines, chemokines and growth factors to the corresponding receptors, and tumour invasion and metastasis. Also, CD44 expression is elevated in many types of malignancies, as compared with the corresponding normal tissues [2]. In particular, the specific isoform CD44v6 was determined as the major one overexpressed in various types of malignancy. RHAMM, or Cluster determinant 168 (CD168), is present in the cytoplasm and nucleus and can be found also in the cellular surface, being known to mediate cell migration and proliferation [2]. Also, it is overexpressed in the surface of some types of cancer cells.

TSG-6 and GHAP has also been identified as HyA-binding proteins. The first one is associated with inflammatory or autoimmune diseases, and the later is found surrounding myelinated optic nerve axons [25] [2].

This introduction focuses on the synthesis, biological properties and applications of different nanoparticulate delivery systems that include HyA in their structure. We intend to report the work done in the past few years with HyA, including HyA-based nanocarriers, but also conjugates that are chemically or physically bound the polysaccharide chain. We review the intracellular delivery and targeting of the HyA-based nanosystems and the *in vivo* biodistribution and their therapeutic effect.

5. Hyaluronic acid-based nanocarrier systems – synthesis strategies and modifications

HyA can be chemically modified in two major ways: crosslinking or conjugation.

The chemical modification of HyA can be performed on the two available functional sites: the carboxylic acid group and the hydroxyl group (figure 1). An amino group can also be recovered by deacetylation of the N-acetyl group. It is not known which of the hydroxyl groups reacts, though it is reasonable to assume that the reaction occurs mainly on the hydroxyl of the C6 of the N-acetylglucosamine moiety of HyA because of the better accessibility.

5.1. HyA - Drug conjugates

Conjugation of drugs to HyA, as a means to improve delivery, was first reported in 1991 [26]. The covalent linking of a drug to a polymer molecule forms a so-called “polymer prodrug”. A prodrug is an inactive form of a drug that when delivered to a specific organ, tissue or cell is activated by the endogenous metabolism. Certain aspects have to be taken into account such as: i) the drug-polymer bond has to be sufficiently stable to allow reaching the target site; ii) cleavage of the the drug-polymer linkage must release an intact and functional drug molecule; iii) the carrier itself must be stable in the bloodstream [4, 27].

Hyaluronic acid is very attractive for conjugation with hydrophobic/hydrophilic drugs and others therapeutic agents (Table 1) due to the presence of multiple functional groups (hydroxyl and carboxylic acid). Carboxylic group reactions include amidation and esterification, while the hydroxyl groups give origin to ester and ether linkages. Also, Hya can bear reductive amination in the one aldehyde group at the reducing end of the polymer. Through deacetylation of the N-acetyl group it is possible to recover an amine and by periodate oxidation diahdehyde groups via ring opening of the D-glucoronic acid residue (figure2).

Paclitaxel (PTX) is a highly hydrophobic anti-cancer drug, which has been widely utilized in conjugation with HyA. Xin, Wang and Xiang [28] have described the use of amino acids as spacers between paclitaxel and HyA to achieve a higher release of the drug in physiological environment owing to enzymatic action. PTX was first modified with valine, leucine and phenylalanine in the presence of 1-Ethyl-3-(3 dimethylaminopropyl) carbodiimide (EDC)/ 4-Dimethylaminopyridine (DMAP) and piperidine and then conjugated with HyA-tetrabutylammonium (TBA) in dimethylformamide (DMF) and EDC/ N-hydroxysuccinimide (NHS) through an amide bond. The engineered conjugate exhibited higher cytotoxicity in Michigan Cancer Foundation-7 (MCF-7) human breast cancer cell line in comparison to the free paclitaxel.

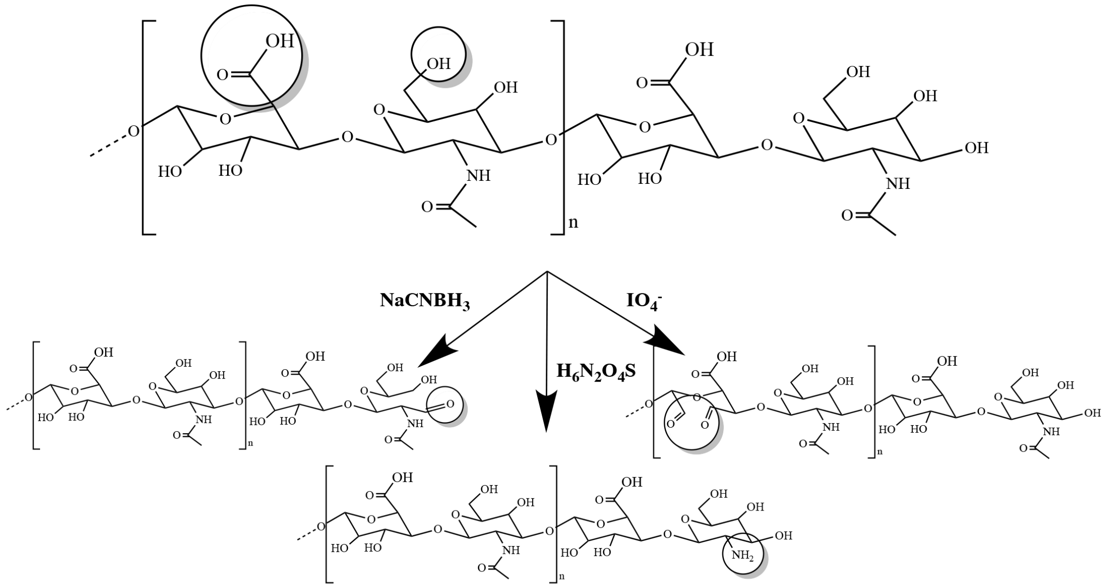

Figure 2: Hyaluronic acid functional groups and chemical modifications that result in new and the introduction of new ones, that become target sites for chemical modification and the grafting of other molecules.

Other authors have used different ligands to obtain HyA-PTX conjugates, potentiating or complementing the PTX effect. Yao, J. et al. [29], described the combination of g-all-trans retinoid acid (ATRA) with HyA-PTX conjugate to enhance PTX tumour induced death and regression. ATRA a retinoid is known to inhibit cell proliferation and induce differentiation in various tumors and enhances PTX effect in tumor regression and cell death. HyA reacted through an amide bond with aminated ATRA in DMF and the presence of EDC/NHS. The amphiphilic conjugate of HyA-ATRA self-assembled into nanostrutures and could entrap the hydrophobic PTX. The resulting multifunctional nanosystem was effective in simultaneously targeting and delivering PTX and ATRA to tumour cells, by a combination of EPR effect and HyA mediated endocytosis. ONCOFIDTM-P [30, 31] is a HyA paclitaxel conjugate developed for the treatment of refractory bladder cancer and peritoneal carcinosis. Due to promising antitumour efficacy, *in vitro* and *in vivo* phase I and II studies are ongoing in six European countries. The studies are being performed in fifteen patients with refractory bladder cancer.

Another common example of therapeutic agents conjugated with HyA are, peptides. Peptides can be modified with an aminooxy N-terminus and react directly with HyA through an oxime bond. Sestak, J. et al. [32] grafted multiple sclerosis antigen (PLP) and an ICAM-1 ligand (LABL) to HyA through an oxime bond. The resulting HyA grafted PLP and LABL significantly inhibited the disease in mice with experimental autoimmune encephalomyelitis, a model of multiple sclerosis.

HyA-Interferon alpha (IFNα) conjugates have been widely used in polymer therapeutics as immunomodulators. IFNα conjugation to biodegradable polymers can mask activity and enhance stability in the bloodstream [33, 34].

Peptides with a terminal amine group can react directly to HyA without any additional modification process. Such is the case of anti-Flt1 peptide - the antagonist peptide against vascular endothelial growth factor receptor 1 (VEGFR1) coupling [35] - and Tat peptide - a kind of cell-penetrating peptide [36]. Although peptides can be coupled to HyA backbone through their amine groups, HyA can also be modified with a spacer prior to the peptide coupling. Yang, J. A. [37] described the transdermal delivery of HyA-human growth hormone (hGH) conjugate, synthesized by coupling the ethylene glycol modified HyA with the N-terminal primary amine of hGH.

Nair et al. [38] described the synthesis of a HyA-bound letrozole conjugate to target long-term letrozole-treated tumours (LTLT) cells. HyA-letrozole nanoparticles (NPs) were prepared by nanoprecipitation using biodegradable PLGA-PEG co-polymer. The engineered NPs restored and maintained a prolonged sensitivity and targeted delivery of letrozole by inhibiting ρ-glycoprotein-mediated multidrug resistance. Table 1 presents a list of recent papers published on the development of HyA-drug conjugates.

Table 1: Hyaluronic acid conjugates.

Conjugate	Therapeutic agent	Solvent and Linker and/or catalyst	Reaction	Application	Reference
Acetylated HyA-pheophorbide	Pheophorbide	DMSO, DCC / DMAP	Esterification	Photodynamic therapies	[14]
HyA – selenium	Selenium	dH_2O, Ascorbic acid	Physical adsorption by hydrogen bonds	Cancer treatment	[39, 40]
HyA-QDot	QDot	PBS, EDC / sulfo-NHS,	Amide bond formation	Bioimaging	[41] [42] [43]
HyA– Cdot	CDot	dH_2O, EDC,	Amide bond formation	Bioimaging for liver diseases	[44]
HyA–Curcumin	Curcumin	dH_2O /DMSO, DCC / DMAP,	Esterification	Drug delivery to CD44 overexpressing cells	[45]
HyA-g-all-trans retinoid acid	g-all-trans retinoid acid / PTX	Formamide, EDC / NHS	Amide bond formation	Drug delivery cancer cells	[29]
HyA-	Trypsin/EGF	dH_2O,	Amide bond	Bioresponsive protein	[33]

PUMPT		EDC/NHS	formation	therapy	
Pyrenyl Hyaluronan	Magnetic nanoclusters	dH_2O, EDC / Sulfo-NHS	Amide bond formation	Detection of CD44 overexpressing cells	[46]
HyA-L-cysteine	Thiolated polymer	dH_2O, EDC / NHS	Amide bond formation	Mucoadhesive drug delivery	[47]
HyA-bound letrozole	Letrozole	Acetoniltrile, PLGA / PEG,	Nanoprecipitation	letrozole-resistant (LTLT-Ca) cells	[38]
HyA–paclitaxel	Paclitaxel	DMF/ dH_2O, EDC/NHS,	Amide bond	Drug delivery cancer cells	[48] [28]
	Paclitaxel	DCM/CAN/PBS NHS, ADH	Amide bond	Drug delivery cancer cells	[49]
	Paclitaxel	DMF, NHS	Ester bond	Drug delivery cancer cells	[50] [51]
HyA-insulin	Insulin	W/O emulsion, EDC / ADH	Cross-linking	Oral insulin delivery	[52]
HyA-apoptosis inducing ligand	Apoptosis inducing ligand (TRAIL)	PBS, -	Electrostatic interactions	Drug delivery rheumatoid arthritis	[53]
HyA- Cisplatin	Cisplatin		-	Intrapulmonary Drug	[54]

				delivery	
HyA-pepetide	Sclerosis antigen (PLP), ICAM-1 ligand (LABL)	dH_2O, -	Oxime bond formation	Pepetide delivery	[32]
	tat	MES, EDC / NHS	Amide bond formation	Enhanced Gene delivery	[36]
	anti-Flt1	Organic solvents, DIPEA, TMP	Amide bond formation	Peptide delivery	[35]
HyA- MTX	MTX	dH_2O /THF, PEG	Amide bond formation	Anti-inflamatory	[55]
HyA- IFNα	IFNα	dH_2O, sodium cyanoborohydride	Coupling reaction	Immune response to viral infections	[34]
HyA- hGH	hGH	dH_2O, sodium cyanoborohydride	Hydrazone bond	Protein Transdermal delivery	[37]
HyA-flavonoids	Epigallocatechin gallate (EGCG)	dH_2O, DA / NHS / EDC	Aldehyde mediated conjugation	Drug delivery cancer cells	[56]

Abbreviations

ADH - Adipic acid dihydrazide
CDots – Carbon Dots
MTX - Methotrexate
NHS - N-hydroxysuccinimide

DA - diethoxyethyl amine	NP - Nanoparticle
DCC - 1, 3-dicyclohexyl carbodiimide	PBS - Phosphate buffered saline
DIPEA - N,N-diisopropyl ethylamine	PEG - Polyethylene glycol
DMAP – 4-Dimethylaminopyridine	PLGA- Poly(lactic-co-glycolic acid)
DMF - Dimethylformamide	PTX - Paclitaxel
DMSO – Dimethyl sulfoxide	PUMPT - Polymer-masked UnMasked Protein Therapy
EDC - 1-Ethyl-3-(3-dimethylaminopropyl)carbodiimide	QDots - Quantum dots
EGF - Epidermal growth factor	Sulfo-NHS - N-hydroxysulfosuccinimide
hGH - Human growth hormone	THF - Tetrahydrofuran
IFNα - Interferon alpha	TMP - 2,2,6,6-tetramethylpiperidine
MES - 2-(N-morpholino)ethanesulfonic acid buffer	W/O – Water in oil

5.2. Self-assembled Nanoparticles

Polymeric amphiphilic molecules have been the focus of attention of many researchers because they can self-assemble into core-shell nanoparticles (NPs) and exhibit singular physicochemical characteristics in aqueous solution. Their unique features are due to the inner hydrophobic core capable of entrapping therapeutic and/or imaging hydrophobic molecules. The outer HyA hydrophilic shell prevents undesirable protein adsorption and evades de immune system. These nanoparticles are also called nanogel due to their hydrogel like composition in which the cross-linkers are provided by the association of hydrophobic groups.

The chemical conjugation of hydrophobic molecules in the HyA backbone can be performed in two available functional sites: the carboxylic acid group and the hydroxyl group (figure 1). Also, by deacetylation of the N-acetyl group it is possible to recover another functional group, an amine. Other common modifications that introduces new functional groups to HyA is the periodate oxidation, which results in two new aldehyde groups and the reduction of the terminal reducing sugar with sodium borohydride that results in another aldehyde group (figure 2).

Several methods have been reported for HyA chemical conjugation. Some methods are performed in water while others need to be performed in organic solvents- most commonly DMF or DMSO – since they use reagents sensitive to hydrolysis,). In this case, the native HyA sodium salt first needs to be modified to render soluble in organic solvents, as we already discussed.

Ceramide has been used as a hydrophobic segment anchored to Hya backbone by ether bond formation with 4-chloromethylbenzoyl chloride as a linker [18] [19] [21] [57], to produce self-assembled NPs. Based in this model, Cy5.5 and Gd3+ were successfully anchored to HyA-ceramide

(HACE) to achieve a dual bioimaging nanoprobe, for near-infrared fluorescence (NIRF) and magnetic resonance (MR) imaging. The engineered nanoprobe proved efficiency in recognising CD44 receptor-overexpressed cells, as assessed by confocal laser scanning microscopy [18]. The same nanosystem has been used to incorporate hydrophobic drugs, such as Doxorubicin (DOX) [19] [21], Docetaxel (DCT) [57], also for CD44 targeting over expressing cells. Table 2 presents a list of recent papers published on the development of HyA derivatives. A new HACE based system has been reported [58] that allows the embedding of PLGA-DCT nanoparticles to the self-assembled HACE nanostructure. This method has been previously used in inorganic nanoparticles, but its application to polymer based nanoparticles was innovative.

Hyaluronic acid can be grafted with aliphatic polyesters, such as Polylactic acid (PLA), poly(lactic-co-glycolic acid) (PLGA), poly(allylamine) (PAH) and poly(ι-lysine) (PLL) by different approaches. Some researchers have chemically linked the polyester molecules to HyA chain by amide bond formation. Yadav, A. et al. [59] designed HyA-PLGA conjugates linked with polyethylene glycol (PEG), for tumour targeting. 5-Fluorouracil (5-FU), an anti-cancer drug was loaded in the HyA-PEG-PLGA triblock copolymer to reach Ehlich Ascites tumour (EAT) cells. HyA-PEG-PLGA NPs were synthetized via amide reaction of one of the amino groups of PEG-bis-amine with carboxylic group of HyA. Further, the second free amino group of PEG was reacted with PLGA. Young-Il Jeong, et al. [60] and Chia Chang Liu et al. [61] used the same approach to synthetize amphiphilic polyester-HyA diblock copolymers. The strategy adopted entailed the reductive amination of HyA and further amid bond formation with PLGA [60] or PLA [61]. Since polysaccharides have one reductive end, HyA was treated with sodium cyanoborohydride to obtain a formyl group that would react with a diamine molecule. The aminated-HyA then reacted via amide bond formation with NHS activated PLGA [60] or N, N′-dicyclohexylcarbodiimide (DCC) activated PLA [61]. These engineered

NPs revealed great potential for drug encapsulation and delivery to cancer cells using CD44 receptor-mediated endocyotosis. Giovanna Pitarresi et al. [62] described the synthesis of HyA grafted copolymers having a balance between hydrophobic PLA and hydrophilic PEG chains, capable of self-assembling into micelles, in aqueous solutions.
The grafting process followed an esterification reaction between the NHS activated PLA chain and HyA, in DMSO, after HyA ion exchange with TBA. The coupling of the PEG molecules was performed by the same methodology. Researchers [63, 64] [65] have been able to synthetize poly(benzyl-L-glutamate)-HyA block copolymers by Huisgen 1,3-dipolar cycloaddition. In summary, HyA was end functionalized by reductive amination and then modified with 1-azido-3-aminopropane [65] or by an alkyne function [63] [64]. The Huisgen's 1,3-Dipolar Cycloaddition (''click reaction'') was performed in DMSO using copper bromide (CuBr) as the catalyst and pentamethyldiethylenetriamine (PMDETA) as a ligand. Hsuen-Tseng Chang et al. [66] patented the synthesis of HyA derivatives by the reaction of HyA hydroxyl groups with polyester isocyanate groups, via a urethane linkage.

Table 2: Hyaluronic acid derivatives.

Carrier	Therapeutic agent	Solvent, Linker/Catalyst	Reaction	Application	Reference
HyA-Ceramide	DTPA + Cy5.5	THF/Acetonitrile Chloromethylbenzoyl chloride	Ether bond formation	MR imaging	[18]
	DOX, DCT	THF/Acetonitrile Chloromethylbenzoyl chloride	Ether bond formation	Drug delivery cancer cells	[19] [21] [57]
	DCT loaded PLGA NPs	THF/acetonitrile Chloromethylbenzoyl chloride	Ether bond formation	Drug delivery cancer cells	[58]
HyA-catechol (dopamine)	Gold NPs, IONs, Qdots	PBS, EDC / Dopamine,	Amide bond formation	High-performance devices or materials	[67]
HyA-polyarginine	Future work	dH_2O, glycerol,	Electrostatic interactions	Future work	[68]
HyA - protamine sulfate	microRNA-34a	dH_2O	Electrostatic interactions	Drug delivery breast cancer	[69]
HyA-Poly(ethylene glycol)diglyci	Future work	W/O emulsion, -	Cross-linking	Topical/transdermal delivery systems	[70]

dyl ether					
HyA-l-phenylalanine ethyl ester	Future work	-	Amide bond	Future work	[71]
HyA-aliphatic polyesters (PLA, PLGA PAH, PLL and PLI)	Ellagic acid / lidocaine chloride,	DMSO/PBS, EDC /NHS/ Sodium cyanoborohydride,	Reductive amination/amide formation	Topical/transdermal delivery systems	[61]
	-	dH_2O, EDC/NHS	Covalent cross-linking	Drug delivery	[72] [73]
	5-fluorouracil	DMSO, DCC/NHS,	Amide bond formation	Drug delivery cancer cells	[59]
	DOX	DMSO, DEA/NHS,	Ester bond	Drug delivery cancer cells	[62]
	DOX	dH_2O /DMSO, sodium cyanoborohydride/ hexamethylene diamine/NHS	Reductive amination / amide bond	Drug delivery cancer cells	[60]
	DOX	DMSO, CuBr/ PMDETA,	Huisgen 1,3-dipolar cycloaddition	Drug delivery cancer cells	[63] [64]

		DMSO, CuBr/ PMDETA,	Huisgen 1,3-dipolar cycloaddition	Drug delivery	[65]
		DMSO, diisocyanate and di-n-butyltin dilaurate, di-n-butyltin diacetate, sodium phenate, ferric chloride, copper acetylacetonate, zinc naphthenate, or tributylphosphine[74]	Urethane bond	Drug delivery	[66]
	IRT	Poloxamers	O/W emulsion	Drug delivery to CD44 overexpressing cells	[74]
PLGA-Pluronic F127- Chitosan- HyA	DOX, IRT	PVA/dH2O	W/O/W doble emulsion	Drug delivery to cancer stem-like cells	[75]

HyA–spermine	Silencer Select siRNAs for COX-2	dH_2O, EDC / NHS	Amide bond formation	Drug delivery to CD44 overexpressing cells	[76], [77]
Glycyrrhetinic acid - HyA	Glycyrrhetinic acid / PTX	Formamide, EDC / NHS	Amide bond formation	Drug delivery cancer cells	[78]
HyA–5β-cholanic acid	SPIONs, Cy5.5	DMSO, EDC/NHS	Amide bond formation	Optical and magnetic resonance (MR) dual imaging probe	[79]
	DOX	DMSO, EDC/NHS	Amide bond formation	Drug delivery cancer cells	[80] [81]
	carbonic anhydrase B	DMSO, EDC/NHS	Amide bond formation	Protein sustained release	[82]
	-	DMSO, EDC / NHS,	Amide bond formation	Drug delivery	[83] [84] [85] [86]
	PTX	DMSO, EDC/NHS	Amide bond formation	Drug delivery	[87]
	PTX	PBS, Cysteamine / EDC / NHS	Amide bond formation	Drug delivery	[88]
	DOX, CPT	DMSO, EDC/NHS	Amide bond formation	Drug delivery	[89]

	IRT	DMSO, EDC/NHS	Amide bond formation	Drug delivery cancer cells	[90]
	chlorin e6	DMSO, EDC / NHS	Amide bond formation	Photodynamic imaging, photodynamic therapy	[91]
HyA-polyethyleneimine	plasmid pIRES2-eGFP-p53	dH_2O, sodium borohydride,	Imine reaction	Gene delivery	[92]
	pDNA	dH_2O, L-cysteine/ EDC/NHS,	Amide bond/disulfide bond	Gene delivery	[93, 94]
	siRNA	dH_2O, $NaBH_3CN$	Reductive amination	Gene silencing	[95]
branched poly(ethyleneimine)-HyA	eGFP DNA	Sodium borate buffer, sodium cyanoborohydrate,	Reductive amination	Gene delivery	[96]
HyA-mesoporous silica NPs	Rhodamine B	dH_2O, EDC/NHS,	Amide bond formation	Drug delivery cancer cells	[97]
	Camptothecin	dH_2O, EDC/NHS,	Amide bond formation	Drug delivery cancer cells	[98]
acetylated HyA	Doxorubicine	Formamide, pyridine,	Acetylation	Drug delivery cancer cells	[17]
chitosan–HyA	siRNA	HBSS buffer,	Ionotropic	Gene silencing	[99]

NPs		-	gelation		
	Plasmid DNA	dH_2O, -	Ionotropic gelation	Gene delivery	[100] [101] [102]
	Plasmid DNA	dH_2O, -	Electrostatic interactions	Gene delivery	[103]
	Eudragit S100 encapsulated oxaliplatin	PBS, EDC,	Amide bond formation	Drug delivery cancer cells	[104]
	Dorzolamide hydrochloride /Timolol maléate	dH_2O, -	Ionotropic gelation	Mucadhesive drugs delivery	[105]
	siRNA/pDNA	dH_2O, tripolyphosphate (TPP),	Cross-linking	Gene delivery/silencing	[106]
	VEGF and PDGF-BB	dH_2O, TPP	Cross-linking	Bioregeneration	[107]
	mannitol	dH_2O, TPP	Ionotropic gelification	Lung delivery	[108]
	-	PBS, -	Disulfide cross-linking	Mucoadhesive oral delivery system	[109]
		dH_2O,	Cross-linking	Drug delivery	[110]

		TPP			
	Curcumanoids	dH_2O	Electrostatic interactions	Drug delivery cancer cells	[111]
	DOX	dH_2O, TPP	Ionotropic gelification	Drug delivery breast cancer	[112]
	microRNA (antimiR-138)	dH_2O, TPP	Ionotropic gelification	Osteogenisis mesenchimal stem cells	[113]
HyA- divinyl sulfone	Iron oxide magnetic NPs/ TMP	W/O microemulsion, AOT	Cross-linking	Multifunctional Drug delivery device	[114]
	Trimethoprim (TMP) / naproxen (NN)	NaOH solution, AOT	Cross-linking	Drug delivery	[13]
HyA-silver	Hemoglobin	dH_2O, -	UV-initiated photoreductio n	Biosensor	[115]
HyA - Monostearin glycerol - monostearate, niosome	α -tocopherol	PBS, EDC/NHS,	Esterification	Transdermal drug delivery system for tumor therapy	[116] [117]
HyA-TOS	D-α-tocopheryl	Formamide EDA/NHS/EDC	Amide bond formation	Drug delivery cancer cells	[118]

	succinate				
Cross-linked HyA	Plasmid DNA	dH_2O, glutaraldehye/ EDC/NHS/4 arm Star PEG/ epichlorohydrin,	Ionic gelation/cross-linking	Gene delivery	[119]
	-	dH_2O /DMSO, glutaraldehyde	Cross-linking	Drug delivery glioma cells	[120]
	polyhexanide	PBS, TDI	Cross-linking by inverse miniemulsion technique	Antibacterial	[121]
	-	dH_2O, EDC/hydrazide,	Amide bond formation	Viscosupplements	[122]
	-	dH_2O, 2,2_(Ethylenedioxy) bis(ethylamine)/ CDI	Amide bond formation		[123] [124]
	-	Alginate/FeCl3,	Electrostatic	-	[125]

			field cross-linking		
	-	dH_2O, ADH / EDC,	Covalent cross-linking	Drug delivery	[126]
	DOX	THF/ACN Ceramide/EDC/NHS/ADH	Covalent cross-linking	Drug delivery cancer cells	[127]
	DOX	DMSO, CuBr/ PMDETA,	Huisgen's 1,3-Dipolar Cycloaddition	Drug delivery cancer cells	[128, 129]
	-	dH_2O, styrylpyridinium	Photocross-linking	Drug delivery	[130]
Hyaluronic acid - 11-amino-undecanethiol	Sinvastatin / Curcumin	DMSO, EDC/NHS/DPDPB	Amide bond/disulfide bond	Drug delivery	[131]
HyA-styrylpyridinium	PTX	dH_2O, UV light,	Electrostatic ineraction/UV cross-linking	Drug delivery cancer cells	[132]
thiolated trimethyl chitosan -	ovalbumin	HEPES, -	Disulfide bonding	Nasal and intradermal vaccination	[133]

thiolated HyA					
HyA-glycerol-monostearate	-	PBS, EDC/NHS,	Esterification	Drug delivery	[134]
Folate-HyA-octadecyl	PTX	Formamide, EDC/NHS,	Amide bond formation	Drug delivery cancer cells	[135]
HyA-cholesterol	DOX/ superparamagnetic iron oxide nanoparticles	DMF, EDC/NHS,	Amide bond formation	Drug delivery cancer cells and bioimaging	[136]
	Etoposide, salinomycin, curcumin.	DMSO, EDC/ HOBT/TEA/DMAP	Ester bond	Drug delivery cancer cells	[137]
	Recombinant human growth hormone, erythropoietin, exendin-4, and lysozyme	DMSO, DMTMM	Condensation	Sustained protein release systems	[20]
HyA-graphene oxide	Photosensitizers (PS; Ce6)	dH_2O, EDC/NHS	Amide bond formation	Phtotodynamic therapy and Drug delivery cancer cells	[138]

HyA-polyamines	siRNA	Formamide, EDC/NHS	Amide bond formation	Gene silencing cancer cells	[139]
	DOX	dH_2O, EDC/NHS/HCl,	Amide bond formation	Drug delivery	[140]
HyA- L-alpha-dioleylphosphatidylethanolamine	pDNA		Amide bond formation	Gene delivery cancer cells	[141]
HyA- N,N-diethylnicotinamide oligomer	PTX	dH_2O, EDC/ HOBt	Amide bond formation	Drug delivery cancer cells	[142]
HyA-octenyl succinic anhydride	-	dH_2O, -	Ether, bond	Drug delivery	[143] [144]
HyA-histidine	DOX	dH_2O, EDC/NHS,	Amide bond formation	Drug delivery cancer cells	[145]
HyA-pyrene	DOX	DMSO, DTT,	Disulfide bond	Drug delivery cancer cells	[22]

Abbreviations

ACN - Acetonitrile

ADH - Adipic acid dihydrazide

IONs - Iron Oxide Nanoparticles

IRT - Irinoteca

AOT - Sodium bis(2-ethylhexyl) sulfosuccinate	MTX - Methotrexate
CDI - 1-[3-(dimethylamino)propyl]-3-ethylcarbodiimide methiodide	NHS - *N*-hydroxysuccinimide
COX-2 - Cyclooxygenase-2	NP - Nanoparticle
CPT - Camptothecin	PBS - Phosphate buffered saline
Cy5.5 – Cyanine Dye 5.5	PDGF-BB - Platelet derived growth factor
DEA - Diethylamine	PAH - poly (allylamine)
DCC - 1, 3-dicyclohexyl carbodiimide	PEG - Polyethylene glycol
DCT - Docetaxel	PLA - Poly(D,L-lactic acid)
DMAP – 4-Dimethylaminopyridine	PLGA- Poly(lactic-co-glycolic acid)
DMF - Dimethylformamide	PLI - Poly-L-lysine-graft-imidazole
DMSO – Dimethyl sulfoxide	PLL - Poly(ι-lysine)
DMTMM - 4-(4,6-Dimethoxy-1,3,5-triazin-2-yl)-4-methylmorpholinium chloride,	PMDETA - N,N,N′,N′,N″-pentamethyldiethylenetriamine
	PTX - Paclitaxel
DOX – Doxorubicin	QDots - Quantum dots
DPDPB - 4-Di-(3'-[2'-pyridyldithio]-propionamido)butane	SPIONs - Super-paramagnetic iron oxide nanoparticles
DTPA - Diethylenetriaminepentaacetic dianhydride	TEA - Triethylamine
EDA - ethylenediamine	TDI - 2,4-toluene diisocyanate
EDC - 1-Ethyl-3-(3-dimethylaminopropyl) carbodiimide	THF - Tetrahydrofuran
HEPES - 4-(2-hydroxyethyl)-1-piperazineethanesulfonic acid buffer	TMP – Trimetoprim
HBSS - Hank's buffered salt solution buffer	TOS - D-α-tocopheryl succinate
HOBT - hydroxybenzotriazole	TPP – Tripolyphosphate
	VEGF - Vascular endothelial growth factor
	W/O – Water in oil

Another great example of hydrophobic molecules, that can be grafted into HyA chain to obtain amphiphilic molecules that self-assemble into nanostrustures, are bile acids, such as 5β-cholanic acid. This was chosen as a hydrophobic moiety for the assembly of HyA NPs once it is non-toxic and biocompatible, as it is present in humans, and can solubilize hydrophobic molecules. Briefly, 5β-cholanic acid must be amino functionalized to allow the reaction with carboxylic acid of HyA via amide formation. Researchers have synthetized and fully characterized these conjugates and their ability to form micelles in water as a result of its amphiphilicity [84, 86]. Amphiphilic HyA–5 β -cholanic acid (HyA–CA) conjugates were synthesized as described earlier, and further modified with a NIRF dye and water-dispersible super-paramagnetic iron oxide nanoparticles (SPION). The engineered nanoparticles were employed as tumour-targeted optical and MR dual imaging contrast agent [79]. The HyA shell of NPs allows prolonged circulation and excellent active targeting of the SPION and NIRF dye, due to the EPR effect and CD44-specific active tumour targeting. Yoon, H., et al. [91] used the same NPs as the carrier of the hydrophobic photosensitizer, chlorin e6 (Ce6) for simultaneous photodynamic imaging and therapy. Hyaluronic acid–5 β -cholanic acid conjugate was further grafted with PEG – to help escape the unintended accumulation in the liver – and black hole quencher3 (BHQ3) – that can effectively quench fluorescent molecules, like Ce6. NPs reached the tumour tissue via passive targeting mechanism and specifically entered tumour cells through CD44-mediated endocytosis. Upon laser irradiation, the Ce6 released from the nanoparticles could generate fluorescence and singlet oxygen inside tumour cells, resulting in effective growth suppression (figure 3). A similar system was developed by Choi and Jeon, et al. [90] using a NIRF imaging dye (Cy 5.5) chemically conjugated onto the HyA backbone to create a theranostic system.

PEG coating of the HyA-5β-cholanic was a strategy used by researchers to improved tumour targetability *in vivo* [57, 83, 90]. Although PEGylation of HyA-5 β-cholanic acid NPs slightly affects their binding affinity to receptors on the cancer cell, it effectively reduces liver uptake and increases the circulation time, leading to accumulation on the tumour site by receptor recognition and EPR effect.

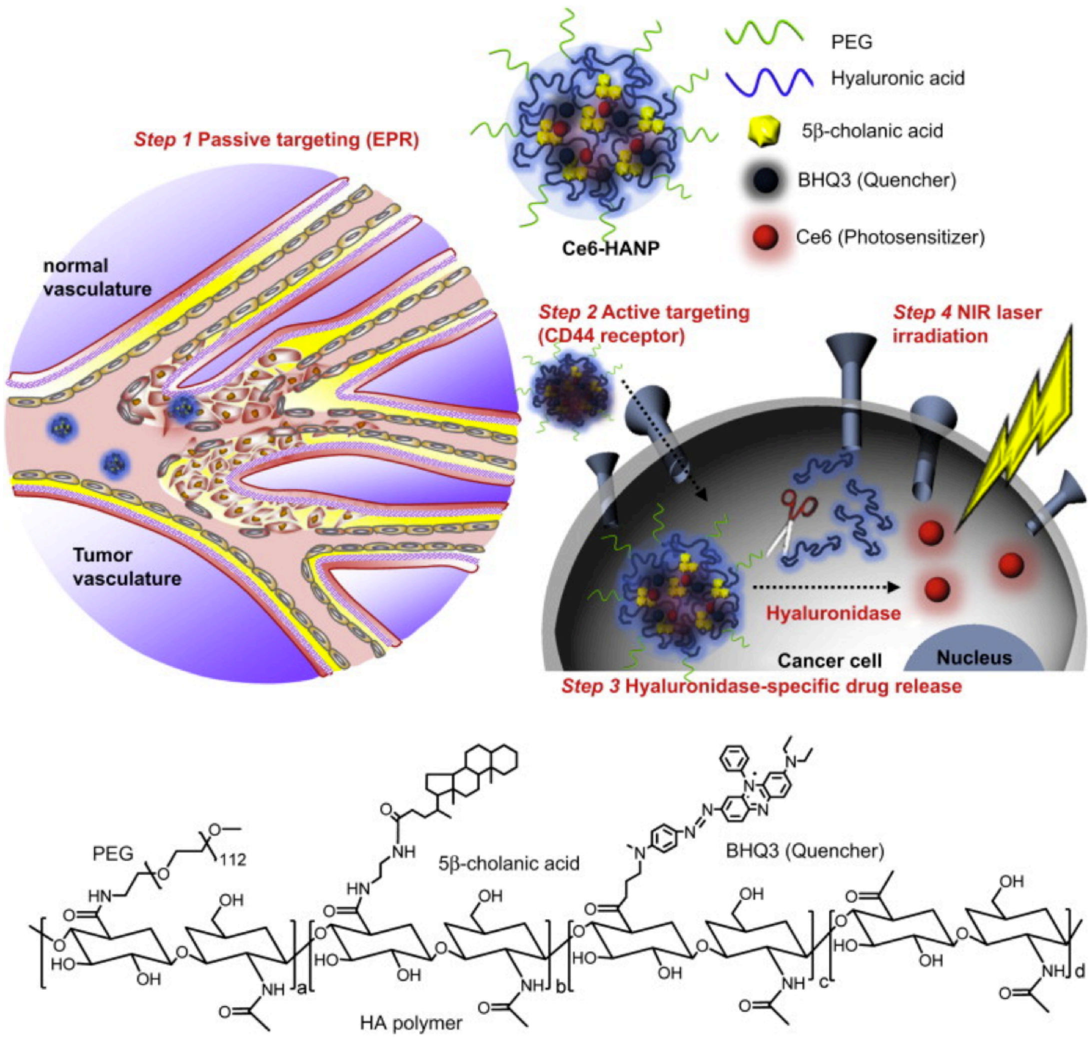

Figure 3: Hyaluronic acid–5 β -cholanic acid (CA) conjugate grafted with PEG molecules and black hole quencher3 (BHQ3) for the intracellular delivery of Ce6. Schematic illustration of the targeting of HyA-CA system by EPR effect and CD44 mediated endocytosis.

Source: Adapted with permission from Yoon, H., et al. (Yoon, H., et al., 2012).

Researchers have recently exploited the use of this nanosystems as anticancer drug carriers. The anticancer drugs include DOX [57, 75, 80, 81], camptothecin (CPT) [57], PTX [87, 88] and irinotecan (IRT) [74, 75, 90]. The drugs are physically encapsulated into de NPs by hydrophobic interactions with 5 β -cholanic acid.

The stability of nanoparticles in blood still remains a critical hurdle for efficient tumour-targeted drug delivery. Researchers recently tried to improve nanoparticle stability and drug release conditions by modifying the engineered NPs by mineralization with calcium phosphate [80, 81]. Mineralized NPs revealed potential as robust drug delivery systems that can release hydrophobic drugs at specific sites under mild acidic conditions, such as found in the extracellular matrix of tumour tissue and in intracellular compartments (e.g., endosome and lysosome).

H.Y. Yoon et al. [87] developed a photo-crosslinked HyA nanoparticles with improved stability and sustained release of loaded drug. NPs were stabilized by ultraviolet (UV)-triggered chemical crosslinking of acrylate groups in the polymer backbone. In a different approach but with the same purpose J. Li et al. [88]developed redox-sensitive micelles based on HyA-deoxycholic acid (HyA-ss-DOCA) conjugates containing cysteamin as bioreducible linkages for intracellular delivery of anticancer drugs. The unique intracellular redox environment has the ability to cleave the disulfide bonds leading to drug release in the intracellular compartment. In a similar approach, Pedrosa et al. [131] developed a crosslinkable hyaluronic acid nanogel by the conjugation with a hydrophobic thiolated chain. Crosslinking was achieved by disulfide bond with, 4-Di-(3'-[2'-pyridyldithio]-propionamido)butane (DPDPB) crosslinkable spacer.

Recent studies have exploited the HyA-5 β-cholanic acid nanosystem as molecular chaperone-like complexes that could entrap and subsequently release biologically active proteins [82]. Carbonic anhydrase B (CAB) was physically encapsulated into HyA-NPs via hydrophobic interaction between the denatured surface of the protein and hydrophobic core of the nanoparticle. Furthermore, researchers observed that nanoparticles assisted protein refolding in a manner similar to the mechanism of molecular chaperones.

5.3. Crosslinked Nanoparticles

Various methods have been developed to produce cross-linked HyA, as hydrogels, films, or particulate systems. In the Table 2 we report a list of recent papers published on the development of HyA-based crosslinked NPS.

A common strategy for developing crosslinked NPs is through their carboxyl groups via carbodiimide chemistry. Carbodiimide (CDI) crosslinked NPs were developed by Fakhari et al. [122] to modify the rheological properties of Orthovisc - used for the management of knee pain caused by ostheoartrites. Maroda et al. [123] also described the synthesis of nano-sized particles by amidation with a bifunctional amine as a cross-linking agent. The particulate systems were obtained by covalent cross-linking of HyA carboxylic groups and 2,2-(ethylenedioxy)bis (ethylamine) in the presence of water soluble CDI, in aqueous solution. Another CDI based crosslinking reaction was used to assemble HyA-block-poly(ethylene glycol)-poly-L-lysine (PLL) complexes [73]. This new methodology envisages the formation of interpolyelectrolyte complexes via the interaction of polysaccharides with opposite charges (HyA and PLL), to induce macromolecular co-assembly, followed by a subsequent crosslinking.

Another usual approach to improve drug-loading and release capacity of HyA nanosystems is the crosslinking with adipic acid dihydrazide (ADH). Park, et al. [127] developed DOX-loaded nanoparticles based on hyaluronic acid-ceramide interconnected with ADH.

Also based in covalent crosslinking via amide bond, Szarpak, A. [72], designed fully biodegradable capsules based on HyA and poly(allylamine) (PAH) or PLL. Although chemically modified, the HyA/PLL or HyA/PAH capsules were still responsive to hyaluronidase, showing higher permeability in the tissues and controlled drug release through a biodegradation process. The fast intracellular rupturing and extracellular resistance offers distinct advantage for delivery of drugs and peptides.

Xu, J. et al. [130, 132] developed a novel photo-crosslinkable micelle based on negatively charged hyaluronan and positively charged styrylpyridinium (SbQ) via an electrostatic self-assembly technique. SbQ, an amphiphilic sensitizer of the styrylpyridinium family, can be dimerized via the [2 + 2]-cycloaddition reaction under UV irradiation. In their report, researchers proved the micelles were photo-crosslinkable.

Bioresponsive crosslinked nanosystems have also been the focus of researchers attention in the last years. Baier et al. have developed stable cross-linked HyA based nanocapsules with trapped polyhexanide, using the inverse miniemulsion technique [121]. Briefly, the crosslinking reaction occurred between the OH groups of HyA acid and the NCO groups of 2,4- toluene diisocyanate (TDI) at the interface of miniemulsion droplets. The HyA nanocapsules containing the antimicrobial agent polyhexanide are specifically cleaved in the presence of hyaluronidase (figure 4).

Yu-Hsien, et al. [125] described a new method for synthesis of HyA nanoparticles by using an electrostatic field system (EFS) in aqueous phase. Alternating electrical polarity of the EFS and the high voltage applied to a dilute HyA solution can dissociated the bio-polymer into separated string. Subsequently, these individual strings coil into nanoparticles under a flip-flop electrostatic field environment and finally assemble into nanoparticles.

Rosso, F. et al. [120] used glutaraldehyde as a crosslinking agent to prepare sub-micron HyA particles. The synthesis consisted in a solvent-non-solvent method followed by glutaraldehyde cross-linking. The resulting particles accumulate with a high efficiency in xenograft tumor site, also due to EPR effect.

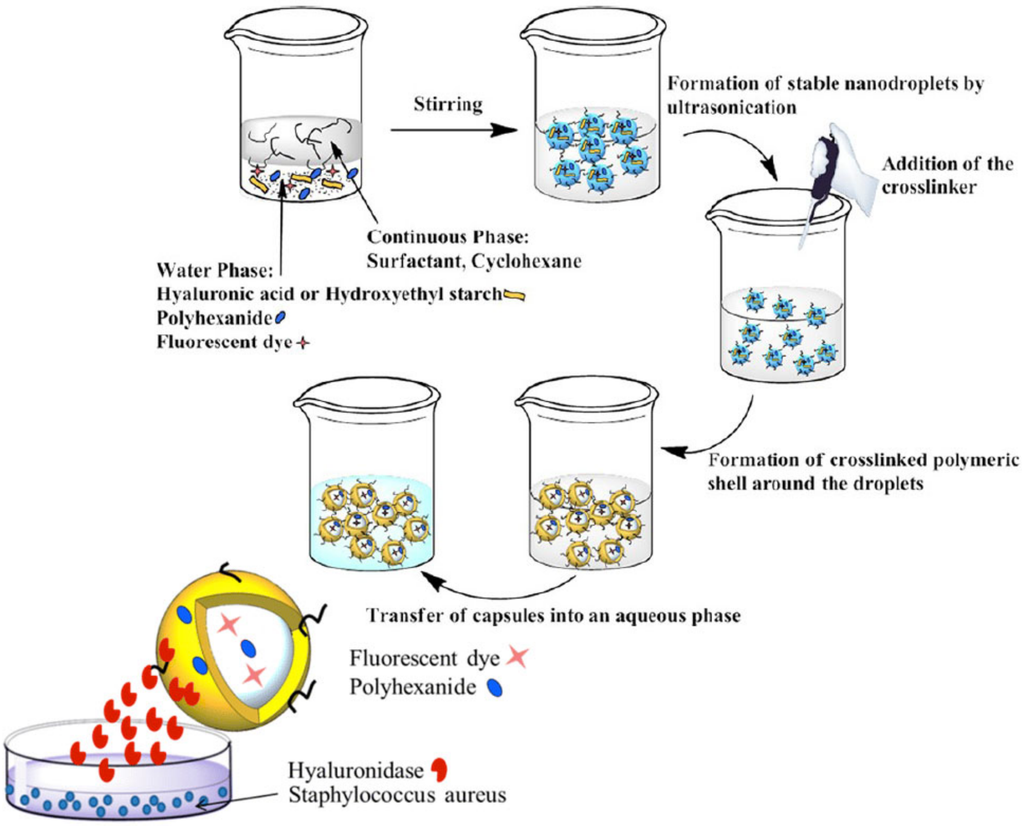

Figure 4: Schematic illustration of the nanocapsules formation through inverse miniemulsion and their cleavage by hyaluronidases.

Reprinted with permission from Baier, G., A. Cavallaro, et al. (2013 Biomacromolecules 14(4): 1103-1112. Copyright 2013 American Chemical Society.

A new method for producing crosslinked HyA-Polyethylene glycol NPs based in an inverse suspension polymerization (w/o) technique was developed by Lim, H. J. et al. [70]. First, the two polymers are solubilized in an aqueous phase and surfactants are dispersed in the oil phase. During emulsification, minimal size emulsion droplets are formed. Then, the crosslink of the HA-based hydrogel nanoparticles occurs by the reaction between OH group of HyA and an epoxide group in the Poly(ethylene glycol)diglycidyl ether (PEGDG) molecule. This nanogel presents ideal features for functioning as a carrier for transdermal drug delivery such as the ability to entrap a high amount of water due to the hydrophilic characteristics of HyA.

Ilgin, P. and Avci, G. et al. [114] and Ekici, S. and Ilgin, P. et al. [13] described the synthesis of divinyl sulfone (DVS) crosslinked HyA nanoparticles. Their approach was based on a water-in-oil microemulsion system and further crosslinking of the HyA molecules with DVS. The resulting nanoporus spherical particles were loaded with magnetic iron particles and Trimethoprim (TMP), an antibacterial drug, to produce a novel type of superior multitask drug delivery devices [114]. Ekici, S. et al. [13] used the engineered system to study the drug loading and release efficiency of Naproxen (NN), a nonsteroidal and anti-inflammatory drug, in physiological conditions.

The limited physiological stability of polyelectrolyte nanocomplexes of chitosan and HyA led to the development of covalently stabilized nanoparticles. Dissulfide crosslinking was used to synthetize chitosan-HyA nanoparticles for nasal and intradermal vaccination [133]. Thiolated trimethylchitosan (TMC) and thiolated HyA were coupled via ionic gelification followed by spontaneous disulfide formation after incubation at pH 7.4 and 37 °C. The disulfide-crosslinked NPs showed superior stability in saline solutions compared to non-stabilized particles but readily disintegrated upon incubation with dithiothreitol. Nasal and intradermal immunization study, with OVA loaded crosslinked particles demonstrated immunogenicity compared to non-stabilized particles.

Mahor, S. et al. [119] investigated the effect of different crosslinkers in pDNA loaded HyA nanoparticles. They concluded that glutaradehyde based cross-linked nanoparticles were the most cytotoxic followed by the Epichlorohydrin and EDC/4-arm Star PEG cross-linked nanoparticles.

5.4. NANOCOMPLEXES

Recent approaches have exploited the complexation of HyA to chitosan (CS) to form nanoparticles, mostly by ionic bond due to the opposite charges. Polycations such as chitosan are particularly attractive for gene delivery not only because of its high density of positive charges, which are essential to condensate the negatively charged siRNA but also for its biodegradability, biocompatibility, mucoadhesivity, and permeation-enhancing effect. The complexation with HyA reduces non-specific interactions with serum proteins and at the same time improves their internalization by cells expressing HyA receptors. Also, the trafficking of HyA particles inside the cells seem to exclude lysossomal compartments, favoring rapid accumulation in the perinuclear region and cell nuclei, which is favorable for gene delivery. HyA is believed to act in this nanocomplexes as a transcriptional activator, probably by loosening the tight binding between the gene and carrier.

CS-HyA NPs can be synthetized by ionotropic gelation as described by Al-Qadi, S. et al. [99]. HyA incorporation in CS-siRNA complex seems to improve cell biocompatibility and also promote the gene release by competing with siRNA for binding to CS, so loosening the CS-si-RNA bond.

Several authors [100, 104, 105, 107, 108] have designed nanosystems of chitosan/HyA by the ionotropic gelation technique using tripolyphosphate (TPP), a polyphosphate penta-anion. TPP interacts with ammonium groups of chitosan, performing as an ionic crosslinker.

Zambito, Y., et al. [109] developed mucoadhesive polymeric nanoparticles for drug delivery across the gastrointestinal mucosa entailing quaternary ammonium–chitosan and HyA conjugates. The NPs were also produced by ionotropic gelation, using thiolated chitosan derivative and the polyanion HyA. The nanoparticles showed a significant mucoadhesivity, due to the positive surface charge and free thiol groups of thiolated quaternary ammonium–chitosan.

Another approach to the development of Cs-HyA NPs involves the additional complexation with PEG. Raviña, M., et al. [106] developed a new nanoparticle formulation, composed by HyA and CS-g-PEG that could be applied for a broad range of gene delivery applications. The strategy embraced was as well the ionic gelification technique in the presence of TPP. The engineered NPs exhibited clear benefits in terms of pDNA delivery compared to classic CS nanoparticles.

It has been reported [146] the synthesis of new liposome-HyA hybrid NP produced by ionic complexation between N-[1-(2,3-Dioleoyloxy)propyl]-N,N,N-trimethylammonium (DOTAP) and thiolated HyA. In this case also, nanosystem was further stabilized by reacting the thiolated HyA layer on the outer shell with thiolated PEG.

Lu, H.-D., et al. [102], Duceppe, N. and Tabrizian, M.[147], and Liu, Y., et al. [103] described the synthesis of HyA-CS–plasmid DNA nanoparticles obtained by complexing chitosan with HyA. These NPs were crafted as novel, non-viral gene delivery vectors targeted to osteoarthritis and other joint diseases. The transfection efficiency of HyA/CS-plasmid nanoparticles was significantly higher than that of CS-plasmid nanoparticles under the same conditions.

Kim, E. et al. [148] developed a nanovector consisting of HyA and poly-L-lysine-graft-imidazole (PLI)-based polyplexes containing Bcl-xL-specific shRNA-encoding plasmid DNA for gastric cancer therapy. The HyA-PLI-pDNA polyplexes were assembled by electrostatic interactions. These polyplexes exhibited targetability to CD44-overexpressing gastric cancer cells, which induced substantial cell death by knockdown of an antiapoptotic gene.

A nanoparticulate system composed of polyarginine (PArg) and HyA was successfully synthetized by Oyarzun-Ampuero, F. et al. [68] through an extremely mild process. Adjusting the polymer ratio, the surface charge of the nanocarrier can be altered therefore allowing interaction with targets that recognize PArg or HyA. This approach allows nanoparticle customization for the incorporation of positively or negatively charged drug molecules.

Fei Zhang, Juan Wu and Hongbin Zhang [115] developed a novel method to produce layer-by-layer (LBL) films with hemoglobin (Hb) and HyA nanoparticles. HyA-Silver (Ag^+) nanoparticles were prepared by UV-initiated photoreduction and then assembled in layers alternately with Hb on a glass carbon electrode. HyA negatively charged carboxyl groups interacts electrostatically with Ag+ to form a complex that photoreduce Ag+ into Ag nanostructure. Further, the UV-photoirradiation finalizes de production of the HyA-Ag nanostrustures in wich HyA function as reducer, catalyst, and stabilizing agent. The combining of HyA biocompatibility and silver antibacterial properties, with enzyme-like catalytic activity of Hb brings great potential as biosensors for *in vitro* and *in vivo* applications. Table 2 presents a list of recent reports on the use of HyA in nanocomplexes systems.

5.5. HyA as a decoration agent

HyA has been extensively used as a coating material (table 3). Overall, coating intends to protect the nanoparticles, prevent protein adsorption and subsequent phagocytosis, and mainly regulate the circulation time and biodistribution through the targeting ability of HyA. The major distinct feature is that HyA decorated NPs contain HyA molecules only in the outer shell of the particles, in contrast with HyA nanogels where the chains are commingled in all the structure. HyA coating requires the covalent bond of the HyA molecule to appropriate functionalities in the surface of the NPs or the exploitation of secondary forces between the two entities.

Liposomes are commonly surface bound with HyA to gain stability against aggregation, long circulation time and high affinity to recognition sites that are overexpressed in tumours. Mizrahy, et al. [15] reported the covalent attachment of pre-activated HyA to the surface of lipidic NPs by amide bond formation. The purpose was to extend the circulation time of NPs and achieve a specific targeting towards HyA receptors (CD44 and CD168) highly expressed on tumours. The interactions of hyaluronan modified liposomes with macrophages, as drug carriers for the treatment of inflammatory diseases, was investigated by Glucksam-Galnoy et al. [149]. HyA surface modified liposomes were able to reduce Tumor necrosis factor α (TNF-α) production in LPS-stimulated macrophages on its own, even before loading with an anti-inflammatory drug. Gan, Wang, et al. [150] reported the surface modification of core-shell lipid nanoparticles with HyA for the treatment of retinal inflammation. HyA coated NPs were obtained by amide bond between the glucuronic acid moiety of HyA and the primary amine of 1,2-dioleoyl-sn-glycero-3-phosphoethanolamine (DOPE) in the pre-formed liposome shell. The surface modification of the liponanoparticles greatly enhanced the targeting to retinal pigment epithelium (RPE) cells, which overexpress CD44 receptors in inflamed human eyes. HyA revealed a viable option to PEG coating when passive delivery is required, due to the lack of adverse effects such as complement activation and cytokine induction, while awarding active targeting to CD44 overexpressing cells and aberrantly activated leukocytes in inflammation. Researchers [151] had also used the targeting ability of hyaluronic acid towards CD44 receptors, in magnetic nanoparticles, to selectively collect and detect leukemia cells.

Self-assembled lipid NPs based on neutral phospholipids and cholesterol were coated with EDC pre-activated HyA, by covalent bond in the similar way as described in the previous reports [152]. The engineered NPs were loaded with siRNA against the multidrug resistance extrusion pump, p-glycoprotein (P-gp) for the treatment of cancer cells. Also intending to synthetize tumour-targeted HyA coated liponanoparticles, Rivkin [153] assembled a PTX- dilauroyl-phosphatidylethanolamine (PE) cluster. The strategy was based on the solubility of PTX in lipids further covalently coated with HyA. Once again, HyA coating allowed selective delivery of PTX into tumour cells in a CD44-dependent manner.

Table 3: Hyaluronic acid as decorating agent

Nanosystem	Reaction	Purpose	Reference
Iron oxide NPs and Magnetic nanoparticle	Ligand exchange reaction with oleic acid	Drug delivery, Cellular trafficking and *in vivo* imaging	[154]
	Amide bond	Bio imaging for atherosclerotic plaques	[155]
	Amide bond	Imaging and drug delivery to activated macrophages	[156]
	Amide bond	Detection and separation leukemia cells	[151]
Titania NPs	Electrostatic interactions	Study physicochemical and biological effects of the HyA coating on Titania NP's	[157]
Silica nanoparticles	Amide formation	Drug delivery cancer cells	[158, 159] [160]

	Layer by layer adsortion	Phtotodynamic therapy and Drug delivery cancer cells	[161]
Mesoporous silica	Dissulfide bond	Drug delivery cancer cells	[162]
DNA/Poliethylenimine	Electrostatic interactions	Gene delivery	[163] [164] [165] [36]
Cell-penetrating peptides-liposomes	Amide formation	Drug delivery cancer cells	[166]
$MnFe_2O_4$ nanocrystal	Amide formation	Magnetic resonance contrast agents	[167]
Lipid-based nanoparticles (LNPs)	Amide formation	siRNA delivery for cancer cells	[152]
	Ionic/electrostatic interactions	Drug delivery	[168] [169] [170]
	Covalent bond	Drug delivery cancer cells / Anti-inflamatory	[15] [149] [150]
	Emusionation/ sonication	Drug delivery	[171, 172]
PTX-Lipid NPs	Covalent bond	Drug delivery	[153]
Polyacrylamide nanoparticle	Physical adsortion	NP pH sensor system that targets CD44	[173]
Chitosan/triphosphate nanoparticles	Electrostatic adosortion	CD44 recognition and delivery	[174] [175]
Gold NPs	Adsorption by irradiation	Drug delivery	[176] [177]
Maghemite NPs	Amide bond	Magnetic resonance imaging	[178]

Polyesters NPs (PLGA/ PLI/ PLA)	Emulsification	Drug delivery	[179]
	Electrostatic interactions	Tissue regeneration	[180] [181]
	Electrostatic interactions	Gene delivery cancer cells	[148]
	Esterification	Drug delivery for arthritis and/or osteoarthritis by intrarticular delivery	[182]
N,N'-cystaminebisacrylamide-4- aminobutanol /pDNA complex	Electrostatic interactions	Retinal gene therapy	[183]

A different approach to modify the surface of lipid NPs can be based on electrostatic interactions. Toriyabe and coworkers [170] studied the effect of HyA coating in liver endothelial cells targeting. Cationic liposomes were coated with free HyA by electrostatic interactions and with HyA-stearylamine (HA-SA) by hydrophobic interactions. They concluded that HyA-SA conjugate allowed an appropriate display of HyA in the surface of liposomes, which was not observed in the case of the free HyA coating. Oyarzun-Ampuero, et al. [168] and Yang, Li, et al. [169] reported the synthesis of lipid nanostructured carriers for the delivery of paclitaxel [169] and docetaxel [168], surface modified with HyA by electrostatic interactions. These surface modified nanocarriers are easy to prepare, do not involve the formation of covalent linkages nor the use of chemical reagents and are able to successfully encapsulate the hydrophobic drugs in their lipid core, merely by exploiting the surface cationic charge of the lipid NPs and the negatively charged hyaluronan.

The biochemical properties of HyA in wound healing and its angiogenic effects were exploited by investigators to produce HyA coated poly(de-co-glycolide) (PLGA) nanoparticles [180] [181]. The engineered NPs were embedded into porcine small intestinal submucosa (SIS) to create a stable microarchitecture for tissue repair and regeneration through enhanced angiogenesis. Results showed that these NPs represent a new approach for modifying derived SIS biomaterials for tissue regeneration.

Kim, E. et al. [148] formulated a HyA- poly-L-lysine-graft-imidazole (PLI)-pDNA ternary polyplexes for gene delivery. PL (poly-L-lysine), a naturally derived polymeric vector for gene delivery, was modified with imidazole to confer buffering abilities in acidic pH conditions. The PLI/pDNA polyplexes were capped with HyA molecules by electrostatic interactions, which added valuable features such as physiological stability and safety and high target ability to CD44-overexpressing gastric cancer cells.

Researchers have studied the potential toxic effect of poly(D,L-lactic/glycolic acid) (PLGA) or poly(D,L-lactic acid) (PLA) NPs coated with HyA. They measured the expression of mRNA of IL-1β and TNF-α - of two cytokines known to be early inflammation markers – and evaluated the change in the synthesis of proteoglycans. Results showed that surface modification with HyA augments the biocompatibility of the engineered NPs. HyA was chemically esterified to the surface of the PLA or PLGA NPs [182].

Dellacherie et al. [179] patented the synthesis of HyA coated polyester NPs. The polyesters mentioned in the invention are polylactic acid, poly (glycolic acid) or poly-caprolactone, and their copolymers. The NPs are assembled in an oil-in-water type emulsion containing the polyester and active substances in the organic phase and hyaluronan in the aqueous phase. In table 3 we present a list of recent papers published on the use of HyA as a coating agent.

A recent approach used hyaluronic acid as surface decorating agent conjugated by disulfide bond to mesoporous silica NPs in a dual-stimuli responsive drug delivery system. In brief, Silica NPs were loaded with DOX and surface modified with sulfhydryl bond that was conjugated with thiolated hyaluronic acid. This coating banded DOX release and allowed a redox/enzyme (HYALs) dual-stimuli responsive targeted delivery system [162].

6. Conclusion and perspectives

Owing to its versatile physicochemical and biological properties, such as biocompatibility, biodegradability, non-immunogenicity, and selective uptake by specific cancer cells, HyA has been widely used as an important constituent in numerous carrier systems. Hyaluronic acid also offers broad range of chemical modification options due to the various functional groups in its structure. A great variety of nanoparticulate materials including HyA in its formulations have been reported in recent years. The availability of medical grade HyA makes it a biomaterial with a huge potential in the field of biomedicine.

7. Acknowledgments

This work was supported by Fundação para a Ciência e a Tecnologia (FCT) under Grant SFRH/BD/61516/2009.

8. References

1. Goodarzi, N., et al., *A review of polysaccharide cytotoxic drug conjugates for cancer therapy.* Carbohydr Polym, 2013. **92**(2): p. 1280-93.
2. Choi, K.Y., et al., *Hyaluronic acid-based nanocarriers for intracellular targeting: interfacial interactions with proteins in cancer.* Colloids Surf B Biointerfaces, 2012. **99**: p. 82-94.
3. Arpicco, S., G. De Rosa, and E. Fattal, *Lipid-Based Nanovectors for Targeting of CD44-Overexpressing Tumor Cells.* J Drug Deliv, 2013. **2013**: p. 860780.
4. Ossipov, D.A., *Nanostructured hyaluronic acid-based materials for active delivery to cancer.* Expert Opin Drug Deliv, 2010. **7**(6): p. 681-703.
5. Misra, S., et al., *Hyaluronan-CD44 interactions as potential targets for cancer therapy.* FEBS J, 2011. **278**(9): p. 1429-43.
6. Gaffney, J., et al., *Therapeutic applications of hyaluronan.* Mol Biosyst, 2010. **6**(3): p. 437-43.
7. Oh, E.J., et al., *Target specific and long-acting delivery of protein, peptide, and nucleotide therapeutics using hyaluronic acid derivatives.* Journal of Controlled Release, 2010. **141**(1): p. 2-12.
8. Haidar, Z.S., *Bio-Inspired/-Functional Colloidal Core-Shell Polymeric-Based NanoSystems: Technology Promise in Tissue Engineering, Bioimaging and NanoMedicine.* Polymers, 2010. **2**(3): p. 323-352.
9. Muzzarelli, R.A.A., et al., *Chitosan, hyaluronan and chondroitin sulfate in tissue engineering for cartilage regeneration: A review.* Carbohydrate Polymers, 2012. **89**(3): p. 723-739.
10. Schanté, C.E., et al., *Chemical modifications of hyaluronic acid for the synthesis of derivatives for a broad range of biomedical applications.* Carbohydrate Polymers, 2011. **85**(3): p. 469-489.
11. Liu, Y., et al., *Amphiphilic polysaccharide-hydrophobicized graft polymeric micelles for drug delivery nanosystems.* Curr Med Chem, 2011. **18**(17): p. 2638-48.
12. Cheng, R., et al., *Dual and multi-stimuli responsive polymeric nanoparticles for programmed site-specific drug delivery.* Biomaterials, 2013. **34**(14): p. 3647-57.
13. Ekici, S., et al., *Hyaluronic acid hydrogel particles with tunable charges as potential drug delivery devices.* Carbohydrate Polymers, 2011. **84**(4): p. 1306-1313.
14. Li, F., B.C. Bae, and K. Na, *Acetylated Hyaluronic Acid/Photosensitizer Conjugate for the Preparation of Nanogels with Controllable Phototoxicity: Synthesis, Characterization,*

Autophotoquenching Properties, and in vitro Phototoxicity against He La Cells. Bioconjugate Chemistry, 2010. **21**(7): p. 1312-1320.

15. Mizrahy, S., et al., *Hyaluronan-coated nanoparticles: the influence of the molecular weight on CD44-hyaluronan interactions and on the immune response.* J Control Release, 2011. **156**(2): p. 231-8.
16. El-Dakdouki, M.H., et al., *Development of multifunctional hyaluronan-coated nanoparticles for imaging and drug delivery to cancer cells.* Biomacromolecules, 2012. **13**(4): p. 1144-51.
17. Park, W., et al., *Cancer cell specific targeting of nanogels from acetylated hyaluronic acid with low molecular weight.* European Journal of Pharmaceutical Sciences, 2010. **40**(4): p. 367-375.
18. Cho, H.J., et al., *Hyaluronic acid-ceramide-based optical/MR dual imaging nanoprobe for cancer diagnosis.* J Control Release, 2012. **162**(1): p. 111-8.
19. Jin, Y.-J., et al., *Hyaluronic Acid Derivative-Based Self-Assembled Nanoparticles for the Treatment of Melanoma.* Pharm Res, 2012. **29**(12): p. 3443-3454.
20. Nakai, T., et al., *Injectable hydrogel for sustained protein release by salt-induced association of hyaluronic acid nanogel.* Macromol Biosci, 2012. **12**(4): p. 475-83.
21. Cho, H.J., et al., *Polyethylene glycol-conjugated hyaluronic acid-ceramide self-assembled nanoparticles for targeted delivery of doxorubicin.* Biomaterials, 2012. **33**(4): p. 1190-200.
22. Yang, X., et al., *Preparation of hyaluronic acid nanoparticles via hydrophobic association assisted chemical cross-linking-an orthogonal modular approach.* Soft Matter, 2011. **7**(16): p. 7517-7525.
23. Lee, H., K. Lee, and T.G. Park, *Hyaluronic acid-paclitaxel conjugate micelles: synthesis, characterization, and antitumor activity.* Bioconjug Chem, 2008. **19**(6): p. 1319-25.
24. Li, F., B.C. Bae, and K. Na, *Acetylated hyaluronic acid/photosensitizer conjugate for the preparation of nanogels with controllable phototoxicity: synthesis, characterization, autophotoquenching properties, and in vitro phototoxicity against HeLa cells.* Bioconjug Chem, 2010. **21**(7): p. 1312-20.
25. Fakhari, A. and C. Berkland, *Applications and emerging trends of hyaluronic acid in tissue engineering, as a dermal filler and in osteoarthritis treatment.* Acta Biomaterialia, 2013. **9**(7): p. 7081-7092.
26. Drobnik, J., *Hyaluronan in drug delivery.* Advanced Drug Delivery Reviews, 1991. **7**(2): p. 295-308.
27. Khandare, J. and T. Minko, *Polymer–drug conjugates: Progress in polymeric prodrugs.* Progress in Polymer Science, 2006. **31**(4): p. 359-397.
28. Xin, D., Y. Wang, and J. Xiang, *The use of amino acid linkers in the conjugation of paclitaxel with hyaluronic acid as drug delivery*

system: synthesis, self-assembled property, drug release, and in vitro efficiency. Pharm Res, 2010. **27**(2): p. 380-9.
29. Yao, J., et al., *Efficient simultaneous tumor targeting delivery of all-trans retinoid acid and Paclitaxel based on hyaluronic acid-based multifunctional nanocarrier.* Mol Pharm, 2013. **10**(3): p. 1080-91.
30. Campisi, M. and D. Renier, *ONCOFID-P a Hyaluronic Acid Paclitaxel Conjugate for the Treatment of Refractory Bladder Cancer and Peritoneal Carcinosis.* Current Bioactive Compounds, 2011. **7**(1): p. 27-32.
31. Montagner, I.M., et al., *Paclitaxel-hyaluronan hydrosoluble bioconjugate: Mechanism of action in human bladder cancer cell lines.* Urologic Oncology: Seminars and Original Investigations, (0).
32. Sestak, J., et al., *Single-step grafting of aminooxy-peptides to hyaluronan: A simple approach to multifunctional therapeutics for experimental autoimmune encephalomyelitis.* J Control Release, 2013. **168**(3): p. 334-40.
33. Ferguson, E.L., A.M. Alshame, and D.W. Thomas, *Evaluation of hyaluronic acid-protein conjugates for polymer masked-unmasked protein therapy.* Int J Pharm, 2010. **402**(1-2): p. 95-102.
34. Yang, J.A., et al., *Target specific hyaluronic acid-interferon alpha conjugate for the treatment of hepatitis C virus infection.* Biomaterials, 2011. **32**(33): p. 8722-9.
35. Hahn, S.K., et al., *Drug delivery system using hyaluronic acid-peptide conjugate micelle*. 2012, POSTECH ACADEMY-INDUSTRY FOUNDATION (Pohang, KR)
36. Tang, S., et al., *Tat-conjugated hyaluronic acid enveloping polyplexes with facilitated nuclear entry and improved transfection.* Colloids and Surfaces A: Physicochemical and Engineering Aspects, 2013. **423**(0): p. 124-130.
37. Yang, J.A., et al., *Transdermal delivery of hyaluronic acid -- human growth hormone conjugate*. Biomaterials, 2012. **33**(25): p. 5947-54.
38. Nair, H.B., et al., *Hyaluronic acid-bound letrozole nanoparticles restore sensitivity to letrozole-resistant xenograft tumors in mice*. J Nanosci Nanotechnol, 2011. **11**(5): p. 3789-99.
39. Zhang, Y., J. Wang, and L. Zhang, *Creation of Highly Stable Selenium Nanoparticles Capped with Hyperbranched Polysaccharide in Water.* Langmuir, 2010. **26**(22): p. 17617-17623.
40. Yuena Ren, T.Z., Guanghua Mao, Min Zhang, Fang Li, Ye Zou, and X.W. Liuqing Yang, *Antitumor activity of hyaluronic acid–selenium nanoparticles.* International Journal of Biological Macromolecules, 2013. **57**: p. 57-62.
41. Kim, K.S., et al., *Bioimaging for targeted delivery of hyaluronic Acid derivatives to the livers in cirrhotic mice using quantum dots.* ACS Nano, 2010. **4**(6): p. 3005-14.

42. Kim, K.S., et al., *In vivo real-time confocal microscopy for target-specific delivery of hyaluronic acid-quantum dot conjugates.* Nanomedicine, 2012. **8**(7): p. 1070-3.
43. Ki Su, K., et al. *Real-time bioimaging of hyaluronic acid derivatives using quantum dots for biopharmaceutical delivery applications*. in *Nano/Molecular Medicine and Engineering (NANOMED), 2010 IEEE 4th International Conference on*. 2010.
44. Goh, E.J., et al., *Bioimaging of Hyaluronic Acid Derivatives Using Nanosized Carbon Dots.* Biomacromolecules, 2012. **13**(8): p. 2554-2561.
45. Manju, S. and K. Sreenivasan, *Conjugation of curcumin onto hyaluronic acid enhances its aqueous solubility and stability.* Journal of Colloid and Interface Science, 2011. **359**(1): p. 318-325.
46. Lim, E.K., et al., *Hyaluronan-modified magnetic nanoclusters for detection of CD44-overexpressing breast cancer by MR imaging.* Biomaterials, 2011. **32**(31): p. 7941-50.
47. Li, X., et al., *Hyaluronic acid L-cysteine conjugate exhibits controlled-release potential for mucoadhesive drug delivery.* Pharmazie, 2012. **67**(3): p. 224-8.
48. Galer, C.E., et al., *Hyaluronic acid-paclitaxel conjugate inhibits growth of human squamous cell carcinomas of the head and neck via a hyaluronic acid-mediated mechanism.* Oral Oncol, 2011. **47**(11): p. 1039-47.
49. Xu, C., et al., *Self-assembled nanoparticles from hyaluronic acid-paclitaxel prodrugs for direct cytosolic delivery and enhanced antitumor activity.* Int J Pharm, 2015. **493**(1-2): p. 172-81.
50. Lee, S.J., et al., *Metronomic activity of CD44-targeted hyaluronic acid-paclitaxel in ovarian carcinoma*. Clin Cancer Res, 2012. **18**(15): p. 4114-21.
51. Luo, Y., M.R. Ziebell, and G.D. Prestwich, *A Hyaluronic Acid−Taxol Antitumor Bioconjugate Targeted to Cancer Cells.* Biomacromolecules, 2000. **1**(2): p. 208-218.
52. Han, L., et al., *Insulin-Loaded pH-Sensitive Hyaluronic Acid Nanoparticles Enhance Transcellular Delivery.* AAPS PharmSciTech, 2012. **13**(3): p. 836-845.
53. Kim, Y.J., et al., *Ionic complex systems based on hyaluronic acid and PEGylated TNF-related apoptosis-inducing ligand for treatment of rheumatoid arthritis.* Biomaterials, 2010. **31**(34): p. 9057-64.
54. Xie, Y., et al., *Pulmonary delivery of cisplatin-hyaluronan conjugates via endotracheal instillation for the treatment of lung cancer.* Int J Pharm, 2010. **392**(1-2): p. 156-63.
55. Homma, A., et al., *Synthesis and optimization of hyaluronic acid-methotrexate conjugates to maximize benefit in the treatment of osteoarthritis.* Bioorg Med Chem, 2010. **18**(3): p. 1062-75.

56. Motoichi Kurisawa, S.N., Joo Eun Chung, *Particulate hyaluronic acid formulations for cellular delivery of bioactive agents*, T.A.R. AGENCY FOR SCIENCE, Editor. 2012: Singa.
57. Cho, H.J., et al., *Self-assembled nanoparticles based on hyaluronic acid-ceramide (HA-CE) and Pluronic(R) for tumor-targeted delivery of docetaxel.* Biomaterials, 2011. **32**(29): p. 7181-90.
58. Park, J.H., et al., *Development of poly(lactic-co-glycolic) acid nanoparticles-embedded hyaluronic acid-ceramide-based nanostructure for tumor-targeted drug delivery.* Int J Pharm, 2014. **473**(1-2): p. 426-33.
59. Yadav, A.K., et al., *Development and characterization of hyaluronic acid decorated PLGA nanoparticles for delivery of 5-fluorouracil.* Drug Deliv, 2010. **17**(8): p. 561-72.
60. Jeong, Y.I., et al., *Self-assembled nanoparticles of hyaluronic acid/poly(DL-lactide-co-glycolide) block copolymer.* Colloids Surf B Biointerfaces, 2012. **90**: p. 28-35.
61. Liu, C., K. Chang, and Y. Wang, *A novel biodegradable amphiphilic diblock copolymers based on poly(lactic acid) and hyaluronic acid as biomaterials for drug delivery.* Journal of Polymer Research, 2010. **17**(4): p. 459-469.
62. Pitarresi, G., et al., *Self-assembled amphiphilic hyaluronic acid graft copolymers for targeted release of antitumoral drug.* J Drug Target, 2010. **18**(4): p. 264-76.
63. Upadhyay, K.K., et al., *The in vivo behavior and antitumor activity of doxorubicin-loaded poly(gamma-benzyl l-glutamate)-block-hyaluronan polymersomes in Ehrlich ascites tumor-bearing BalB/c mice.* Nanomedicine, 2012. **8**(1): p. 71-80.
64. Upadhyay, K.K., et al., *The intracellular drug delivery and anti tumor activity of doxorubicin loaded poly(gamma-benzyl L-glutamate)-b-hyaluronan polymersomes.* Biomaterials, 2010. **31**(10): p. 2882-92.
65. Bonduelle, C., et al., *Synthesis and self-assembly of "tree-like" amphiphilic glycopolypeptides.* Chem Commun (Camb), 2012. **48**(67): p. 8353-5.
66. Hsuen-Tseng Chang, J.-H.C., Yu-Hua Chen, Muh-Lan Chen, Shu-Hua Jan, Mei-Jung Liu, Bin-Hong Tsai, *Biodegradable hyaluronic acid derivative and biodegradable polymeric micelle composition*, I.T.R. Instittute, Editor. 2010: Taiwan.
67. Lee, Y., et al., *A Bioinspired Polymeric Template for 1D Assembly of Metallic Nanoparticles, Semiconductor Quantum Dots, and Magnetic Nanoparticles.* Macromolecular Rapid Communications, 2010. **31**(24): p. 2109-2114.
68. Oyarzun-Ampuero, F.A., et al., *A new drug nanocarrier consisting of polyarginine and hyaluronic acid.* European Journal of Pharmaceutics and Biopharmaceutics, 2011. **79**(1): p. 54-57.

69. Wang, S., et al., *Degradable hyaluronic acid/protamine sulfate interpolyelectrolyte complexes as miRNA-delivery nanocapsules for triple-negative breast cancer therapy.* Adv Healthc Mater, 2015. **4**(2): p. 281-90.
70. Lim, H.J., et al., *A novel approach for the use of hyaluronic acid-based hydrogel nanoparticles as effective carriers for transdermal delivery systems.* Colloids and Surfaces a-Physicochemical and Engineering Aspects, 2012. **402**: p. 80-87.
71. Zhang, C., et al., *Polymer vesicles prepared from the (l-phenylalanine ethyl ester)-modified hyaluronic acid.* Materials Letters, 2016. **164**: p. 15-18.
72. Szarpak, A., et al., *Designing hyaluronic acid-based layer-by-layer capsules as a carrier for intracellular drug delivery.* Biomacromolecules, 2010. **11**(3): p. 713-20.
73. Novoa-Carballal, R., D.V. Pergushov, and A.H.E. Muller, *Interpolyelectrolyte complexes based on hyaluronic acid-block-poly(ethylene glycol) and poly-l-lysine.* Soft Matter, 2013. **9**(16): p. 4297-4303.
74. Giarra, S., et al., *Spontaneous arrangement of a tumor targeting hyaluronic acid shell on irinotecan loaded PLGA nanoparticles.* Carbohydrate Polymers, 2016. **140**: p. 400-407.
75. Wang, H., et al., *Hyaluronic acid-decorated dual responsive nanoparticles of Pluronic F127, PLGA, and chitosan for targeted co-delivery of doxorubicin and irinotecan to eliminate cancer stem-like cells.* Biomaterials, 2015. **72**: p. 74-89.
76. Shen, Y., et al., *Synthesis and characterization of low molecular weight hyaluronic acid-based cationic micelles for efficient siRNA delivery.* Carbohydrate Polymers, 2009. **77**(1): p. 95-104.
77. Shen, Y., et al., *A novel tumor-targeted delivery system with hydrophobized hyaluronic acid-spermine conjugates (HHSCs) for efficient receptor-mediated siRNA delivery.* International Journal of Pharmaceutics, 2011. **414**(1-2): p. 233-243.
78. Zhang, L., et al., *Glycyrrhetinic acid-graft-hyaluronic acid conjugate as a carrier for synergistic targeted delivery of antitumor drugs.* International Journal of Pharmaceutics, 2013. **441**(1-2): p. 654-664.
79. Lee, D.E., et al., *Amphiphilic hyaluronic acid-based nanoparticles for tumor-specific optical/MR dual imaging.* Journal of Materials Chemistry, 2012. **22**(21): p. 10444-10447.
80. Han, S.-Y., et al., *Mineralized hyaluronic acid nanoparticles as a robust drug carrier.* Journal of Materials Chemistry, 2011. **21**(22): p. 7996-8001.
81. Han, H.S., et al., *Robust PEGylated hyaluronic acid nanoparticles as the carrier of doxorubicin: Mineralization and its effect on tumor targetability in vivo.* J Control Release, 2013. **168**(2): p. 105-14.

82. Sivasubramanian, M., et al., *Molecular chaperone-like hyaluronic acid nanoparticles: Implications as the carrier for protein delivery systems.* Macromolecular Research, 2012. **20**(10): p. 1007-1010.
83. Choi, K.Y., et al., *PEGylation of hyaluronic acid nanoparticles improves tumor targetability in vivo.* Biomaterials, 2011. **32**(7): p. 1880-9.
84. Dong, X. and C. Liu, *Preparation and Characterization of Self-Assembled Nanoparticles of Hyaluronic Acid-Deoxycholic Acid Conjugates.* Journal of Nanomaterials, 2010. **2010**.
85. Choi, K.Y., et al., *Self-assembled hyaluronic acid nanoparticles as a potential drug carrier for cancer therapy: synthesis, characterization, and in vivo biodistribution.* Journal of Materials Chemistry, 2009. **19**(24): p. 4102-4107.
86. Choi, K.Y., et al., *Self-assembled hyaluronic acid nanoparticles for active tumor targeting.* Biomaterials, 2010. **31**(1): p. 106-14.
87. Yoon, H.Y., et al., *Photo-crosslinked hyaluronic acid nanoparticles with improved stability for in vivo tumor-targeted drug delivery.* Biomaterials, 2013. **34**(21): p. 5273-80.
88. Li, J., et al., *Redox-sensitive micelles self-assembled from amphiphilic hyaluronic acid-deoxycholic acid conjugates for targeted intracellular delivery of paclitaxel.* Biomaterials, 2012. **33**(7): p. 2310-20.
89. Choi, K.Y., et al., *Smart nanocarrier based on PEGylated hyaluronic acid for cancer therapy.* ACS Nano, 2011. **5**(11): p. 8591-9.
90. Choi, K.Y., et al., *Theranostic nanoparticles based on PEGylated hyaluronic acid for the diagnosis, therapy and monitoring of colon cancer.* Biomaterials, 2012. **33**(26): p. 6186-93.
91. Yoon, H.Y., et al., *Tumor-targeting hyaluronic acid nanoparticles for photodynamic imaging and therapy.* Biomaterials, 2012. **33**(15): p. 3980-9.
92. Yao, J., et al., *Amphoteric hyaluronic acid derivative for targeting gene delivery.* Biomaterials, 2010. **31**(35): p. 9357-9365.
93. Yeh, P.-H., et al., *Stimuli-responsive HA-PEI Nanoparticles Encapsulating Endostatin Plasmid for Stem Cell Gene Therapy.* Rsc Advances, 2013.
94. Park, J.S., et al., *Receptor-mediated gene delivery into human mesenchymal stem cells using hyaluronic acid-shielded polyethylenimine/pDNA nanogels.* Carbohydr Polym, 2016. **136**: p. 791-802.
95. Park, K., et al., *Target specific tumor treatment by VEGF siRNA complexed with reducible polyethyleneimine-hyaluronic acid conjugate.* Biomaterials, 2010. **31**(19): p. 5258-65.
96. Needham, C.J., et al., *Engineering a polymeric gene delivery vector based on poly(ethylenimine) and hyaluronic acid.* Biomacromolecules, 2012. **13**(5): p. 1429-37.

97. Chen, Z.W., et al., *Bioresponsive Hyaluronic Acid-Capped Mesoporous Silica Nanoparticles for Targeted Drug Delivery.* Chemistry-a European Journal, 2013. **19**(5): p. 1778-1783.
98. Ma, M., et al., *Hyaluronic acid-conjugated mesoporous silica nanoparticles: excellent colloidal dispersity in physiological fluids and targeting efficacy.* Journal of Materials Chemistry, 2012. **22**(12): p. 5615-5621.
99. Al-Qadi, S., et al., *Chitosan-hyaluronic acid nanoparticles for gene silencing: the role of hyaluronic acid on the nanoparticles' formation and activity.* Colloids Surf B Biointerfaces, 2013. **103**: p. 615-23.
100. Gwak, S.J., et al., *Chitosan/TPP-Hyaluronic Acid Nanoparticles: A New Vehicle for Gene Delivery to the Spinal Cord.* J Biomater Sci Polym Ed, 2011.
101. Contreras-Ruiz, L., et al., *Intracellular trafficking of hyaluronic acid-chitosan oligomer-based nanoparticles in cultured human ocular surface cells.* Mol Vis, 2011. **17**: p. 279-90.
102. Lu, H.-D., et al., *Novel hyaluronic acid–chitosan nanoparticles as non-viral gene delivery vectors targeting osteoarthritis.* International Journal of Pharmaceutics, 2011. **420**(2): p. 358-365.
103. Liu, Y., et al., *Self-assembled nanoparticles based on amphiphilic chitosan derivative and hyaluronic acid for gene delivery.* Carbohydr Polym, 2013. **94**(1): p. 309-16.
104. Jain, A., et al., *Design and development of ligand-appended polysaccharidic nanoparticles for the delivery of oxaliplatin in colorectal cancer.* Nanomedicine, 2010. **6**(1): p. 179-90.
105. Wadhwa, S., et al., *Hyaluronic acid modified chitosan nanoparticles for effective management of glaucoma: development, characterization, and evaluation.* J Drug Target, 2010. **18**(4): p. 292-302.
106. Ravina, M., et al., *Hyaluronic acid/chitosan-g-poly(ethylene glycol) nanoparticles for gene therapy: an application for pDNA and siRNA delivery.* Pharm Res, 2010. **27**(12): p. 2544-55.
107. Parajo, Y., et al., *Hyaluronic acid/Chitosan nanoparticles as delivery vehicles for VEGF and PDGF-BB.* Drug Deliv, 2010. **17**(8): p. 596-604.
108. Al-Qadi, S., A. Grenha, and C. Remuñán-López, *Microspheres loaded with polysaccharide nanoparticles for pulmonary delivery: Preparation, structure and surface analysis.* Carbohydrate Polymers, 2011. **86**(1): p. 25-34.
109. Zambito, Y., et al., *Mucoadhesive nanoparticles made of thiolated quaternary chitosan crosslinked with hyaluronan.* Carbohydrate Polymers, 2013. **92**(1): p. 33-39.
110. Alonso Fernandez, M.J.E.C.-C.s., E-15782 Santiago de Compostela, ES) , F.F.M.E.C.-C.s. De La, E-15782 Santiago de Compostela, ES) , and M.B.E.C.-C.s. Seijo Rey, E-15782 Santiago de Compostela, ES)

Hyaluronic acid nanoparticles. 2012, Advanced In, Vitro Cell Technologies S. L. .
111. Yang, L., et al., *Hyaluronic acid/chitosan nanoparticles for delivery of curcuminoid and its in vitro evaluation in glioma cells.* Int J Biol Macromol, 2015. **72**: p. 1391-401.
112. Deng, X., et al., *Hyaluronic acid-chitosan nanoparticles for co-delivery of MiR-34a and doxorubicin in therapy against triple negative breast cancer.* Biomaterials, 2014. **35**(14): p. 4333-44.
113. Wu, G., et al., *Improving the osteogenesis of rat mesenchymal stem cells by chitosan-based-microRNA nanoparticles.* Carbohydr Polym, 2016. **138**: p. 49-58.
114. Ilgin, P., et al., *Colloidal drug carries from (sub)micron hyaluronic acid hydrogel particles with tunable properties for biomedical applications.* Carbohydrate Polymers, 2010. **82**(3): p. 997-1003.
115. Zhang, F., J. Wu, and H.B. Zhang, *Construction of hyaluronan-silver nanoparticle-hemoglobin multilayer composite film and investigations on its electrocatalytic properties.* Journal of Solid State Electrochemistry, 2012. **16**(4): p. 1683-1692.
116. Kong, M., et al., *Construction of hyaluronic acid noisome as functional transdermal nanocarrier for tumor therapy.* Carbohydrate Polymers, 2013. **94**(1): p. 634-641.
117. Kong, M., et al., *Investigations on skin permeation of hyaluronic acid based nanoemulsion as transdermal carrier.* Carbohydrate Polymers, 2011. **86**(2): p. 837-843.
118. Liang, D.S., et al., *Tumor-specific penetrating peptides-functionalized hyaluronic acid-d-alpha-tocopheryl succinate based nanoparticles for multi-task delivery to invasive cancers.* Biomaterials, 2015. **71**: p. 11-23.
119. Mahor, S., et al., *Controlled release of plasmid DNA from hyaluronan nanoparticles.* Curr Drug Deliv, 2011. **8**(4): p. 354-62.
120. Rosso, F., et al., *Cross-linked hyaluronic acid sub-micron particles: in vitro and in vivo biodistribution study in cancer xenograft model.* J Mater Sci Mater Med, 2013.
121. Baier, G., et al., *Enzyme responsive hyaluronic acid nanocapsules containing polyhexanide and their exposure to bacteria to prevent infection.* Biomacromolecules, 2013. **14**(4): p. 1103-12.
122. Fakhari, A., et al., *Hyaluronic Acid nanoparticles titrate the viscoelastic properties of viscosupplements.* Langmuir, 2013. **29**(17): p. 5123-31.
123. Maroda, M., et al., *Preparation and investigation of a cross-linked hyaluronan nanoparticles system.* Carbohydrate Polymers, 2011. **83**(3): p. 1322-1329.
124. Magdolna Bodnar, J.B., Ildiko Schriffertne Denyicska, Tunde Rente, *Hyaluronic acid-based cross-linked nanoparticles*. 2011.

125. Yu-Hsien, K., et al., *Preparation of bio-polymeric nanoparticles by electrostatic field system.* Micro & Nano Letters, IET, 2012. **7**(10): p. 997-1000.
126. Bicudo, R.C.S. and M.H.A. Santana, *Production of hyaluronic acid (HA) nanoparticles by a continuous process inside microchannels: Effects of non-solvents, organic phase flow rate, and HA concentration.* Chemical Engineering Science, 2012. **84**(0): p. 134-141.
127. Park, J.H., et al., *Interconnected hyaluronic acid derivative-based nanoparticles for anticancer drug delivery.* Colloids Surf B Biointerfaces, 2014. **121**: p. 380-7.
128. Han, H.S., et al., *Bioreducible core-crosslinked hyaluronic acid micelle for targeted cancer therapy.* J Control Release, 2015. **200**: p. 158-66.
129. Han, H.S., et al., *Bioreducible shell-cross-linked hyaluronic acid nanoparticles for tumor-targeted drug delivery.* Biomacromolecules, 2015. **16**(2): p. 447-56.
130. Xu, J., et al., *Self-assembly behavior between native hyaluronan and styrylpyridinium in aqueous solution.* Carbohydrate Polymers, 2011. **86**(2): p. 678-683.
131. Pedrosa, S.S., et al., *A novel crosslinked hyaluronic acid nanogel for drug delivery.* Macromol Biosci, 2014. **14**(11): p. 1556-68.
132. Tao, Y.H., et al., *Core cross-linked hyaluronan-styrylpyridinium micelles as a novel carrier for paclitaxel.* Carbohydrate Polymers, 2012. **88**(1): p. 118-124.
133. Verheul, R.J., et al., *Covalently stabilized trimethyl chitosan-hyaluronic acid nanoparticles for nasal and intradermal vaccination.* J Control Release, 2011. **156**(1): p. 46-52.
134. Ming Kong, X.C., Hyunjin Park, *design and investigation of nano emulsified carrier based on amphiphile-modified hyaluronic acid.* Carbohydrate Polymers, 2011. **83**: p. 462-469.
135. Liu, Y., et al., *Dual targeting folate-conjugated hyaluronic acid polymeric micelles for paclitaxel delivery.* Int J Pharm, 2011. **421**(1): p. 160-9.
136. Deng, L., et al., *Enzymatically triggered multifunctional delivery system based on hyaluronic acid micelles.* Rsc Advances, 2012. **2**(33): p. 12909-12914.
137. Wei, X., et al., *Hyaluronic acid-based nanogel-drug conjugates with enhanced anticancer activity designed for the targeting of CD44-positive and drug-resistant tumors.* Bioconjug Chem, 2013. **24**(4): p. 658-68.
138. Li, F., et al., *Hyaluronic acid-conjugated graphene oxide/photosensitizer nanohybrids for cancer targeted photodynamic therapy.* Journal of Materials Chemistry B, 2013. **1**(12): p. 1678-1686.

139. Ganesh, S., et al., *Hyaluronic acid based self-assembling nanosystems for CD44 target mediated siRNA delivery to solid tumors.* Biomaterials, 2013. **34**(13): p. 3489-502.
140. Han, M., et al., *Overcoming drug resistance of MCF-7/ADR cells by altering intracellular distribution of doxorubicin via MVP knockdown with a novel siRNA polyamidoamine-hyaluronic acid complex.* Journal of Controlled Release, 2012. **163**(2): p. 136-144.
141. Dufay Wojcicki, A., et al., *Hyaluronic acid-bearing lipoplexes: physico-chemical characterization and in vitro targeting of the CD44 receptor.* J Control Release, 2012. **162**(3): p. 545-52.
142. Saravanakumar, G., et al., *Hydrotropic hyaluronic acid conjugates: Synthesis, characterization, and implications as a carrier of paclitaxel.* Int J Pharm, 2010. **394**(1-2): p. 154-61.
143. Eenschooten, C., et al., *Novel self-associative and multiphasic nanostructured soft carriers based on amphiphilic hyaluronic acid derivatives.* Carbohydrate Polymers, 2012. **87**(1): p. 444-451.
144. Eenschooten, C., et al., *Preparation and structural characterisation of novel and versatile amphiphilic octenyl succinic anhydride–modified hyaluronic acid derivatives.* Carbohydrate Polymers, 2010. **79**(3): p. 597-605.
145. Wu, J.L., et al., *Preparation and characterization of nanoparticles based on histidine-hyaluronic acid conjugates as doxorubicin carriers.* J Mater Sci Mater Med, 2012. **23**(8): p. 1921-9.
146. Fan, Y., et al., *Cationic liposome-hyaluronic acid hybrid nanoparticles for intranasal vaccination with subunit antigens.* J Control Release, 2015. **208**: p. 121-9.
147. Duceppe, N. and M. Tabrizian, *Factors influencing the transfection efficiency of ultra low molecular weight chitosan/hyaluronic acid nanoparticles.* Biomaterials, 2009. **30**(13): p. 2625-31.
148. Kim, E., et al., *Hyaluronic acid receptor-targetable imidazolized nanovectors for induction of gastric cancer cell death by RNA interference.* Biomaterials, 2013. **34**(17): p. 4327-38.
149. Glucksam-Galnoy, Y., T. Zor, and R. Margalit, *Hyaluronan-modified and regular multilamellar liposomes provide sub-cellular targeting to macrophages, without eliciting a pro-inflammatory response.* J Control Release, 2012. **160**(2): p. 388-93.
150. Gan, L., et al., *Hyaluronan-modified core-shell liponanoparticles targeting CD44-positive retinal pigment epithelium cells via intravitreal injection.* Biomaterials, 2013. **34**(24): p. 5978-87.
151. Zhou, Y. and Q. Xie, *Hyaluronic acid-coated magnetic nanoparticles-based selective collection and detection of leukemia cells with quartz crystal microbalance.* Sensors and Actuators B: Chemical, 2016. **223**: p. 9-14.
152. Landesman-Milo, D., et al., *Hyaluronan grafted lipid-based nanoparticles as RNAi carriers for cancer cells.* Cancer Letters, 2013. **334**(2): p. 221-227.

153. Rivkin, I., et al., *Paclitaxel-clusters coated with hyaluronan as selective tumor-targeted nanovectors.* Biomaterials, 2010. **31**(27): p. 7106-14.
154. El-Dakdouki, M.H., et al., *A simple method for the synthesis of hyaluronic acid coated magnetic nanoparticles for highly efficient cell labelling and in vivo imaging.* Rsc Advances, 2011. **1**(8): p. 1449-1452.
155. El-Dakdouki, M.H., et al., *CD44 Targeting Magnetic Glyconanoparticles for Atherosclerotic Plaque Imaging.* Pharm Res, 2013.
156. Kamat, M., et al., *Hyaluronic acid immobilized magnetic nanoparticles for active targeting and imaging of macrophages.* Bioconjug Chem, 2010. **21**(11): p. 2128-35.
157. Pasqui, D., et al., *Chemical and biological properties of polysaccharide-coated titania nanoparticles: the key role of proteins.* Biomacromolecules, 2011. **12**(4): p. 1243-9.
158. El-Dakdouki, M.H., E. Pure, and X. Huang, *Development of drug loaded nanoparticles for tumor targeting. Part 1: Synthesis, characterization, and biological evaluation in 2D cell cultures.* Nanoscale, 2013. **5**(9): p. 3895-903.
159. El-Dakdouki, M.H., E. Pure, and X. Huang, *Development of drug loaded nanoparticles for tumor targeting. Part 2: Enhancement of tumor penetration through receptor mediated transcytosis in 3D tumor models.* Nanoscale, 2013. **5**(9): p. 3904-11.
160. Yu, M., et al., *Hyaluronic acid modified mesoporous silica nanoparticles for targeted drug delivery to CD44-overexpressing cancer cells.* Nanoscale, 2013. **5**(1): p. 178-83.
161. Gary-Bobo, M., et al., *Hyaluronic acid-functionalized mesoporous silica nanoparticles for efficient photodynamic therapy of cancer cells.* Photodiagnosis and Photodynamic Therapy, 2012. **9**(3): p. 256-260.
162. Zhao, Q., et al., *Dual-stimuli responsive hyaluronic acid-conjugated mesoporous silica for targeted delivery to CD44-overexpressing cancer cells.* Acta Biomater, 2015. **23**: p. 147-56.
163. Ito, T., et al., *DNA/polyethyleneimine/hyaluronic acid small complex particles and tumor suppression in mice.* Biomaterials, 2010. **31**(10): p. 2912-8.
164. He, Y., et al., *Polyethyleneimine/DNA polyplexes with reduction-sensitive hyaluronic acid derivatives shielding for targeted gene delivery.* Biomaterials, 2013. **34**(4): p. 1235-45.
165. Tian, H., et al., *RGD targeting hyaluronic acid coating system for PEI-PBLG polycation gene carriers.* J Control Release, 2011. **155**(1): p. 47-53.
166. Jiang, T.Y., et al., *Dual-functional liposomes based on pH-responsive cell-penetrating peptide and hyaluronic acid for tumor-*

targeted anticancer drug delivery. Biomaterials, 2012. **33**(36): p. 9246-9258.
167. Lee, T., et al., *Efficient CD44-targeted magnetic resonance imaging (MRI) of breast cancer cells using hyaluronic acid (HA)-modified MnFe2O4 nanocrystals.* Nanoscale Research Letters, 2013. **8**: p. 1-9.
168. Oyarzun-Ampuero, F.A., et al., *Hyaluronan nanocapsules as a new vehicle for intracellular drug delivery.* European Journal of Pharmaceutical Sciences, 2013(0).
169. Yang, X.-y., et al., *Hyaluronic acid-coated nanostructured lipid carriers for targeting paclitaxel to cancer.* Cancer Letters, 2013. **334**(2): p. 338-345.
170. Toriyabe, N., et al., *Synthesis and evaluation of stearylated hyaluronic acid for the active delivery of liposomes to liver endothelial cells.* Biol Pharm Bull, 2011. **34**(7): p. 1084-9.
171. Tran, T.H., et al., *Development of vorinostat-loaded solid lipid nanoparticles to enhance pharmacokinetics and efficacy against multidrug-resistant cancer cells.* Pharm Res, 2014. **31**(8): p. 1978-88.
172. Tran, T.H., et al., *Hyaluronic acid-coated solid lipid nanoparticles for targeted delivery of vorinostat to CD44 overexpressing cancer cells.* Carbohydr Polym, 2014. **114**: p. 407-15.
173. Sun, H., et al., *Hyaluronic acid immobilized polyacrylamide nanoparticle sensors for CD44 receptor targeting and pH measurement in cells.* Bioconjug Chem, 2012. **23**(11): p. 2247-55.
174. Almalik, A., et al., *Hyaluronic acid (HA) presentation as a tool to modulate and control the receptor-mediated uptake of HA-coated nanoparticles.* Biomaterials, 2013. **34**(21): p. 5369-5380.
175. Zaki, N.M., A. Nasti, and N. Tirelli, *Nanocarriers for cytoplasmic delivery: cellular uptake and intracellular fate of chitosan and hyaluronic acid-coated chitosan nanoparticles in a phagocytic cell model.* Macromol Biosci, 2011. **11**(12): p. 1747-60.
176. Hien, N.Q., et al., *Radiation synthesis and characterization of hyaluronan capped gold nanoparticles.* Carbohydrate Polymers, 2012. **89**(2): p. 537-541.
177. Kumar, C.S., et al., *Hyaluronic acid co-functionalized gold nanoparticle complex for the targeted delivery of metformin in the treatment of liver cancer (HepG2 cells)*. Carbohydr Polym, 2015. **128**: p. 63-74.
178. Babic, M., et al., *The use of dopamine-hyaluronate associate-coated maghemite nanoparticles to label cells.* Int J Nanomedicine, 2012. **7**: p. 1461-74.
179. Dellacherie, E., et al., *Particles which are surface coated with hyaluronan or one of the derivatives thereof and the use of same as biological vectors for active substances*. 2013, Centre National De La Recherche Scientifique.

180. Roth, C.C., et al., *Bladder regeneration in a canine model using hyaluronic acid-poly(lactic-co-glycolic-acid) nanoparticle modified porcine small intestinal submucosa.* Bju International, 2011. **108**(1): p. 148-155.
181. Mondalek, F.G., et al., *Enhanced angiogenesis of modified porcine small intestinal submucosa with hyaluronic acid-poly(lactide-co-glycolide) nanoparticles: from fabrication to preclinical validation.* J Biomed Mater Res A, 2010. **94**(3): p. 712-9.
182. Zille, H., et al., *Evaluation of intra-articular delivery of hyaluronic acid functionalized biopolymeric nanoparticles in healthy rat knees.* Biomed Mater Eng, 2010. **20**(3): p. 235-42.
183. Martens, T.F., et al., *Coating nanocarriers with hyaluronic acid facilitates intravitreal drug delivery for retinal gene therapy.* J Control Release, 2015. **202**: p. 83-92.

CHAPTER II

A NOVEL CROSSLINKED HYALURONIC ACID NANOGEL FOR DRUG DELIVERY

Adapted from

Pedrosa, S. S., et al. (2014).

Macromolecular Biosciences 14(11): 1556-1568.

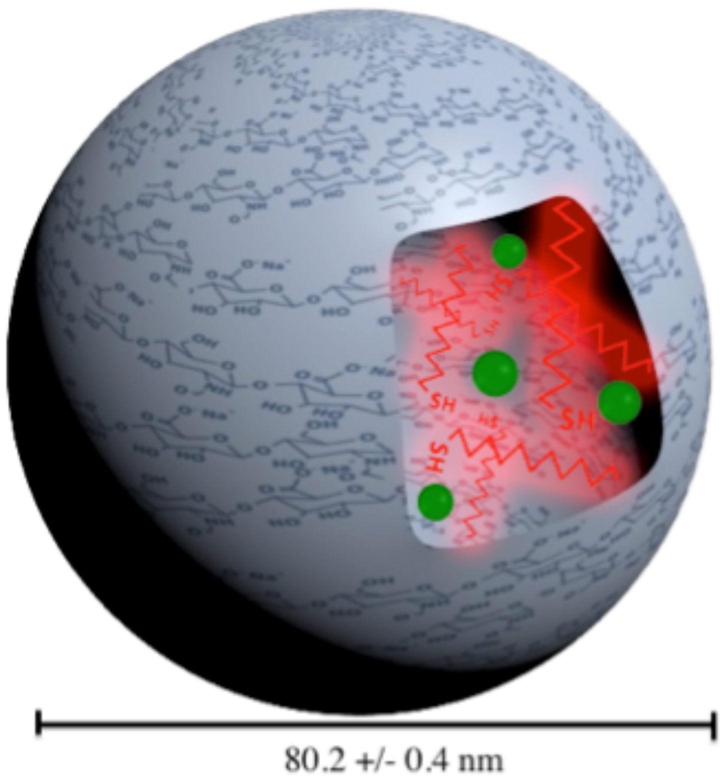

ABSTRACT

An amphiphilic hyaluronic acid conjugate is successfully developed based on grafting a thiolated hydrophobic molecule to the polysaccharide backbone. The engineered conjugate is capable of assembling into nanostructures once dispersed in water, with average diameter of 80.2 +/- 0.4 nm (n=5), stable up to 6 months. The thiolated HyA conjugate is reticulated by dissulfide bond with a homofunctional crosslinker - 1,4-Bis(3-[2-pyridyldithio]propionamido)butane (DPDPB). The drug loading efficiency of the reticulated and non-reticulated nanogel is accessed with two hydrophobic drugs, curcumin and simvastatin. Results suggest that crosslinked nanogel exhibit higher stability upon dilution and drug loading efficiency and proves to be a redox sensitive material. The nanogels hold great potential as stealth carriers of lipophilic drugs.

1. INTRODUCTION

Polymeric nanogels are a class of nanocarrier systems based on biodegradable polymers that can be applied in drug sustained release. These systems display prolonged blood circulation time, enhanced drug solubility and selective accumulation at tumour tissues by enhanced permeability and retention (EPR) effect [1, 2].

Hyaluronic acid (HyA) is a natural polysaccharide composed of disaccharide units of D-glucuronic acid and N-acetyl-D-glucosamine with β(1,4) and β(1,3) glucosidic bonds, ubiquitous on the human body [3, 4]. It is a highly hydrophilic polysaccharide with great potential as a drug carrier due to its physicochemical and biological properties, such as biocompatibility, biodegradability and non-immunogenicity [1]. Also, HyA allows several chemical modifications including ones that can originate amphiphilic materials capable of self-assembling into nanostructures. Moreover, hyaladherins – a group of high affinity HyA proteins – that include the receptor for hyaluronan-mediated motility (RHAMM) and the HyA receptor CD44, among others, are important mediators of cancer development and detection. HyA exhibits specific affinity for various cancer cells that overexpress HyA receptors and therefore have great potential for tumour targeting [1, 5, 6].

Various cross-linking approaches have been adopted to improve nanogel features. The cross-linking of nanocarriers could take place on the hydrophilic shell [7], within the hydrophobic core [8, 9], or at the core–shell interface [10]. Redox sensitive nanogel usually containing dissulfide bounds have been used to trigger burst release in response to redox environments. Disulfide bonds represent an interesting approach once though they are stable in the extracellular compartments, may be prone to rapid cleavage with intracellular reducing molecules. Tumour tissues unveil highly reducing ambiences compared with normal ones, with high concentrations of glutathione – a redox molecule [11].

In the present work we developed a new amphiphilic HyA conjugate by grafting a thiolated hydrophobic chain by amide bond formation, yielding hyaluronic acid - 11-Amino-1-undecanethiol hydrochloride (HyA-AT). We studied the self-assembly of the HyA-AT in aqueous environment by ^{1}H nuclear magnetic resonance (NMR) and fluorescence spectroscopy with Nile red, as fluorescent probe. The properties of the resulting nanogel were characterized as to – structure, size, shape, zeta potential, stability and the ability to entrap small hydrophobic molecules and by ^{1}H NMR, fluorescence, cryo-field emission scanning electron microscopy (cryo-FESEM), dynamic light scattering (DLS) and SAX analysis. Further, the engineered nanogel was crosslinked by dissulfide bond with a homofunctional crosslinker - 1,4-Bis(3-[2-pyridyldithio]propionamido)butane (DPDPB) and its – size, structure, stability and ability to entrap hydrophobic drugs was also studied.

2. MATERIALS

All reagents were of analytical grade. Sodium hyaluronate (MW= 7.46 KDa) was purchased from Lifecore Biomedical (USA). AG 50W – X8 resin was purchased from Bio-Rad (USA). Absolute ethanol was purchased from Apllichem (Germany). Dimethyl sulfoxide (DMSO), Tetrabutylammonium fluoride hydrate (TBA-F), 11-Amino-1-undecanethiol hydrochloride (AT), N-hydroxysulfosuccinimide (NHS), 1-ethyl-3-[3-dimethylaminopropyl]carbodiimide hydrochloride (EDC), 1,4-Bis(3-[2-pyridyldithio]propionamido)butane (DPDPB) were purchased from Sigma Aldrich (Italy). The water used for nanogel synthesis and characterization was distillated and ultrapurified (Milli-Q).

3. METHODS

3.1. SYNTHESIS OF AMPHIPHILIC HYALURONIC ACID CONJUGATE

Sodium hyaluronate was chemically grafted with a long thiolated alkyl chain by amide bond formation to produce an amphiphilic conjugate, as presented in 1 [2, 12-14].

To render sodium hyaluronate soluble in DMSO, the sodium ions of HyA were exchanged with the lipophilic tetrabutylammonium (TBA) ion as described by Oudshoorn [15]. Ion exchange was performed using AG 50W-X8 cation exchange resin. AG 50W (1g) resin was incubated with an excess of TBA-F (3.5g) in ultrapure water for 1h at room temperature and mild agitation. The resin was elutriated, washed and transferred into a 1% (w/v) HyA solution in ultrapure water. The exchange of the TBA ions on the resin and the sodium ions of HyA was performed at room temperature with agitation, for 2h. The removal of the resin was achieved by centrifugation for 2 min at 5000 rpm (SIGMA® 113 centrifuge). The resulting HyA-TBA solution was lyophilized and the fluffy white material was stored at room temperature. ^{1}H NMR spectroscopy was performed to confirm the Na^{+} ions exchange with TBA-F.

Hydrophobic11-Amino-1-undecanethiol hydrochloride (AT) was chemically conjugated to the backbone of modified HyA-TBA in the presence of EDC and NHS. HyA-TBA (260mg) was dissolved in anhydrous DMSO at 1% (w/v) and EDC (100mg) and NHS (50mg) were added. Finally, AT (15 mg), also dissolved in anhydrous DMSO was added to the reaction mixture, which was stirred for 24h at room temperature. The resulting solution was dialyzed (MWCO=1000Da) first against a NaCl 150 mM solution for 3 days - to exchange again the TBA ions for sodium ions - and then distilled water for 2 days. Finally, the solution was freeze-dried and a white cottony material was obtained, corresponding to the HyA-

AT conjugate. The degree of substitution of AT molecules in the HyA chain was determined by ^{1}H NMR spectroscopy.

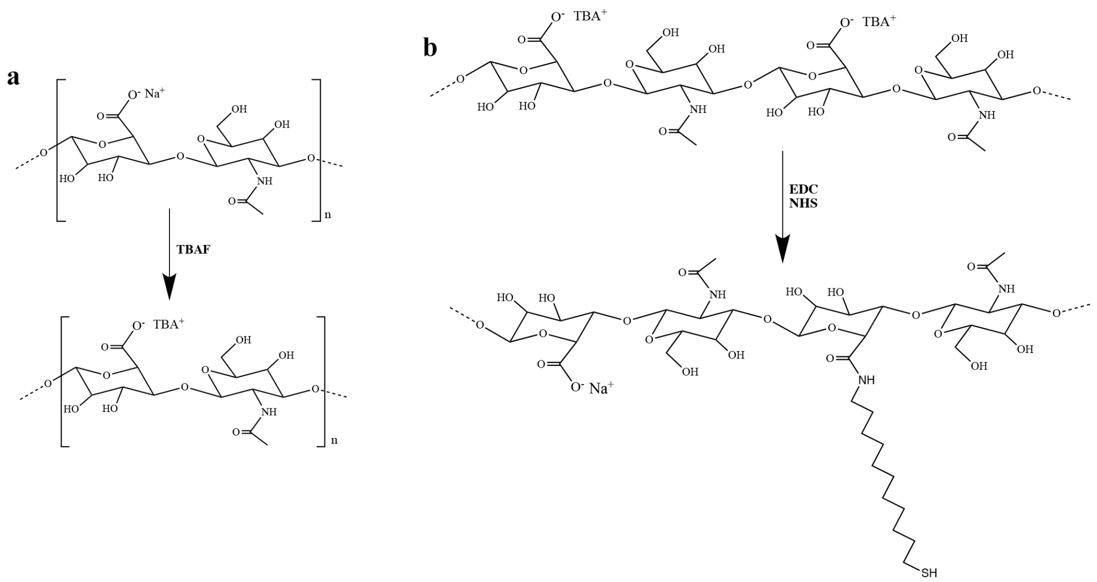

Scheme 1: Representative illustrations of HyA-AT conjugate synthesis, a) ion exchange of sodium hyaluronate and b) amide bond formation reaction.

The ^{1}H NMR spectra were obtained using a Varian Unity Plus 300 spectrometer operating at 299.94MHz and 25°C. The samples were prepared at 10.0 mg/ml in D_2O.

3.2. NANOGEL ASSEMBLY CHARACTERIZATION

3.2.1. PREPARATION OF NANOGEL DISPERSION

The samples were dispersed in distilled water at 1.0 mg/ml and filtered through a membrane of 0.22 μm pore size and stored at 4°C for up to six months.

3.2.2. Dynamic light scattering (DLS) characterization

The obtained nanogel was characterized as to its size distribution (diameter) and zeta potential by DLS analysis (Zetasizer Nano ZS, Malvern Instruments) at 25ºC. Nanogel dispersion (1.0 mL) was analysed in a polystyrene cell or in a folded capillary cell, for size and volume distribution or zeta potential measurements, respectively, using a He-Ne gas laser (wavelength of 633 nm) and a detector angle of 173º. The results presented represent the mean values of polydispersity index (PdI), hydrodynamic diameter and zeta potential of the particles, obtained after five repeated measurements. The Zeta potential values were calculated using Henry's equation.

3.2.3. Cryo-Field-Emission Scanning Electron Microscopy (Cryo-FESEM)

HyA-AT nanogel, 1.0 mg/ml concentration was dispersed at in distilled water and frozen in liquid nitrogen at -200ºC. The sample was transferred to the cryo stage (Gatan, Alto 2500, UK) of an electron microscope (SEM/EDS: FESEM JEOL JSM6301F/Oxford Inca Energy 350). Sample was then fractured and sublimated for 10 minutes at -95ºC to remove the superficial ice layer and allow the nanogel to be exposed. Finally, the sample was sputter-coated with gold and palladium at -140ºC using an accelerating voltage of 10kV. The observation was performed at -140ºC and 15kV.

3.2.4. Fluorescence spectroscopy

The critical aggregation concentration (cac) of HyA-AT nanogel was determined fluorometrically resorting to a hydrophobic probe - Nile Red

(NR). Nile red is a hydrophobic fluorescent probe whose fluorescence intensity shifts according to the polarity of the environment. The lyophilized nanogel was dispersed in water in a range of concentrations between 50 ng/ml and 1.0 mg/ml (final volume of 1ml), by consecutive dilutions. A stock solution of 4.0 x 10^{-5} M solution of NR in ethanol was prepared, and 5 µL of this solution was added to each sample, resulting in a final concentration of NR of 2.0 x 10^{-7}M and an ethanol content of 0.5%. The samples were agitated overnight at room temperature for homogenisation. Samples fluorescence spectrum were analysed in a Spex Fluorolog 3 spectrofluorimeter at room temperature. The cac was determined by the maximum emission shift of NR and the change of the fluorescence intensity as a function of HyA-AT nanogel concentration.

3.2.5. SAXS EXPERIMENT

SAXS experiment was carried at the European Synchrotron Radiation Facility (Grenoble, France) on the BM2-D2AM beamline. Nanogel samples were set in silica tubes (external diameter 3 mm, wall thickness 0.2 mm, 76 mm long, from Deutero GmbH) with elastomer closure caps to avoid water evaporation (Deutero GmbH). The incidence photon energy was 16.000 keV and a 2D CCD X-ray detector (Ropper Scientific) was used. The images were corrected for camera distortion, dark image reading and flat field response of the detector. Finally, the image center ("gravity center" of the incident beam) was determined with attenuators and radial averages yielded 1D profiles (processing carried on the beamline, with bm2img software). Silver behenate powder was used as standard for calibration. The scattering contribution was eliminated by subtracting the attenuation coefficient of water filled glass tube. HyA-AT nanogel was prepared as described earlier at 10.0 mg/ml and 30.0 mg/ml concentration.

3.3. DPDPB MEDIATED CROSSLINKING

3.3.1. CROSSLINKED NANOGEL SYNTHESIS

1,4-Bis(3-[2-pyridyldithio]propionamido)butane (DPDPB), is a homobifunctional crosslinking agent that contains dithiopyridyl groups on both ends of the molecule that react with free sulfhydryl groups.

Lyophilized HyA-AT was dispersed in water at a concentration of 1.0 mg/ml as described earlier. As reported by Wittrup, 2012 [16], a 10 mg/ml stock solution of DPDPB in DMSO was prepared and added to the nanogel dispersion at a molar ratio of 2:1 free sulfhydryl groups of HyA-AT conjugate. The amount of DMSO in the reaction was inferior to 1% (v/v). Air was injected through a syringe in the reaction mixture for 15 minutes. Then, the suspension was gently stirred overnight at 30°C.

The reaction was then dialyzed against water in an MWCO= 1KDa membrane bag. The resulting solution was freeze-dried and lyophilized.

The crosslinked HyA-AT-DPDPB nanogel was analysed by ^{1}H NMR spectroscopy using a Varian Unity Plus 300 spectrometer operating at 299.94MHz and 25°C.

3.3.2. CROSSLINKED NANOGEL CHARACTERIZATION

3.3.2.1. UV-VIS SPECTROSCOPY

The successful disulfide linkage between DPDPB and free sulfhydryl groups of HyA-AT nanogel causes a shift of the DPDPB absorbance peaks of 237 nm ($\varepsilon = 1.2 \times 10^{4}\ M^{-1}cm^{-1}$) to 272 nm and the peak at 287 nm ($\varepsilon = 8.8 \times 10^{3}\ M^{-1}cm^{-1}$) is shifted to 343 nm (ε = 8.08 ± 0.3 x 103 M-1cm-1) [17]. Therefore, UV–Vis absorption spectra of a 200 μL sample of the HyA-AT-DPDPB reaction mixture was recorded on a JASCO V560 equipment. A control with unreacted DPDPB molecule dispersed in DMSO at a concentration of 0.2 mg/ml was also analysed. The dialyzed suspension was again analysed by UV-Vis spectroscopy to ascertain the elimination of the two pyridine-2-thione a product of the DPDPB conjugation with AT and responsible for the 343 nm peak.

3.3.2.2. Cryo-Field-Emission Scanning Electron Microscopy (Cryo-FESEM)

HyA-AT-DPDPB nanogel was dispersed at a concentration of 1.0 mg/ml in distilled water and frozen in liquid nitrogen at -200ºC. The sample were analysed in an electron microscope (SEM/EDS: FESEM JEOL JSM6301F/Oxford Inca Energy 350) as described earlier.

3.3.2.3. Dynamic light scattering (DLS) characterization

The lyophilized crosslinked nanogel (HyA-AT-DPDPB) were dispersed in distilled water at 1.0 mg/ml and filtered through a 0.22 μm membrane pore and diluted sequentially to a concentration of 1.0 μg/ml. The solutions were then characterized as to its hydrodynamic size diameter by DLS analysis (Zetasizer Nano ZS, Malvern Instruments) at 25º. The values presented represent the mean values of polydispersity index (PdI) and size diameter of particles after five repeated measurements.

3.3.3. Redox sensitive crosslinked nanogel characterization

To assess the susceptibility of crosslinked nanogel to reducing environment that disrupt dissulfide bonds, more diluted sample of HyA-AT-DPDPB nanogel – 1.0 μg/ml - was further treated with dithiothreitol

(DTT), a potent reducing agent. DTT was used to reduce the dissulfide bonds between DPDPB molecules and AT residues of the HyA-AT-DPDPB nanogel. To the HyA-AT-DPDPB solution with 1.0 μg/ml in distilled water, a DTT stock solution in DMSO was added, to a final concentration of 1.0 mM. The final solution was stirred and incubated for 30 minutes. The sample was characterized as to its hydrodynamic diameter by DLS analysis soon after preparation and two weeks after, to assess its stability under redox conditions. The values presented represent the mean values of polydispersity index (PdI) and diameter of particles after five repeated measurements.

3.4. Drug loading efficiency

Curcumin (CM) is a hydrophobic drug insoluble in aqueous solvents but soluble in organic ones. Simvastatin (SV) is also a hydrophobic drug poorly soluble in water (less than 1.0 mg/L) and soluble in organic solvents (PubChem Substance and Compound database, substance identifier number SID:54454) [18]. Curcumin was solubilized in ethanol at a concentration of 1.0 mg/ml as a stock solution. A volume of 10 μL of the curcumin stock solution was incubated with 1.0 mg/ml nanogel dispersions of HyA-AT and HyA-AT-DPDPB, prepared as described earlier. The final curcumin concentration attained in the samples was 30 mM and the ethanol content was 1% (v/v). In a similar way, a 5.0 mg/ml stock solution of ethanol solubilized SV was prepared and 6.0 μL were added to analogous nanogel samples. The final SV concentration in the samples was 71.7 μM and the ethanol content was less than 1% (v/v). Also, a negative control and a positive control of drug loading were performed in the same volume and with the same final concentration, in water and ethanol, respectively. The samples were incubated overnight at room temperature in a turning wheel. Finally, all the samples were centrifuged at 13,000 rpm (SIGMA 113 centrifuge) for 10 minutes to remove the insoluble drugs. The samples supernatant were analysed in a JASCO V560 system and the UV-Vis absorption spectra was recorded. Soluble CM has a yellow tone colour and a maximum absorbance at 428 nm. Soluble SV is a colourless solution with maximum absorbance at 238 and 247 nm.

4. Results

4.1. Synthesis of amphiphilic hyaluronic acid conjugate

Amphiphilic hyaluronic acid conjugate was synthetized as shown in Scheme 1a. Sodium hyaluronate was first converted to its tetrabutylammonium salt to enhance the solubility in polar aprotic organic solvents. The exchange with the lipophilic cation was confirmed by ^{1}H NMR in D_2O by the peaks at δ=0.97 (m, 12H, N^+–[$(CH_2)_3$–$\mathbf{CH_3}$]$_4$); δ=1.40 (m, 8H, N^+–[(CH_2–CH_2–$\mathbf{CH_2}$–CH_3]$_4$); δ=1.64 (m, 8H, N^+–[(CH_2–$\mathbf{CH_2}$–CH_2–CH_3]$_4$) and δ=3.82 (m, 8H, N^+–[($\mathbf{CH_2}$–CH_2–CH_2–CH_3]$_4$) [19]. The degree of substitution (DS) of the sodium ion by the tetrabutylammonium ion, defined, as the number of TBA molecules per 100 residues of HyA, was calculated based on the ^{1}H NMR in D_2O of HyA-TBA. The DS obtained for different batches was reproducible and approximately 100%.

Further conjugation of hyaluronate TBA salt with 11-Amino-1-undecanethiol (AT) by amide bond formation was performed as shown in Scheme 1b. The amino group of AT reacted with the carboxylic groups of hyaluronic acid in the presence of 1-ethyl-3(3-dimethylaminopropyl)carbodiimide (EDC) and N-hydroxysuccinimide (NHS) through carbodiimide chemistry. The grafting of the hydrophobic chain and the respective DS, defined as the number of AT molecules per 100 disaccharide units of HyA, were confirmed by ^{1}H NMR spectroscopy, as shown in figure 1. The assignments and chemical shifts of the ^1H signals in D_2O used in the determination of the DS are indicated in figure 1. The peaks correspondent to hyaluronic acid used to the calculus are assigned to 11 protons – and are identified in figure 1, with the number 2 - which are: δ=4.51 (G1), δ=4.61 (N1), δ=3.92 (N2), δ=3.63 (G3), δ= 3.74–3.85 (N3, N6, G4, G5) and δ=3.51–3.62 (N4, N5) [20]. The peaks assigned to AT protons used in the determination of the DS are δ=1.2-1.4 ($14H^+$, N^+–$(CH_2)_2$–**$(CH_2)_7$**–$(CH_2)_2$–SH). The AT DS was calculated according to the following equation:

$$DS_{AT} = \frac{11\times(\delta 1.2 \ \rightarrow 1.4)}{14\times(\delta 3.51 \rightarrow 4.61)}\times 100$$

The DS was about 11%, meaning that 1 out of every 11 disaccharide units are chemically modified with AT. The yield of the reaction was about 67% and was reproducible in all batches.

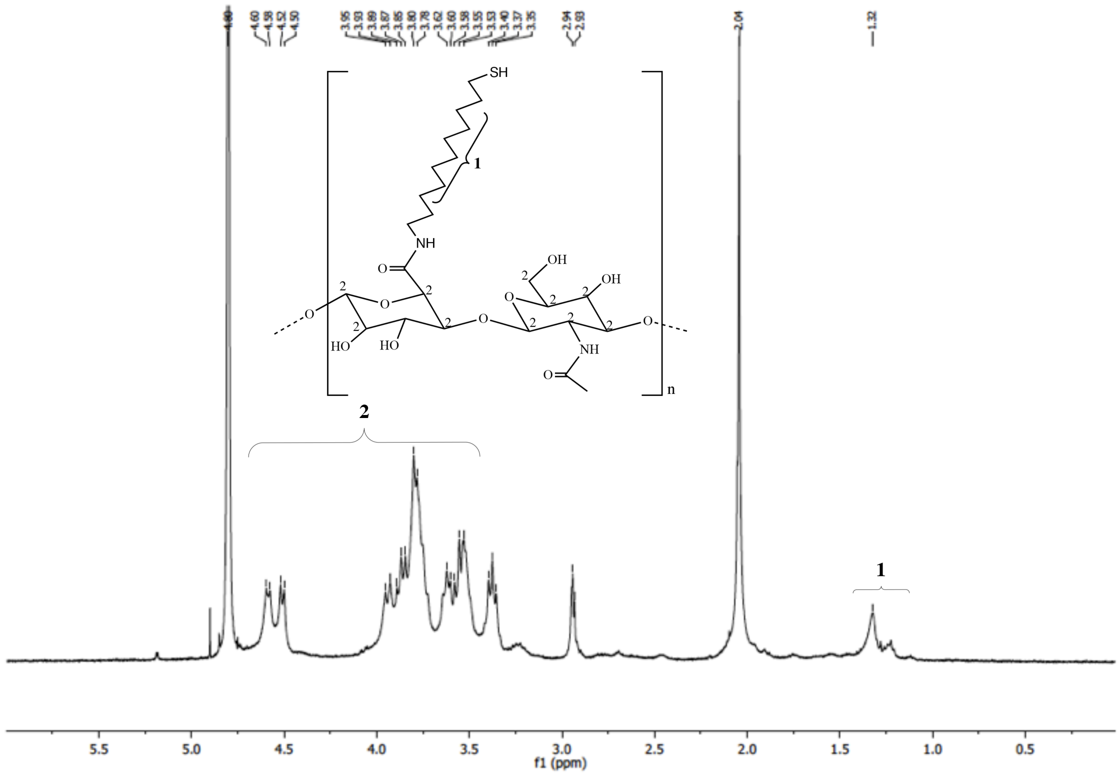

Figure 1: ^1H NMR spectrum of HyA-AT nanogel in D_2O at 25°C and a schematic representation of the HyA-AT conjugate.

4.2. Nanogel characterization

4.2.1. Dynamic light scattering (DLS) characterization

The grafting of AT molecules to hydrophilic backbone of HyA results in an amphiphilic molecule capable of self-assembling into nanostructures in aqueous environment. HyA-AT nanogel was fully characterized by DLS analysis regarding its size distribution by intensity (figure 2a) or volume (figure 2b) and zeta potential (figure 2c). Size distribution is an intensity profile in which the light scattered by the particles is conditioned by its size. The first order result from a DLS experiment is the intensity distribution of particle sizes. The intensity distribution is weighted according to the scattering intensity of each particle fraction. As such, the intensity distribution can be somewhat misleading, in that a small amount of aggregates or larger particles can dominate the distribution.

The intensity distribution (quite sensitive to the presence of larger particles) can be converted, using Mie theory, to a volume distribution. The conversion to volume distribution highlights smaller populations of nanoparticles, leading to, in our opinion, more realistic size distribution.

When dispersed in water at 1.0 mg/ml concentration, the nanogel reveals a bimodal size distribution with a smaller population around 20 nm and another with about 150 nm, corresponding to a mean size diameter of 80.2 +/- 0.4 nm (n=5). The self-assembly of the engineered nanogel was tested in the presence of a reducing agent – DTT - and the resulting mean size diameter was 91.85 +/- 0.410 nm. This proves, that in this case the thiol groups of the hydrophobic chains present in the HyA-AT nanogel do not seem to react with one another, in a spontaneous manner.

Nanocarriers smaller than 200 nm can avoid uptake by the mononuclear phagocyte system, the longer circulation time allowing specific interaction with the target tissues [21]. Analysing the volume distribution profile (figure 2b) the smallest population at 20 nm represents approximately 95% being the main population.

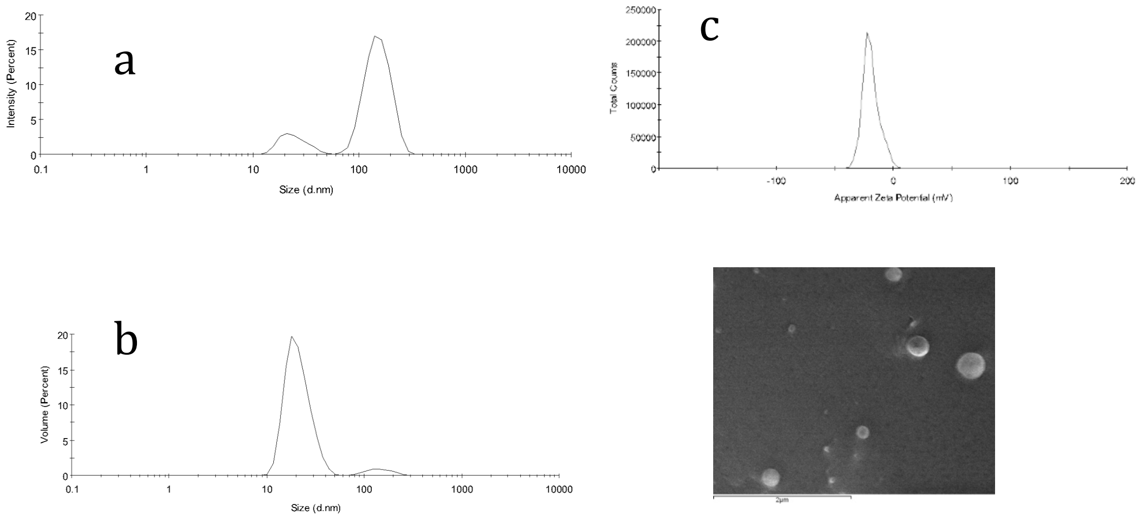

Figure 2: a) Size distribution by intensity and b) by volume and, c) zeta potencial of the HyA-AT nanogel. d) Cryo-FESEM image of HyA-AT nanogel (scale bar = 2µ m).

The polydispersity index of the nanogel size distribution was about 0.4. The zeta potential obtained for HyA-AT nanogel was -19.3 +/- 1.97 mV (n=5) in average. Negatively charged particles have demonstrated enhanced circulation time within the body also due to non-specific binding to serum proteins and allowed high storage stability owing to electrostatic repulsion between the particles [4, 6]. Also, the negative charge of the particles confirms the presence of HyA at the surface of the nanogel as it was expected and is due to the ionized carboxylate groups.

The morphology of the HyA-AT nanogel was examined by Cryofield emission scanning electron microscope (Cryo-FESEM) and is shown in figure 2d. The nanogel particles were well dispersed with spherical shape. Size and volume distribution profiles from DLS analysis were confirmed in the Cryo-FESEM images, where particles with size corresponding to the two populations identified by DLS are indeed visible.

4.2.2. Stability of HyA-AT nanogel

The stability of HyA-AT nanogel was evaluated at different pH and at 25ºC and also following incubation for 7 days at 4ºC. In pH4 phosphate-citrate buffer, the mean size was 112.4 +/- 10.21m (121.8+/-9.2nm after 7 days at 4ºC) and in pH7.4 phosphate buffer saline, the mean size was 90.1 +/- 0.419nm (88.9 +/- 0.4nm after 7 days at 4ºC). The nanogel dispersed in distilled water at 1.0 mg/ml was stored up to 6 months at 4ºC and demonstrated high stability in terms of size distribution as may be seen in figure 3.

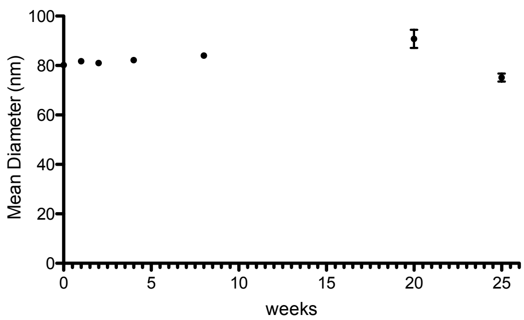

Figure 3: Colloidal stability of HyA-AT nanogel evaluated by average particle size (diameter-nm) of the nanogel as a function of time.

4.2.3. Determination of critical aggregation concentration of the nanogel

Critical aggregation concentration (cac) of the HyA-AT conjugates was determined by fluorescence spectroscopy using Nile Red (NR) as a fluorescent probe. Nile red is a hydrophobic molecule, whose maximum fluorescent emission wavelength is dependent of the polarity of the surrounding environment. When transferred from non-polar to hydrophobic environments, NR emission spectrum is shifted to higher wavelengths and this feature turns it suitable to assess the cac of amphiphilic polymers [22, 23].

For the determination of the cac of HyA-AT conjugate, NR was added to a series of conjugate dispersions with concentration comprised between 10.0 μg/L – 1.0 g/L. The fluorescence emission spectra of NR at different concentrations of HyA-AT nanogel are represented in figure 4 and the plotted maximum fluorescence emission (solid line) and fluorescence intensity (doted line) in figure 5. From these results we may conclude that at concentrations below cac, amphiphilic HyA-AT molecules do not bear any specific organization (premicellar concentration, zone A, figure 4). Near cac, the maximum fluorescence emission wavelength of NR decreased abruptly from about 660 nm to 610 nm (zone B, figure 4 and figure 5) and the fluorescence increases (figure 5, doted line). These changes indicate that the immediate environment of the fluorescent probe changed from polar to less polar due to the interactions between NR and the AT pendant groups of HyA-AT, organized through self-assembling at the higher concentrations, forming hydrophobic nanodomains. Hence, the concentration at which the amphiphilic HyA-AT conjugate self-assembles onto nanostructures with hydrophobic nanodomains is establish between 0.8 mg/L and 1.0 mg/L. The cac reported for similar amphiphilic materials was 0.042 mg/ml for HyA-ceramide conjugate [21], 67.5 mg/L for HyA- g-all-trans retinoid acid [24] and 37.3 to 10.0 μg/mL for HyA-C18 conjugate[13]. These low cac values indicate that HyA-AT nanogel might have good dilution stability in the bloodstreams after intravenous injection [25].

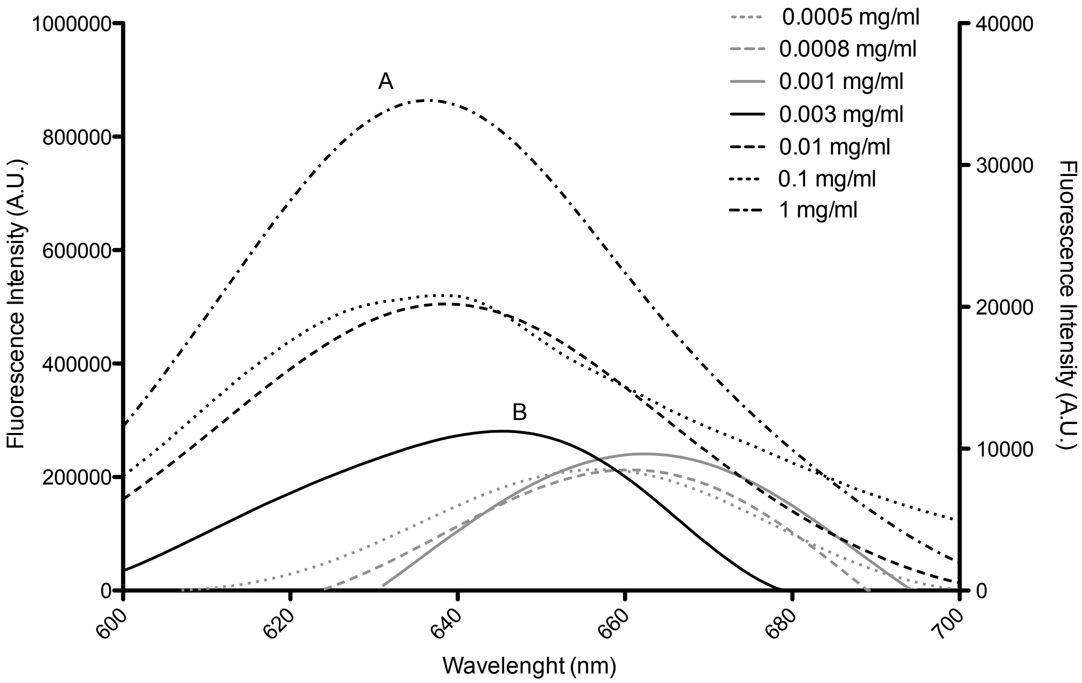

<u>Figure 4:</u> Emission spectra of Nile Red in a concentration of 2.0x 10^{-7} M as a function of HyA-AT nanogel concentration.

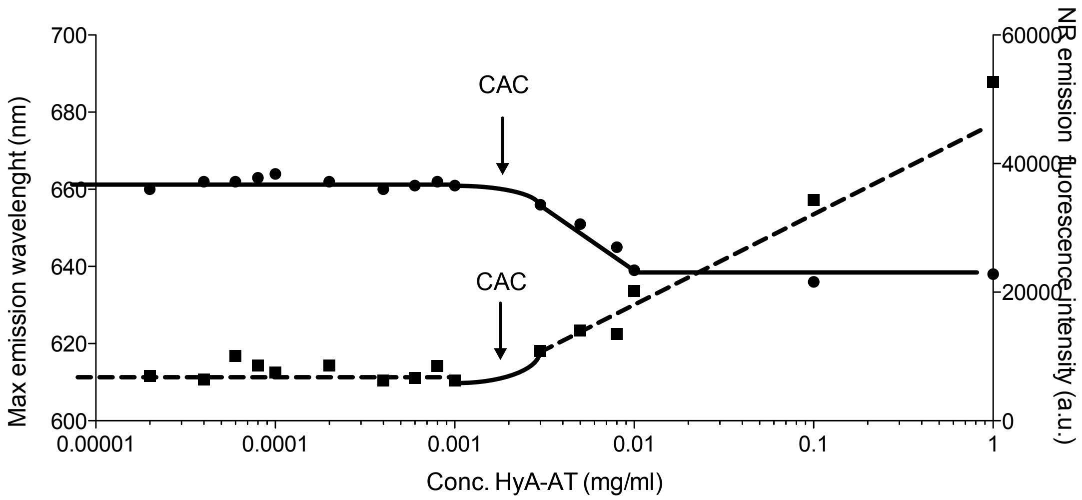

<u>Figure 5:</u> Plot data representation of the fluorescence intensity (•) and maximum emission wavelength ( ) of Nile Red as a function of HyA-AT concentration.

4.2.4. SAXS EXPERIMENTS

The morphology and inner structure of the HyA-AT nanogel was studied by Small Angle
X-ray Scattering (SAXS). The scattering patterns shown in figure 6 demonstrate the existence of hydrophobic nanodomains. These scattering nanodomains present a gyration radius between 4.6 and 4.8 nm and irregular shape, which is an expected feature since they are formed by AT chains. For the nanogel population with lower size (20 nm), it may be speculated that each particle presents at least one hydrophobic nanodomain, surrounded by a hydrophilic corona. However, as observed in a work on a similar material [26], each nanogel particle may contain several hydrophobic nanodomains, as it is quite likely the case for the larger particles.

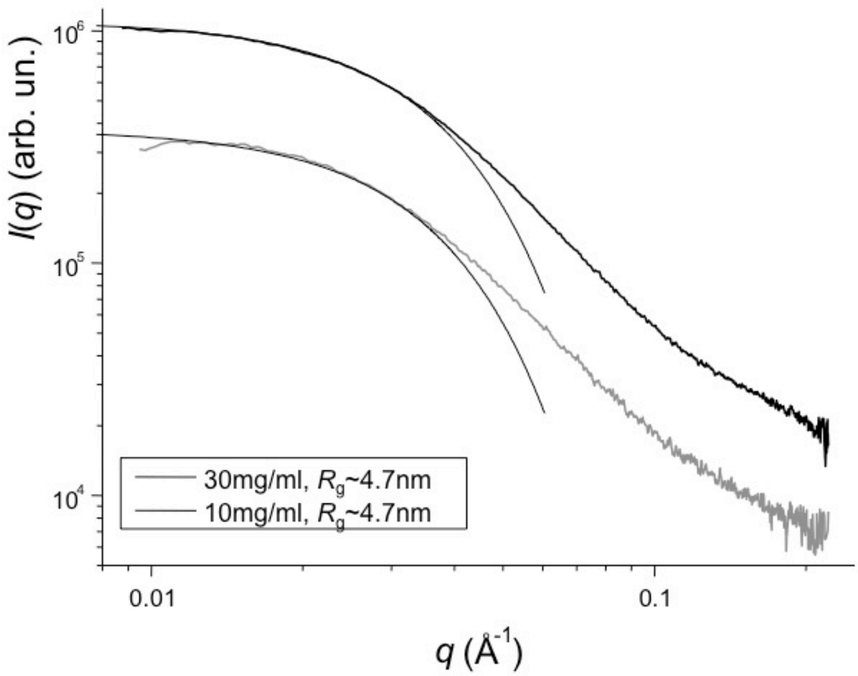

Figure 6: SAXS analysis of HyA-AT nanogel (water dispersion) at 30.0 mg/ml and 10.0mg/ml concentrations.

4.3. DPDPB MEDIATED CROSSLINKING

4.3.1. CROSSLINKED NANOGEL SYNTHESIS

We developed an original way of reticulating the hydrophobic polymer chains of HyA-AT nanogel, by redox-sensitive bonds, as represented in figure 7. The reticulation of the chains of amphiphilic hyaluronic acid conjugates was fulfilled using a homobifunctional sulfhydryl-reactive crosslinker - 1,4-Bis(3-[2-pyridyldithio]propionamido)butane (DPDPB). DPDPB reacts with the sulfhydryl groups of AT residues releasing the two pyridine-2-thione of the terminus of the molecule. Conjugation with DPDPB results in a 14-atom spacer of approximately 16 Å in length (figure 7).

A ^{1}H NMR spectrum of the crosslinked and non crosslinked HyA-AT nanogel was performed to confirm the successful conjugation of DPDPB, which was indeed confirmed by the presence of the peaks at 1.36-1.38 ppm, 1.55 ppm and 1.85 ppm assigned to the methyl groups of DPDPB (figure 8).

4.3.2. CROSSLINKED NANOGEL CHARACTERIZATION

4.3.2.1. UV-VIS SPECTROSCOPY

The release of the two pyridine-2-thione during the conjugation reaction causes the shift of the DPDPB absorbance peaks of 237 nm (ε = 1.2 x 104 M-1cm-1) that is shifted to 272 nm and the peak at 287 nm (ε = 8.8 x 103 M-1cm-1) that is shifted to 343 nm (ε = 8.08 ± 0.3 x 103 M-1cm-1) (Hermanson, 2010). Therefore, the coupling of DPDPB was confirmed by monitoring the absorbance spectrum of DPDPB by UV-Vis spectroscopy (JASCO V560) and the appearance of the 343 nm peak (figure 9).

The monitoring of the conjugation by UV spectroscopy was performed prior and after dialysis, once the dialysis was intended to eliminate the released pyridine-2-thione and the unreacted DPDPB (figure 8). The peak at 343 nm in the reticulated nanogel (before dialysis) demonstrates the conjugation of DPDPB and the release of the pyridine-2-thione (doted line, figure 8), effectively removed by dialysis together with the unreacted DPDPB molecules, as proven by the withdrawal of the 343 nm peak and the presence of the 272 nm peak (grey line, figure 9).

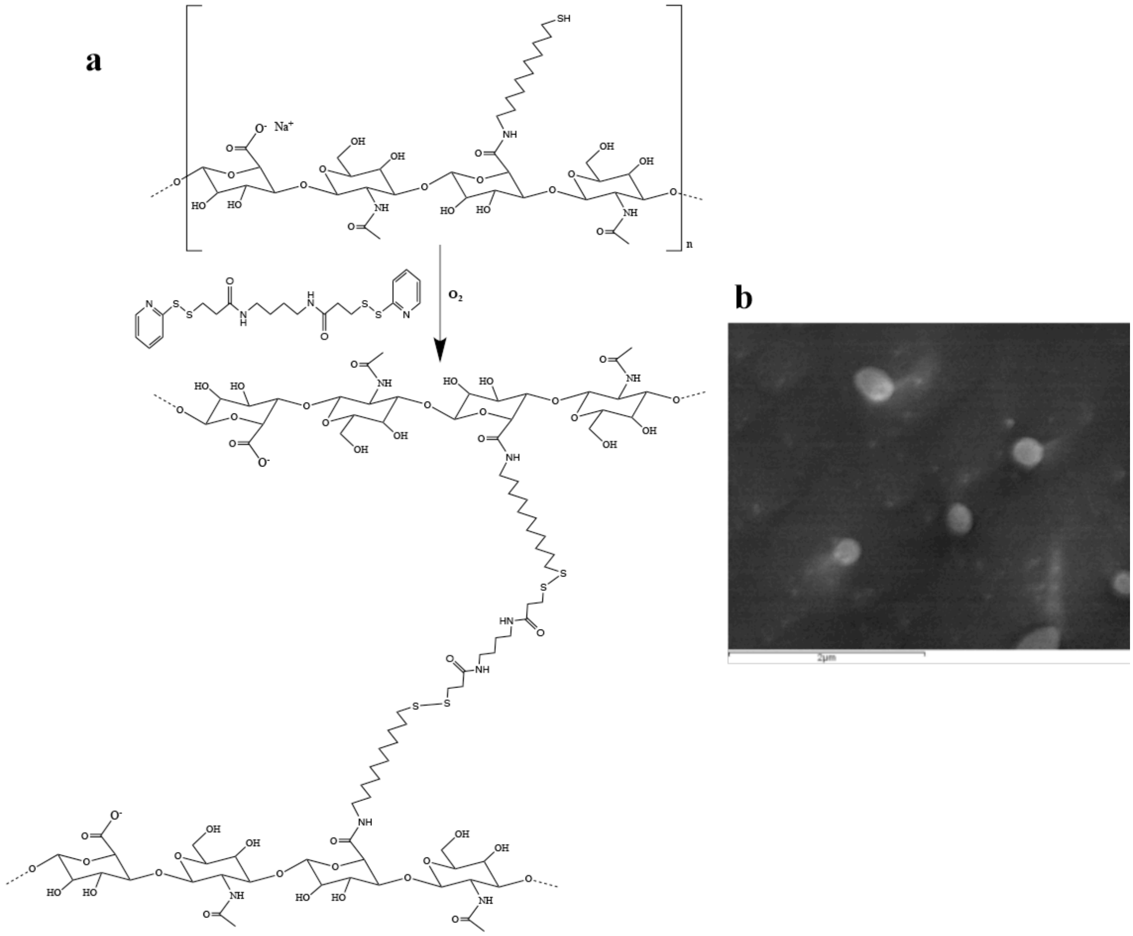

Figure 7: Schematic representation of the crosslinking reaction between HyA-AT conjugate and DPDPB through disulfide bond. B) Cryo-FESEM image of HyA-AT-DPDPB nanogel (scale bar = 2 μm).

4.3.2.2. CRYO-FIELD-EMISSION SCANNING ELECTRON MICROSCOPY (CRYO-FESEM)

HyA-AT-DPDPB nanogel was prepared at a concentration of 1mg/ml in distilled water, frozen and analysed in an electron microscope (SEM/EDS: FESEM JEOL JSM6301F/Oxford Inca Energy 350).
The Cryo-FESEM images show that the reticulated nanogel was also spherical in shape (figure 7).

4.3.2.3. DYNAMIC LIGHT SCATTERING (DLS) CHARACTERIZATION

In figure 10, we present the volume distribution profiles of reticulated and non-reticulated nanogel, using samples with concentrations between 1.0 mg/ml and 0.001 mg/ml – the later, a concentration below de cac of the HyA-AT nanogel. The non-reticulated nanogel showed stability in terms of mean size values and volume distribution profile when diluted to a concentration of 5 μg/ml. Once further diluted, at concentrations below the cac – 1.0 μg/ml – it was possible to detect disassembling of the nanogel as seen in the volume distribution profile and by the mean size value (figure 11).
The study of the dilution effect on the DPDPB-reticulated nanogel was also performed in the same concentration range. The volume distribution profile and the mean size diameter of HyA-AT-DPDPB nanogel were analyzed by DLS (figure 10 and 11). Remarkably, the nanogel volume distribution profile and mean size was maintained even bellow the cac. The lower concentration - 1 μg/ml – was evaluated after two weeks to assess the stability and it was noticeable that the nanogel preserved its supramolecular structure. Similar results were obtained by other researchers [27, 28].

Interestingly, the reticulated nanogel volume distribution showed more equitable populations than in the non-reticulated, indicating that the crosslinking caused an increase in the larger population. This may be due to the effect of the DPDPB spacer in the reorganization of the HyA and AT chains that become deviated increasing the larger population, around 150 nm.

Hence, the reticulated nanogel - although with slightly larger particles - presents a narrower distribution, demonstrated by the smaller PdI values obtained by DLS analysis (figure 11).

4.3.3. REDOX SENSITIVE CROSSLINKED NANOGEL CHARACTERIZATION

Nonetheless, the more diluted sample was further treated with dithiothreitol (DTT), a reducing agent to disrupt the reversible DPDPB conjugation. The reducing agent recoiled the reticulating effect of DPDPB by breaking the disulfide bond between the 14-atom spacer with AT residues of HYA-AT nanogel.

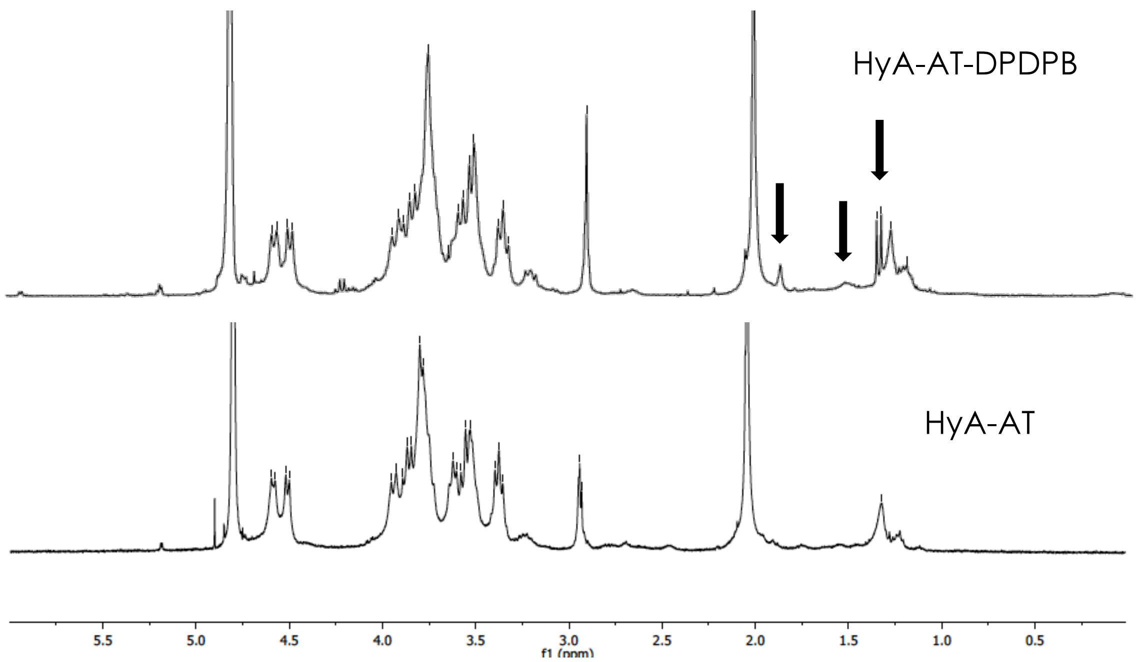

Figure 8: [1]H NMR spectrum of HyA-AT-DPDPB and HyA-AT nanogels in D_2O at 25ºC and the evidence of the presence of DPDPB ascribed peaks.

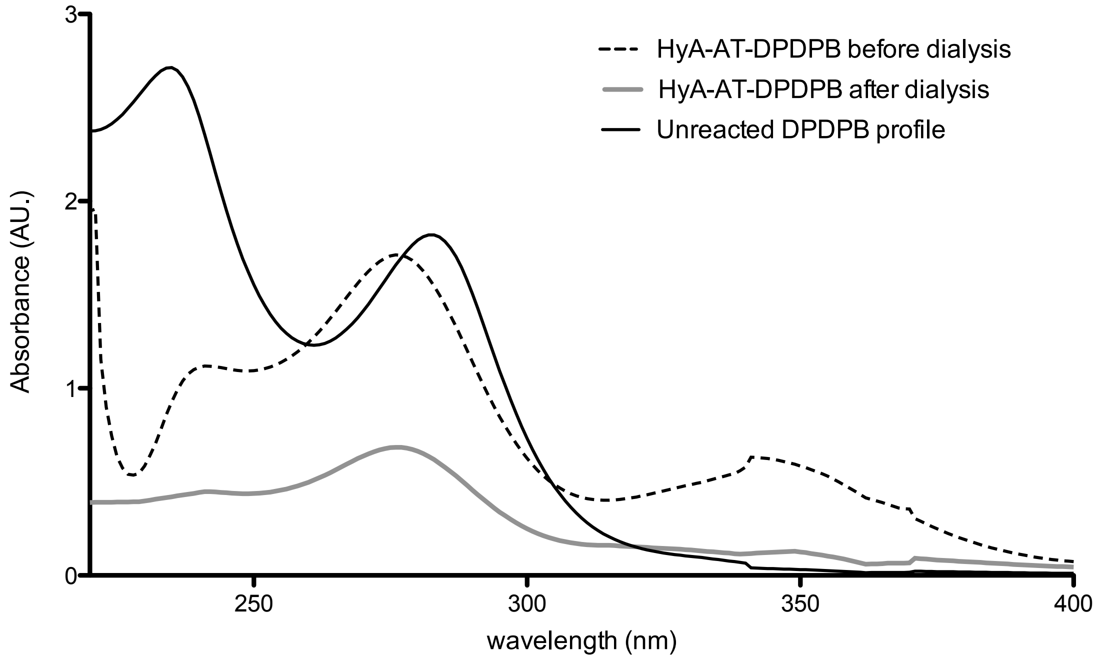

Figure 9: UV-Vis absorbance spectrum of HyA-AT-DPDPB nanogel.

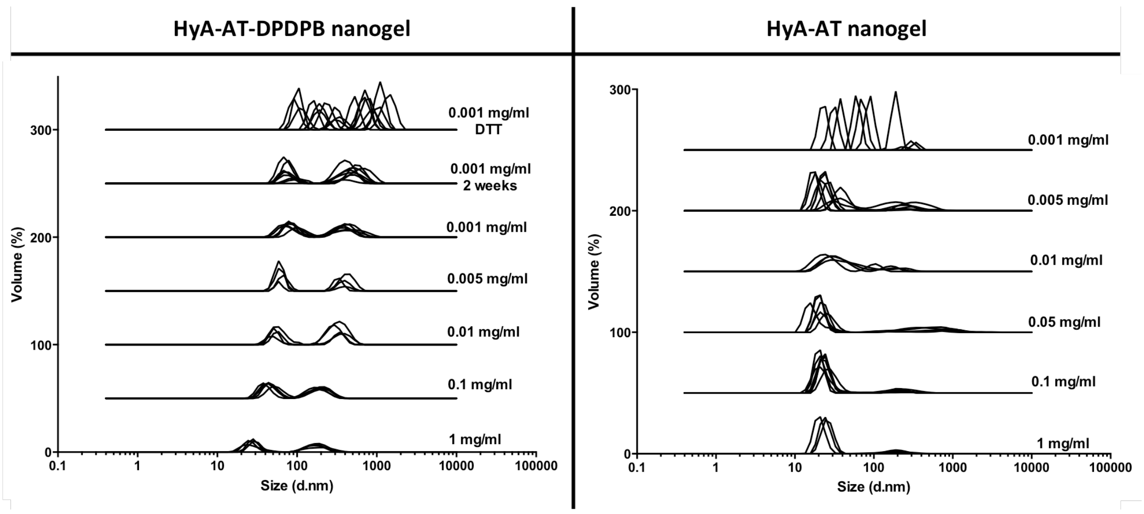

Figure 10: Comparison of hydrodynamic particle volume distribution profile of HyA-AT and HyA-AT-DPDPB nanogels upon dilution, evaluated by DLS analysis

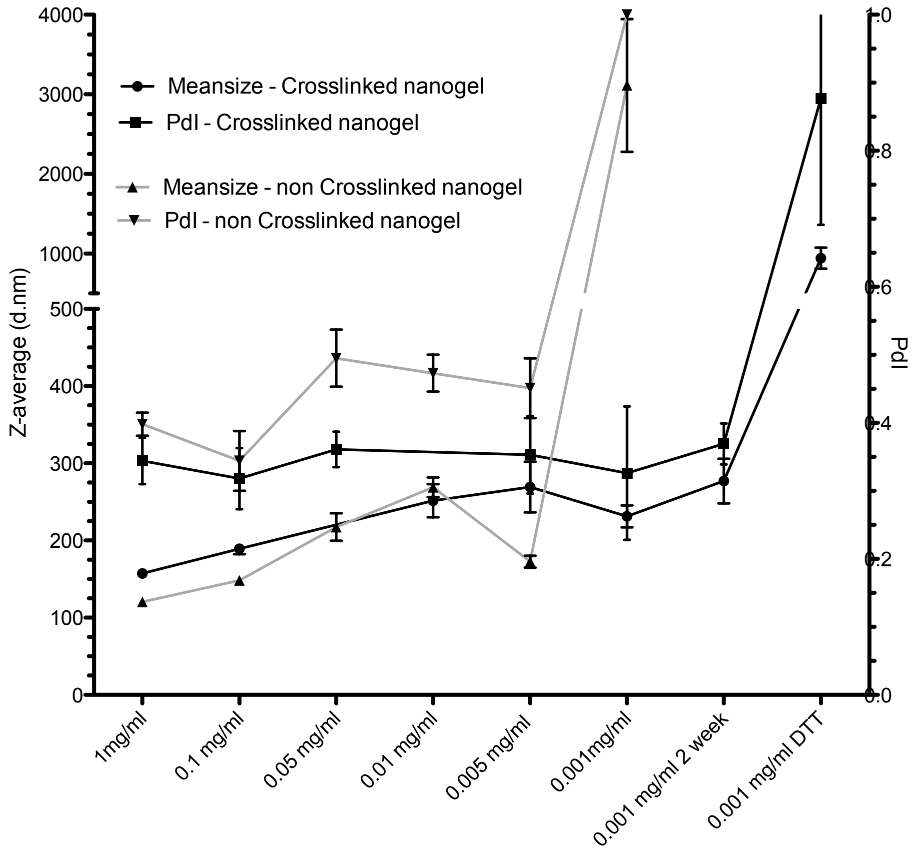

Figure 11: Plot data representation of the mean size diameter of HyA-AT and HyA-AT-DPDPB nanogel particles as function of nanogel concentration and the effect of a reducing agent in the crosslinked nanogel.

4.4. Drug loading efficiency

The drug entrapment efficiency of HyA-AT nanogel was determined using curcumin and simvastatin as model hydrophobic drugs. The encapsulation efficiency (EE) was assessed spectrophotometrically and expressed in concentration of drug incorporated into the nanogel. Simvastatin is a hydrophobic statin [29] used in the treatment of dyslipidaemias and recent findings indicate that also exhibit anti-inflammatory properties such as inhibiting the production of pro-inflammatory cytokines, C-reactive protein, cellular adhesion molecules and chemotaxic molecules [30, 31]. Curcumin (diferuloylmethane) is a low molecular weight natural polyphenolic compound soluble in ethanol and insoluble in water with antioxidant, anti-inflammatory and anticancer properties [32]. These were used as a model drug for assessing the loading capability of HyA-AT nanogel. Since both drugs prefer hydrophobic environments we tested their loading onto de nanogel hydrophobic domains.

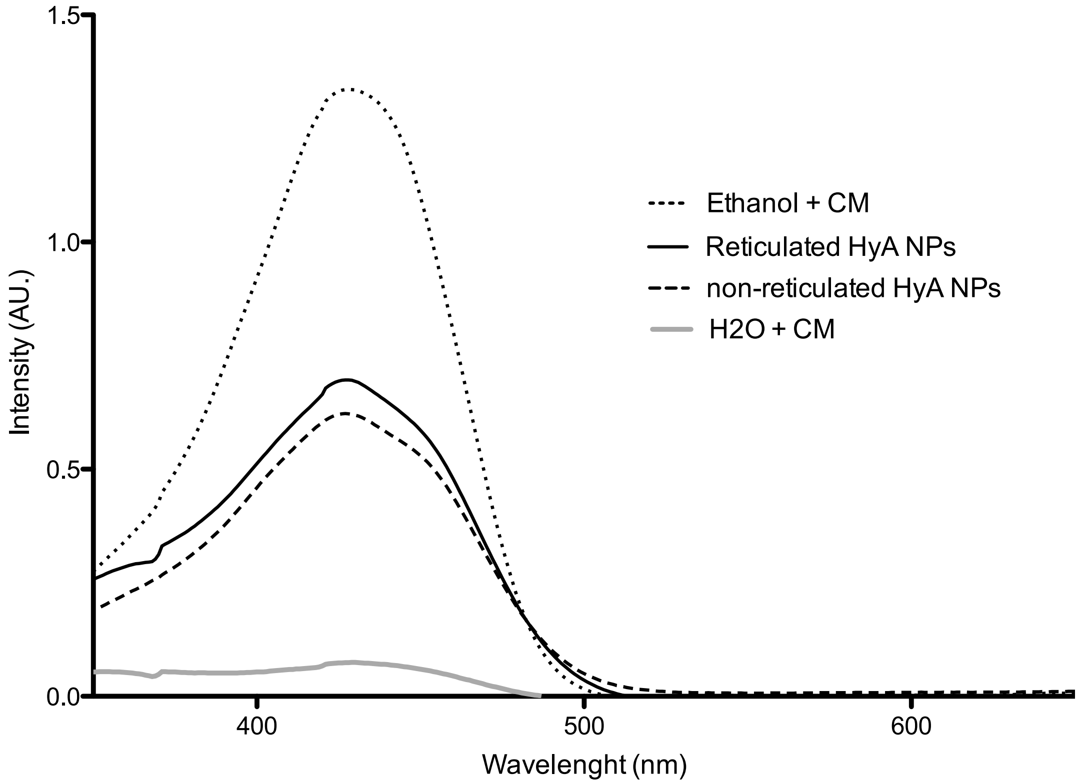

Figure 12: UV-Vis absorbance spectrum of curcumin at a 30 mM concentration solubilized in different solvents and in the presence of HyA-AT and HyA-AT-DPDPB nanogel.

Curcumin (CM) and simvastatin (SV) exhibit strong absorption at 428 nm and at 238 and 247 nm, respectively, allowing the use of spectrophotometrical analysis to quantify the amount of drug incorporated into the nanogel. An ethanolic solution of curcumin (stock solution) was added to 1.0 mg/ml nanogel aqueous suspension - final curcumin concentration of 30mM - precipitation of the (presumably) non-incorporated curcumin being observed. The nanogel dispersion developed a bright yellow colour characteristic of solubilized curcumin. The same dilution of the stock-solution of curcumin was applied in an ethanol control solution, illustrative of the maximum curcumin loading absorption. The absorption at 428 nm confirm the curcumin loading in both the reticulated and non-reticulated nanogel samples, as seen in figure 12, reaching concentrations of 15.63 mM and 13.94 mM, respectively. Similar results were obtained by researchers with PLGA nanogel [33].

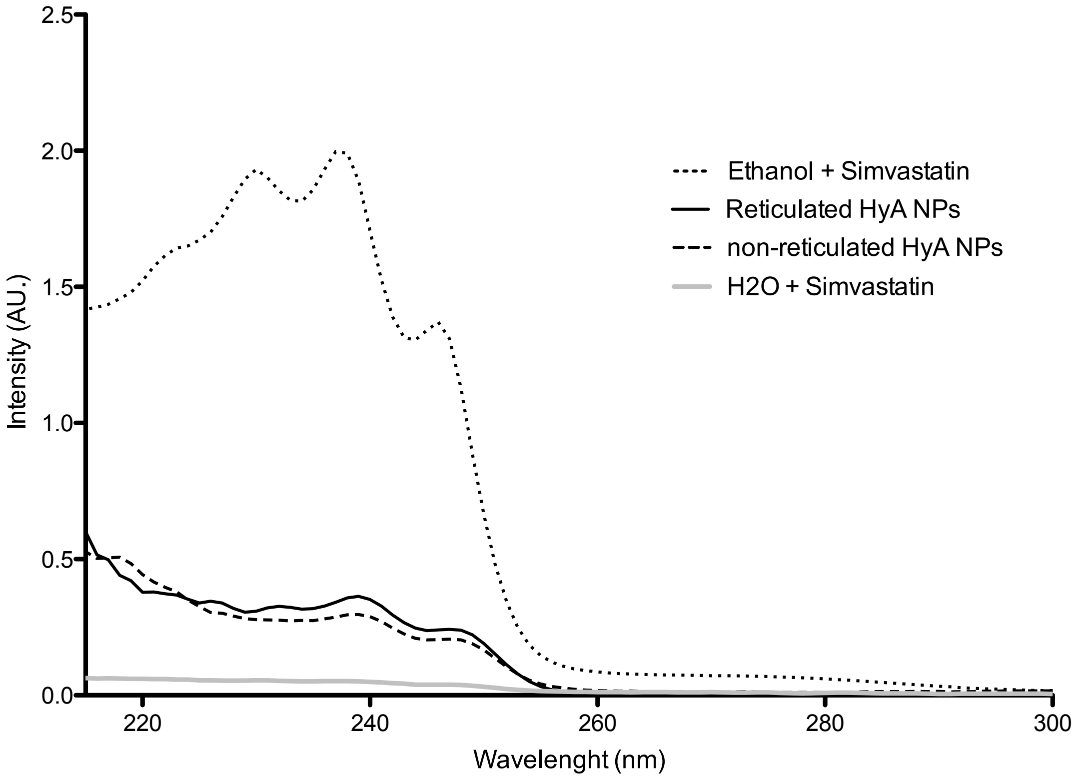

Figure 13: UV-Vis absorbance spectrum of simvastatin at a 71.7 μM concentration in different solvents and in the presence of HyA-AT and HyA-AT-DPDPB nanogel.

Simvastatin loading was performed in a similar way. An ethanolic stock solution of simvastatin was added to 1.0 mg/ml nanogel dispersion, leading to a final simvastatin concentration of 71.7 μM. In figure 13, the characteristic absorption of simvastatin at 238 and 247 nm is detected; settling the entrapment of the hydrophobic drug by the reticulated and non-reticulated nanogels, yielding estimated amounts of soluble simvastatin of 11.85 μg/ml and 13.39 μg/ml, respectively. Similar entrapment concentrations were obtained in other works [24, 34, 35].

The effect of the drug incorporation in the size of the nanogel was assessed by DLS analysis (table 1). The swelling of the non-reticulated nanogels is noticeable, as also observed with similar materials [28, 36]. As expected, the reticulated nanogel exhibited higher size stability and was not significantly affected by the drug loading.

Table 1: DLS results of the hydrodynamic particles size (diameter-nm) of the HyA-AT and HyA-AT-DPDPB nanogel, before and after the drug incorporation. Here is also described the amount of drug loaded and drug loading efficiency of the nanogels.

Sample	Drug loaded	Drug loading	Loading Efficiency	Size (SD)
HyA-AT	-			86.76+/- 2.063 nm
HyA-AT-DPDPB				122.2 +/- 40.70 nm
HyA-AT	Curcumin	13.94 mM	40.46 +/- 1.5 %	175.8 +/- 22.15 nm
HyA-AT-DPDPB		15.63 mM	52.1 +/- 1.8 %	159.3 +/-6.725 nm
HyA-AT	Simvastatin	11.85 μg/ml	39.5 +/- 1.2%	148.2 +/- 3.563 nm
HyA-AT-DPDPB		13.39 μg/ml	44.63 +/- 0.9%	150.3 +/- 18.59 nm

5. CONCLUSION

The synthesis of a thiolated hyaluronic acid conjugate that self – assembles into nanosized structures was achieved in a versatile, easy and reproducible manner. The nanogel presented long-term stability in solution and a fairly low critical aggregation concentration, which envisages good behaviour upon dilution, such as in vivo administration. The nanogel was successfully reticulated by dissulfide bond with a homofunctional crosslinker that linked the thiolated hydrophobic chains between them. Further, with the effective encapsulation of hydrophobic drugs suggest that both nanogels embody good vector systems for drug release and may exhibit redox sensitive trigger burst drug release.

6. ACKNOWLEDGMENTS

We would like to acknowledge the support of FCT for the PhD grant reference SFRH/BD/61516/2009.

7. References

1. Choi, K.Y., et al., *Hyaluronic acid-based nanocarriers for intracellular targeting: interfacial interactions with proteins in cancer.* Colloids Surf B Biointerfaces, 2012. **99**: p. 82-94.
2. Choi, K.Y., et al., *Self-assembled hyaluronic acid nanoparticles as a potential drug carrier for cancer therapy: synthesis, characterization, and in vivo biodistribution.* Journal of Materials Chemistry, 2009. **19**(24): p. 4102-4107.
3. Ekici, S., et al., *Hyaluronic acid hydrogel particles with tunable charges as potential drug delivery devices.* Carbohydrate Polymers, 2011. **84**(4): p. 1306-1313.
4. Li, F., B.C. Bae, and K. Na, *Acetylated Hyaluronic Acid/Photosensitizer Conjugate for the Preparation of Nanogels with Controllable Phototoxicity: Synthesis, Characterization, Autophotoquenching Properties, and in vitro Phototoxicity against He La Cells.* Bioconjugate Chemistry, 2010. **21**(7): p. 1312-1320.
5. Fakhari, A. and C. Berkland, *Applications and emerging trends of hyaluronic acid in tissue engineering, as a dermal filler and in osteoarthritis treatment.* Acta Biomaterialia, 2013. **9**(7): p. 7081-7092.
6. Oh, E.J., et al., *Target specific and long-acting delivery of protein, peptide, and nucleotide therapeutics using hyaluronic acid derivatives.* Journal of Controlled Release, 2010. **141**(1): p. 2-12.
7. Cheng, C., E. Khoshdel, and K.L. Wooley, *One-Pot Tandem Synthesis of a Core−Shell Brush Copolymer from Small Molecule Reactants by Ring-Opening Metathesis and Reversible Addition−Fragmentation Chain Transfer (Co)polymerizations.* Macromolecules, 2007. **40**(7): p. 2289-2292.
8. Li, Y.-L., et al., *Reversibly Stabilized Multifunctional Dextran Nanoparticles Efficiently Deliver Doxorubicin into the Nuclei of Cancer Cells.* Angewandte Chemie International Edition, 2009. **48**(52): p. 9914-9918.
9. Talelli, M., et al., *Core-crosslinked polymeric micelles with controlled release of covalently entrapped doxorubicin.* Biomaterials, 2010. **31**(30): p. 7797-804.
10. Xu, Y., et al., *Reduction-sensitive reversibly crosslinked biodegradable micelles for triggered release of doxorubicin.* Macromol Biosci, 2009. **9**(12): p. 1254-61.
11. Li, J., et al., *Redox-sensitive micelles self-assembled from amphiphilic hyaluronic acid-deoxycholic acid conjugates for targeted intracellular delivery of paclitaxel.* Biomaterials, 2012. **33**(7): p. 2310-20.

12. Ganesh, S., et al., *Hyaluronic acid based self-assembling nanosystems for CD44 target mediated siRNA delivery to solid tumors.* Biomaterials, 2013. **34**(13): p. 3489-502.
13. Liu, Y., et al., *Dual targeting folate-conjugated hyaluronic acid polymeric micelles for paclitaxel delivery.* Int J Pharm, 2011. **421**(1): p. 160-9.
14. Shen, Y., et al., *Synthesis and characterization of low molecular weight hyaluronic acid-based cationic micelles for efficient siRNA delivery.* Carbohydrate Polymers, 2009. **77**(1): p. 95-104.
15. Oudshoorn, M.H.M., et al., *Synthesis of methacrylated hyaluronic acid with tailored degree of substitution.* Polymer, 2007. **48**(7): p. 1915-1920.
16. Wittrup, K.D. and G.L. Verdine, *Protein Engineering for Therapeutics*. 2012: Elsevier Science.
17. Hermanson, G.T., *Bioconjugate Techniques*. 2010: Elsevier Science.
18. Information, N.C.f.B., *SID: 54454*.
19. Palumbo, F.S., et al., *New graft copolymers of hyaluronic acid and polylactic acid: Synthesis and characterization.* Carbohydrate Polymers, 2006. **66**(3): p. 379-385.
20. Bodnár, M., et al., *Preparation and characterization of cross-linked hyaluronan nanoparticles.* Colloid and Polymer Science, 2009. **287**(8): p. 991-1000.
21. Jin, Y.-J., et al., *Hyaluronic Acid Derivative-Based Self-Assembled Nanoparticles for the Treatment of Melanoma.* Pharm Res, 2012. **29**(12): p. 3443-3454.
22. Dutt, G.B. and S. Doraiswamy, *Picosecond reorientational dynamics of polar dye probes in binary aqueous mixtures.* The Journal of Chemical Physics, 1992. **96**(4): p. 2475-2491.
23. Krishna, M.M.G., *Excited-State Kinetics of the Hydrophobic Probe Nile Red in Membranes and Micelles.* The Journal of Physical Chemistry A, 1999. **103**(19): p. 3589-3595.
24. Yao, J., et al., *Efficient simultaneous tumor targeting delivery of all-trans retinoid acid and Paclitaxel based on hyaluronic acid-based multifunctional nanocarrier.* Mol Pharm, 2013. **10**(3): p. 1080-91.
25. Zhang, Y., et al., *Potential of amphiphilically modified low molecular weight chitosan as a novel carrier for hydrophobic anticancer drug: Synthesis, characterization, micellization and cytotoxicity evaluation.* Carbohydrate Polymers, 2009. **77**(2): p. 231-238.
26. Goncalves, C., et al., *New dextrin nanomagnetogels as contrast agents for magnetic resonance imaging.* Journal of Materials Chemistry B, 2013. **1**(42): p. 5853-5864.
27. Mahor, S., et al., *Controlled release of plasmid DNA from hyaluronan nanoparticles.* Curr Drug Deliv, 2011. **8**(4): p. 354-62.
28. Tao, Y.H., et al., *Core cross-linked hyaluronan-styrylpyridinium micelles as a novel carrier for paclitaxel.* Carbohydrate Polymers, 2012. **88**(1): p. 118-124.

29. Salman, H., et al., *Hydrophobic but not hydrophilic statins enhance phagocytosis and decrease apoptosis of human peripheral blood cells in vitro.* Biomed Pharmacother, 2008. **62**(1): p. 41-5.
30. Jain, M.K. and P.M. Ridker, *Anti-inflammatory effects of statins: clinical evidence and basic mechanisms.* Nat Rev Drug Discov, 2005. **4**(12): p. 977-87.
31. Kwak, B., et al., *Statins as a newly recognized type of immunomodulator.* Nat Med, 2000. **6**(12): p. 1399-402.
32. Manju, S. and K. Sreenivasan, *Conjugation of curcumin onto hyaluronic acid enhances its aqueous solubility and stability.* Journal of Colloid and Interface Science, 2011. **359**(1): p. 318-325.
33. Doggui, S., et al., *Neuronal Uptake and Neuroprotective Effect of Curcumin-Loaded PLGA Nanoparticles on the Human SK-N-SH Cell Line.* Journal of Alzheimer's Disease, 2012. **30**(2): p. 377-392.
34. Nath, S.D., et al., *Encapsulation of simvastatin in PLGA microspheres loaded into hydrogel loaded BCP porous spongy scaffold as a controlled drug delivery system for bonetissue regeneration.* J Biomater Appl, 2013.
35. Saravanakumar, G., et al., *Hydrotropic hyaluronic acid conjugates: Synthesis, characterization, and implications as a carrier of paclitaxel.* Int J Pharm, 2010. **394**(1-2): p. 154-61.
36. Yadav, A.K., et al., *Development and characterization of hyaluronic acid decorated PLGA nanoparticles for delivery of 5-fluorouracil.* Drug Deliv, 2010. **17**(8): p. 561-72.

CHAPTER III

BIOCOMPATIBILITY OF A SELF –ASSEMBLED CROSSLINKABLE HYALURONIC ACID NANOGEL

Adapted from

Macromolecular Bioscience, doi:10.1002/mabi.201600221

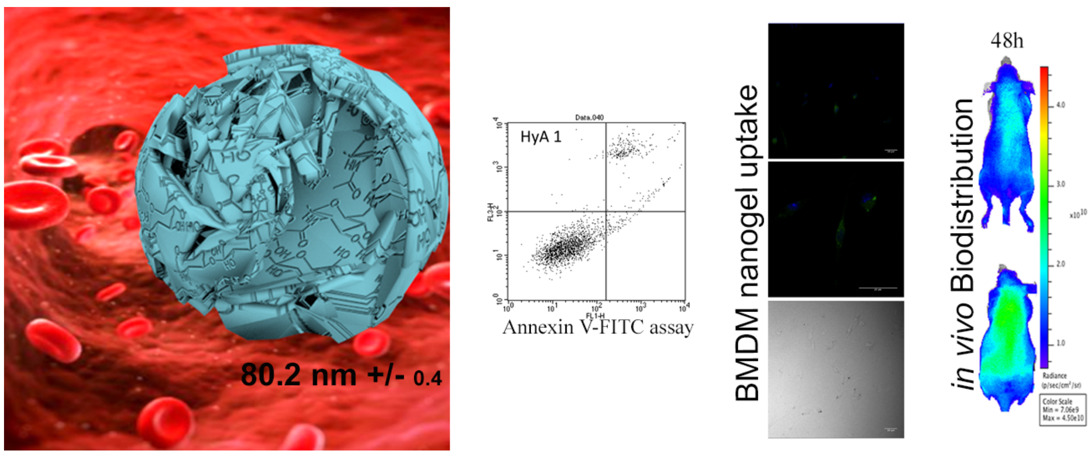

ABSTRACT

Hyaluronic acid nanogel (HyA-AT) is a redox sensitive crosslinkable nanogel, obtained through the conjugation of a thiolated hydrophobic molecule to the hyaluronic acid chain. Engineered nanogel was studied for its biocompatibility, including immunocompatibility and hemocompatability. The nanogel did not compromise the metabolic activity or cellular membrane integrity of 3T3, HMEC and RAW 264.7 cell lines, as determined by the MTT and LDH release assays. Also, we didn't observe any apoptotic effect on these cell lines through the Annexin V-FITC test. Furthermore, the nanogel cell internalization was analysed using murine bone marrow derived macrophages, and the *in vivo* and *ex vivo* biodistribution of the Cy5.5 labelled nanogel was monitored using a non-invasive near-infrared fluorescence imaging system. The HyA-AT nanogel exhibits fairly a long half-live in the blood stream, thus showing potential for drug delivery applications.

1. INTRODUCTION

Nanotechnology is a fast growing field with particular interest for biomedicine research. Nanoparticles and other nanomaterials in general, offer numerous advantages due to their small size, drug loading ability and special pharmacodynamics. Due to their potential and peculiar characteristics are often employed to: i) target-specific delivery of drugs, or other molecules; ii) improve drug stability or solubility, *in vitro* or *in vivo;* iii) reduce side effects of biologically active compound. Therefore, it is not strange to realise that so many nano-systems are being investigated; having several products reached the market, and many more undergoing clinical trials. [1, 2]

However, nanoparticles attractive properties can also be the source of problems, mainly by the interaction with immune system. Engineered nanoparticles can specifically be designed either to target or avoid the immune system [1]. Interactions with immune system are considered beneficial when advantageous medical reactions are obtained, e.g. vaccination or the treatment of autoimmune disorders. However, nanoparticles and especially polymeric nanoparticles may escape the immune system recognition and perform its duty e.g., as drug delivery system. [1, 2] Hyaluronic acid is a naturally occurring polysaccharide, ubiquitous in the human body, and with appealing biological properties [3].

In 2010, Kohane and Langer defined biocompatibility as "an expression of the benignity of the relation between a material and its biological environment". Generally biocompatibility is achieved when materials interact with the body and do not induce unacceptable toxic, immunogenic, thrombogenic and/or carcinogenic effects [4].

A hyaluronic acid nanogel (HyA-AT) crosslinked through redox sensitive bond was prepared in our research group in previous work, demonstrating potential for drug delivery applications [5]. Here, we assess the biocompatibility, immunocompatibility and hemocompatibility of the engineered nanogel. Also, nanogels biosdistribution in healthy mice model was assessed by non-invasive near-infrared (NIR) fluorescence imaging system. Nanogel was labelled with a NIR probe – Cy5.5 hydrazide – and its biodistribution was studied for the course of 48h.

2. EXPERIMENTAL

2.1. MATERIALS

All reagents used were of analytical grade. Sodium hyaluronate (MW= 7.46 KDa) was purchased from Lifecore Biomedical (USA). AG 50W – X8 resin was purchased from Bio-Rad (USA). Dimethyl sulfoxide (DMSO), Tetrabutylammonium fluoride hydrate (TBA-F), 11-Amino-1-undecanethiol hydrochloride (AT), N-hydroxysulfosuccinimide (NHS), 1-ethyl-3-[3-

dimethylaminopropyl]carbodiimide hydrochloride (EDC), 3-(4,5-dimethylthiazol-2-yl)-2,5-diphenyl tetrazolium bromide (MTT), hydrogen nicotinamide adenine dinucleotide (NADH), pyruvate, haemoglobin from bovine blood and Drabkin's reagent were acquired from Sigma-Aldrich (Italy). Fluorescein-5-thiosemicarbazide and Cy5.5 hydrazide were purchased from Life Technologies Ltd (UK). Cell Culture reagents and culture medium were purchased from Biochrom (Germany). The water used was distilled and ultrapurified (Milli-Q system).

2.2. Nanogel assembling

HyA-AT nanogel was produced as described previously [5], by chemical conjugation. Briefly, a thiolated hydrophobic molecule (AT) was grafted in the hyaluronic acid backbone (DS=11%) by carbodiimide chemistry. The resulting amphiphilic hyaluronic acid conjugate was dispersed in water and stirred for a few minutes at room temperature. Dispersion was further filtrated by cellulose acetate serynge filter (pore size 0.22 μm). Engineered nanogel was characterized thoroughly [5] and the nanogel colloidal dispersion in water displayed an average size distribution of 80.2 +/- 0.4 nm. The nanogel dispersions used for *in vitro* and *in vivo* studies were filtered through cellulose acetate syringe filter (pore size 0.22 μm) in aseptic conditions.

HyA-AT nanogel morphology (1.0 mg/ml) was analysed by Cryo-Field-Emission Scanning Electron Microscopy (Cryo-FESEM) in an electron microscope (SEM/EDS: FESEM JEOL JSM6301F/Oxford Inca Energy 350). Sample was frozen in liquid nitrogen and then fractured and sublimated for 10 minutes at -95ºC to expose the nanogel particles. Finally, samples were sputter-coated with gold and palladium at -140ºC using an accelerating voltage of 10kV. The observation was performed at -140ºC and 15kV.

With the intent to evaluate the interaction of the nanogel with protein components of the culture medium we evaluated its size distribution profile by intensity, through dynamic light scattering (DLS). Briefly, HyA-AT nanogel was dispersed in water at 1.0 mg/ml and incubated at room temperature with FBS 1%(v/v). Dispersions were evaluated as to their size distribution profile at: 0h, 24h, 48h and 72h. Also, control samples of nanogel 1mg/ml and FBS 1% were also analysed, following the same protocol.

2.3. Synthesis of HyA-AT-Fluorescein labelled nanogel

For *in vitro* murine BMDM cellular uptake evaluation, HyA-AT nanogel and native HyA were labelled with Fluorescein-5-thiosemicarbazide. Briefly, thiosemicarbazide group reacted with carboxylic group of hyaluronic acid nanogel in the presence of EDC as a coupling agent [6-10]. The molar ratio of Fluorescein-5-thiosemicarbazide to free carboxylic acid groups of HyA-AT nanogel was 0.25. The coupling agent (EDC) was added to the reaction mix at an equimolar ratio to the free carboxylic acid groups of HyA-AT nanogel and native HyA. The reaction was allowed to occur overnight at room temperature, in the dark. The reaction mixture was thoroughly dialysed (MW cut-off 1000 Da) against distilled water to remove non-desired reaction products. Nanogel and polymer labelling was confirmed by UV/VIS spectroscopy at 492 nm.

2.4. Synthesis of HyA-AT-Cy5.5 labelled nanogel

For *in vivo* biodistribution study using near infrared fluorescence (NIRF) technology, HyA-AT nanogel and native HyA were labelled with Cy 5.5 - hydrazide. Hydrazide reactive moiety was conjugated with carboxylic groups of HyA-AT nanogel [8-11] in presence of EDC, as coupling agent. The molar ratio of Cy 5.5 - hydrazide to free carboxylic acid groups of HyA-AT nanogel and native HyA was 0.25. EDC was added in an equimolar ratio to the free carboxylic acid groups. The reaction was allowed to occur overnight at room temperature, in the dark. The reaction mixture was thoroughly dialysed (MW cut-off 2 000 Da) against distilled water to remove non-desired reaction products. Nanogel and polysaccharide labelling was confirmed by UV/VIS spectroscopy at 649 nm.

2.5. Cell lines, cell culture and maintenance

Mus musculus, mouse embryonic fibroblasts (NIH/3T3) cell line was maintained in Dulbecco's modified Eagle's media (DMEM) supplemented with 10% (v/v) newborn calf serum, 100 IU/ml penicillin and 0.1 mg/ml streptomycin. Mouse leukemic monocyte macrophage (RAW 264.7) cell line was grown in Dulbecco's modified Eagle's media (DMEM) supplemented with 10% (v/v) of heat-inactivated (FBS), 100 IU/ml penicillin and 0.1 mg/ml streptomycin. Human microvascular endothelial cells (HMEC) were grown in RPMI-1640 supplemented with 10% FBS, Epidermal Growth Factor (EGF, 10 ng/mL), Hydrocortisone (1 µg/mL), 100 IU/mL penicillin and 0.1 mg/mL streptomycin. All cells were maintained at a 37ºC and 95% humidified air with 5% CO2, environment. RAW 264.7 cells were a courtesy of Dr Hugo Rocha (Federal University of Rio Grande do Norte, Brazil). NIH/3T3 cells and HMEC were already available in our laboratory.

During subculture, cells were detached by trypsinization with 0.05% (w/v) trypsin-EDTA after reaching 80% confluency. RAW 264.7 cells were dislodge with a cell scraper.

Murine Bone Marrow-Derived Macrophages were collected from femoral and tibial mouse bone marrow of female Balb/c mice. Mouse femurs and tibias were collected under aseptic conditions and flushed with RPMI -1640. The resulting cell suspension was centrifuged at 500g for 10 minutes. Pellet was resuspended in RPMI-1640 supplemented with

10mM HEPES, 10% heat-inactivated FBS, 60µg/mL penicillin/streptavidin, 0.005mM β-mercaptoethanol (Complete RPMI) and 10% L929 cell conditioned medium (LCCM). To remove adherent bone marrow cells, cell suspension was incubated on cell culture dishes, overnight at 37°C at 95% humidified air containing 5% CO2 atmosphere. The non-adherent cells were centrifuged at 500g (10min) and seeded in 24 well plates at 5 x 10^5 cells per well, in RPMI complete medium containing 10% of LCCM, and incubated at 37°C in a 5% CO_2 atmosphere. Four days after seeding 10% of LCCM was re-added and the medium was renewed on the seventh day, once again with complete RPMI and 10% LCCM. After 10 days, cells were completely differentiated into macrophages. [12, 13]

2.6. *IN VITRO* CELL TOXICITY

2.6.1. CELL PROLIFERATION ASSAY

Assessment of cell proliferation impairment on 3T3, HMEC and RAW 264.7 cells was performed using the 3-[4,5-dimethylthiazol-2-yl]-2,5-diphenyl tetrazolium bromide (MTT) reduction assay, adapted from Mosmann[14]. Cells were seeded in 24-well cell culture plates at a density of 1×10^4 cells per well for 3T3 and RAW 264.7 cells and of 2×10^4 for HMEC cells, and left adhering in 0.5mL of adequate culture medium overnight. HyA-AT nanogel 0.1mg/ml, 0.5 mg/ml and 1 mg/ml dispersions were suspended in adequate culture medium, resulting in a 1:5 fresh medium dilution. For

RAW 264.7 cell line the maximum concentration tested was 0.5 mg/ml. Untreated cells were used as control of 100% cell viability. Another control with 20% distilled water was used to access the effect of water dilution of samples containing the nanogel. A positive control with 20% of DMSO was used in every analysis. The samples were incubated for 24, 48 and 72h and the cells metabolic activity is calculated due to the reduction of tetrazolium salt of MTT by mitochondrial succinate dehydrogenase enzymes of metabolically active cells. To which well, 10% (v/v) of a MTT solution (5 mg/ml in PBS) was added and it was incubated at 37°C and 5% CO_2 for a period of 4h. In this period of time, the tetrazolium salt is bioreduced to a formazan product that consists in is dark blue crystals that are insoluble in the culture medium. The supernatant was discarded slowly and the crystals were solubilized in dimethyl sulfoxide and quantified spectrophotometrically at 570 nm. The experiments were performed in triplicates as the results are presented as percentage in which 100% viability corresponds to the non-treated cells.

2.6.2. LDH RELEASE ASSAY

The lactate dehydrogenase (LDH) release assay measures the membrane integrity as function of the amount of cytoplasmic LDH leaked through membrane-impaired cells. The lactate is converted to pyruvate in the presence of LDH with parallel reduction of nicotinamide adenine dinucleotide (NAD), detected as a change in absorbance at

340 nm [15]. Cells were seeded in 12-well plate at a density of the $2x10^5$ cells per well for 3T3 and HMEC cell lines and $1x10^5$ for RAW and allowed to settle overnight in 0.5 mL of adequate culture medium. The cells were treated with nanogel dispersions with a concentration of 0.1 and 1.0 mg/ml in suitable culture medium and supplementation. The exception was RAW 264.7 cells that were incubated with 0.1 and 0.5 mg/ml nanogel dosages. Untreated cells were used as control of 100% cell viability. Another control with 20% distilled water was used to access the effect of the water dilution of the samples containing the nanogel. A control with 20% of DMSO was used in every analysis as a positive control. The samples where incubated for 24h and after that period each culture medium from every well was collected and centrifuged at 13000 rpm for 1min and the cell free supernatant was collected and stored on ice for further analysis – Extracellular LDH. Cells were scraped with a Tris solution (15mM) extracellular and further lysed by sonication. The resulting supernatants were used to quantify the LDH present - Intracellular LDH. An aliquot of extracellular (40 µL) or intracellular (10 µL) LDH were assigned into a microplate and 250 µL of the NADH solution 0.31 mM in phosphate buffer 0.05 M, pH7.4 added to each well. Lastly, 10 µL of an 8.96 mM piruvate solution in phosphate buffer (substrate solution) was added and immediately afterwards the variation of the absorbance at 340 nm was read in a microplate spectrophotometer system, as to determine the rate of NADH consumption (slope of the line). LDH

leakage was expressed as the ratio between extracellular and total LDH, corresponding the inverse value to the cell membrane integrity. Each experiment was performed in triplicate.

2.6.3. Apoptosis assay

The FITC Annexin V Apoptosis Detection Kit was used to detect apoptotic and necrotic cells in 3T3, HMEC and RAW cell lines. Cells ($2x10^5$/well) were seeded in a 12-well plate and incubated overnight. Nanogel samples were added to the respective wells in a concentration range of 0.1 to 1.0 mg/ml dispersed in suitable culture medium and incubated for 24h. A negative control without any nanogel sample but with 20% distilled water was used - since preliminary studies revealed that untreated cells and cells incubated with 1:5 distilled water, culture medium ratio had similar results. The positive apoptotic control was prepared by culturing the control cells in medium containing H_2O_2 with different incubation times and concentration accordingly to the cells line (0.5mM and 6h incubation in RAW; 0.2mM and 24h incubation for HMEC; and 5mM and 3h incubation for 3T3) [16, 17]. Cells were then collected by trypsinization 250 µL trypsin/EDTA 0.25%/0.02% in PBS. Cell suspension was transferred to flow cytometry sample tubes (Beckman Coulter) and washed twice with cold PBS. Each sample was incubated with 40 µL of the work solution (1.8 µL of the Annexin V and PI diluted in 36.4 µL of the Annexin V binding buffer) for 15min at room temperature, in the dark.

Finally, 200 µL of Annexin V binding buffer was added to the samples that were then analysed by flow cytometry using a Coulter Epics XL Flow Cytometer (Beckman Coulter Inc., Miami, FL, USA). Cells were set as positive depending on the fluorescence intensity of Annexin V-FITC or PI. The positive of Annexin V-FITC indicates the out-releasing of phospholipid phosphatidylserine (PS), which happens in the early stage of apoptosis. The positive of PI indicates the damage of cell membrane, which occurs either in the end stage of apoptosis, in necrosis or in dead cells. Therefore, the apoptotic cells were identified as Annexin positive, and PI negatives – early apoptosis or Annexin and PI positive PI – late apoptosis. Nonviable cells were identified as PI positive and viable cells as Annexin and PI negative [17].

2.7. Complement activation assay

Complement cascade was studied as reported previously [1] and based on the NCL (Nanotechnology Characterization Laboratory) protocol for qualitative determination of total complement activation by Western blot analysis. Briefly, a pool of human plasma from healthy donors was incubated with 1mg/mL of HyA-AT nanogel in the presence of veronal buffer. Equal volumes (50uL) of plasma, buffer and sample were mixed and incubated at 37 °C for 60 minutes. Cobra venom factor from Quidel Corporation (San Diego, CA, USA), and PBS were used as positive and negative controls, respectively. Proteins were resolved by 10% SDS-PAGE, and then transferred to a membrane (Immun-Blot PVDF Membrane, Biorad, Hercules, USA) using the transblot semidry BioRad transfer equipment (Trans blot SD, BioRad, Hercules, USA). The membranes were incubated for 90 minutes with a mouse monoclonal antibody against human C3 diluted 1:1000 (Abcam, Cambridge, UK), washed and incubation with secondary polyclonal goat anti-mouse IgG antibodies conjugated with alkaline phosphatase diluted 1:2000 (Dako, Glostrup, Denmark). The membrane was finally revealed with 5-Bromo- 4-Chloro-3-Indolyl Phosphate (BCIP) (Sigma). For further analysis, membranes were scanned with ChemiDoc™XRS+ System (Bio-Rad; Hercules, CA). The percentage of the lower band was then quantified with Image Lab™ Software 3.0.

2.8. Murine bone marrow derived macrophages nanogel uptake

The hyaluronic acid nanogel cytocompatibility was further analysed by the phagocytic activity of murine bone marrow derived macrophages (BMDM). Macrophages were seeded in 24 well plates (5 x 10^5 cells/well) on top of coverslip discs and were left adhering overnight. Further, cells were incubated for 6h with 0.2 mg/ml fluorescein labelled nanogel dispersion in culture medium. Dextrin-FITC labelled nanoparticles (0.2 mg/ml) were used as a positive control for phagocytic uptake, as described by Gonçalves et al. [18]. Fluorescein labelled native HyA (0.2

mg/ml) was used to compare its phagocytic internalization with the HyA-AT nanogel. Full medium was removed from all the wells and coverslips were washed twice with PBS at room temperature and fixed with 2% paraformaldehyde solution for 25 minutes. After, 4',6-diamidino-2-phenylindole (DAPI, 120ng/mL) was used to stain the nucleus for 3 minutes at room temperature. Cells were observed in a confocal laser scanning microscope Leica SP2 AOBS SE (Leica Mycrosystems, Germany).

2.9. Haemolysis Index

The haemolysis assay was performed in agreement to the procedure described by the American Society for Testing Materials [19] and used in previous works [20]. Whole blood was collected from three independent healthy donors using citrated blood collection tubes. Briefly, 0.5 mL of diluted blood at 10 mg/mL was added to 3.5 mL of the nanogel solution in PBS at 0.1 mg/ml, 0.5 mg/mL and 0.1 mg/mL and incubated at 37 °C for 3 h. The tubes were gently mixed at 30 minutes frames to homogenize the mixture. Ultrapure water and Phosphate-buffered saline (PBS) were used as positive and negative haemolytic control, respectively. The suspension was centrifuged at 750 g for 15 minutes and 0.5 ml of the supernatant was collected. Then, 0.5ml of Drabkin's reagent was added and the solution was left incubating for15 minutes at room temperature. Finally, the absorbance at 540nm was measured by UV-VIS spectroscopy

(JASCO V560). Haemoglobin standard solutions were prepared from bovine blood haemoglobin to elaborate a calibration curve to infer the haemoglobin content of the samples. Experience was made in triplicates.

2.10. *In vivo* and *ex vivo* near-infrared fluorescence (NIRF) imaging

All experiments with live animals were performed in compliance with the Portuguese General alimentary and Veterinarian Board (authorization number 006315/27/03/2014, from DGAV-Portugal) and animals were kept and used strictly in accordance with National rules and the European Communities Council Directive (86/609/EEC), for the care and handling of laboratory animals. Athymic nude mice CD1-Foxn1nu mice (6-weeks old) were purchased from Charles River Laboratories International, Inc. HyA-AT-Cy5.5 labelled nanogel dispersion and native HyA-Cy5.5 solution were injected intravenously into the mice via tail vein (n=5) at a 5 mg/kg animal body weight. At established time points (2h, 7h, 24h and 48h) mice were anesthetised with Ketamine 75mg/kgBW and Medetomidine 1mg/KgBW solution prior to its analysis and blood sample collection.

The time-dependent biodistribution and accumulation profiles of samples were observed by using a Xenogen's IVIS® Lumina Series and Living Image® Software. To evaluate the blood clearance at all time points, 50μL venous blood was collected from the retro-orbital vein and transferred to a 96-well plate and analysed at each time point. The minimum amount of blood was collected, respecting the animal size and time schedule (50uL per analysis). To observe the organ distribution of the samples, each group of mice was sacrificed with a lethal dose of anesthesia 48h post samples injection. Then, major organs were excised and transferred to a 6-well plate and observed using the Xenogen's IVIS® Lumina Series and Living Image® Software. NIR fluorescence images obtained with a 12-bit CCD camera equipped with a special C-mount lens and Cy5.5 bandpass emission filter (680 nm to 720 nm).

2.11. Statistical Analysis

The results were expressed as mean ± SD of 3 independent experiments (n=3). Statistical analysis was performed with t-test or two-way ANOVA followed by Tukey's comparison test using using GraphPad Prism version 6.00 for Mac OS X, GraphPad Software, La Jolla California USA. Significance of the results is indicated according to P values with one, two, three or four of the used symbols (*, # or +) corresponding to P=0.01 to 0.05; P=0.001 to 0.01; P=0.0001 to 0.001 and P<0.0001, respectively).

3. Results and discussion

3.1. HyA nanogel characterization

The chemical conjugation of a hydrophobic chain to HyA was already fully characterized in our previous study [5]. The resulting amphiphilic molecule (HyA-AT) self assembles in aqueous environment onto nanosized structures. The morphology and size of the nanogel was evaluated by Cryo-FESEM and DLS analysis regarding its size distribution by intensity, as shown in figure 1a. The particles were apparently spherical and well dispersed without any aggregation, and the nanogel reveals a bimodal size distribution with a mean size diameter of 80.2 +/- 0.4 nm (n=5) [5].

It is well known that protein adsorption to nanomaterials has high impact on the interaction of nanomaterials with cells, both *in vivo* and *in vitro*. Therefore, we wanted to assess if the serum supplementation used in culture medium affected the size distribution profile of the nanogel. As can be seen in figure 1.b, we observed the interaction of the nanogel with FBS 1% (v/v) by DLS analysis, in the course of 72h. Indeed, nanogel showed colloidal stability and its average size diameter, around 80nm, maintained constant throughout time. The serum proteins size distribution profile fluctuated through time, probably due to the formation of unstable aggregates.

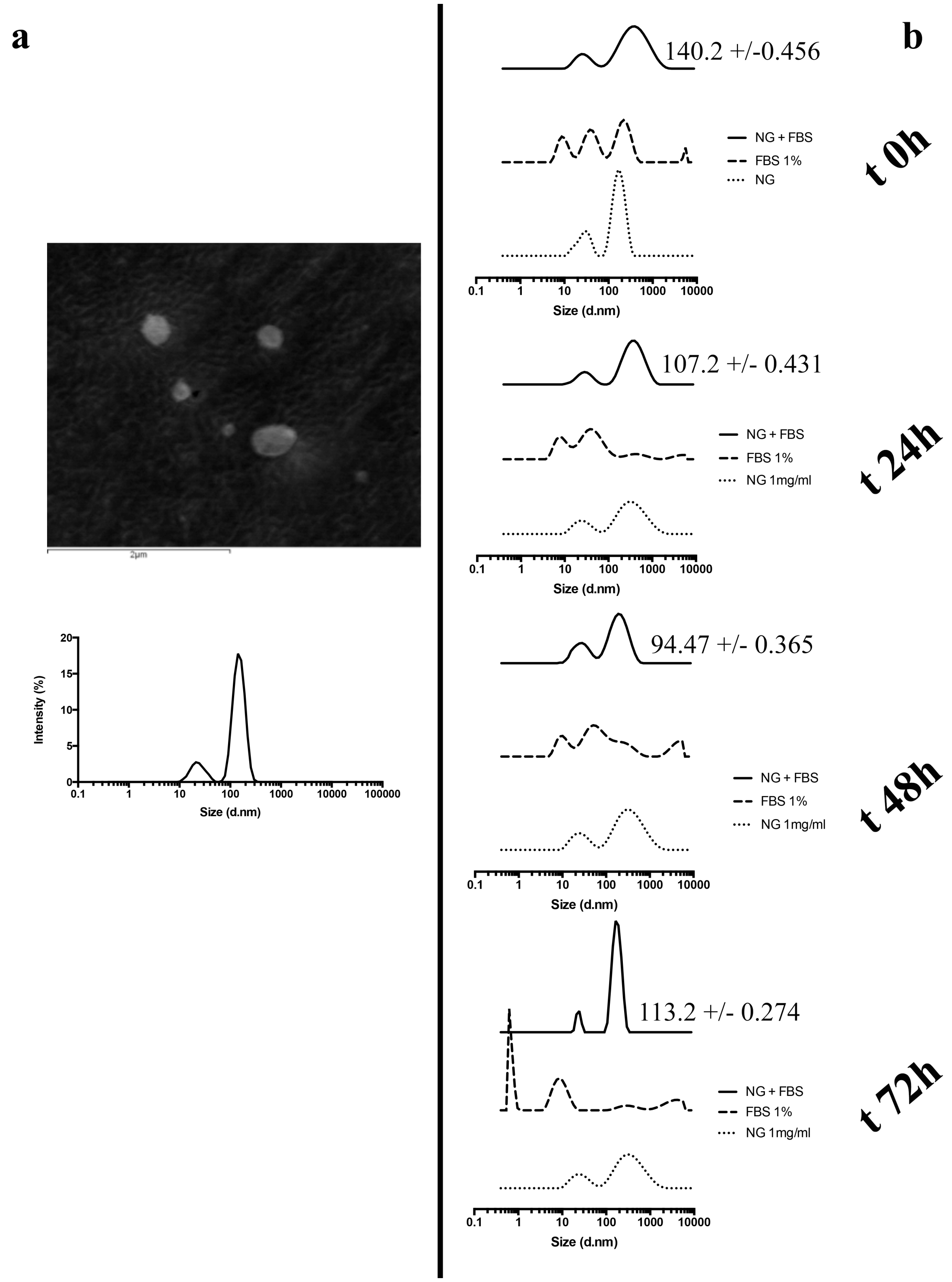

Figure 1: Nanogels size and morphology characterization and serum stability.

Section a: Nanogels size distribution profile by intensity through DLS analysis and Cryo-Field-Emission Scanning Electron Microscopy (Cryo-FESEM).

Section b: Nanogel size stability by intensity through DLS analysis, in the presence of serum proteins (FBS), over time.

3.2. Cytotoxicity studies

Cytotoxicity studies were performed in three cell lines: 3T3, HMEC and RAW 264.7. 3T3 fibroblasts were chosen as a model for stromal cells, which can be found in matrix and connective tissue throughout the body. Human microvascular endothelial cell line (HMEC-1) was used to investigate the possible cytotoxic effects in vasculature. RAW 264.7 are murine macrophages cell line, which are commonly included in nanomaterial toxicity investigations as an inflammatory cell type.

In the case of RAW macrophages we only tested a maximum 0.5 mg/ml, since macrophages can readily phagocytose nanomaterials at a very high rate and lead to overload and cell death. Thus, we didn't feel the need to test higher concentrations in this case. [21, 22] In addition to different nanogel concentrations, DMSO was used as a positive control and two negative controls were performed – one consisting of 100% culture medium and the other of culture medium diluted with 20% water. This last control is actually the most relevant one, since it mimics the water dilution effect with the nanogel samples (which slightly affects the cell growth).

3.2.1. CELL PROLIFERATION

MTT is a colorimetric, easy, fast and safe assay that measures the mitochondrial metabolic activity of viable cells (figure 2). We observed that the water-diluted control had a slightly lower cell growth or activity maybe due to the dilution of nutrients of the culture medium. This effect was most noticed in the longer incubation time (figure 2). The metabolic activity was not, overall, evidently affected be the nanogels presence, however at longer incubation time (72h) and highest dose, a reduced cell proliferation or activity was observed in 3T3 and RAW cells - in comparison to the diluted medium control. RAW cells seem to be more susceptible to nanogel treatment, but even in this case a slightly lower proliferation is observed only with highest incubation time. Similar results were obtained by other researchers [20, 23] when studying nanoparticles effect on macrophage cell lines. For instance, poly(ethylene glycol) (PEG)-conjugated hyaluronic acid nanoparticles, showed dose-dependent cytotoxicity to cancer cells (MDA-MB-231, SCC7, and HCT 116) and significantly lower cytotoxicity against normal fibroblasts (NIH-3T3) [24]. Fairly high nanogel concentrations were tested (up to 1,0 mg/ml) to effectively detect toxic effects and objectively assess the safety of the material.

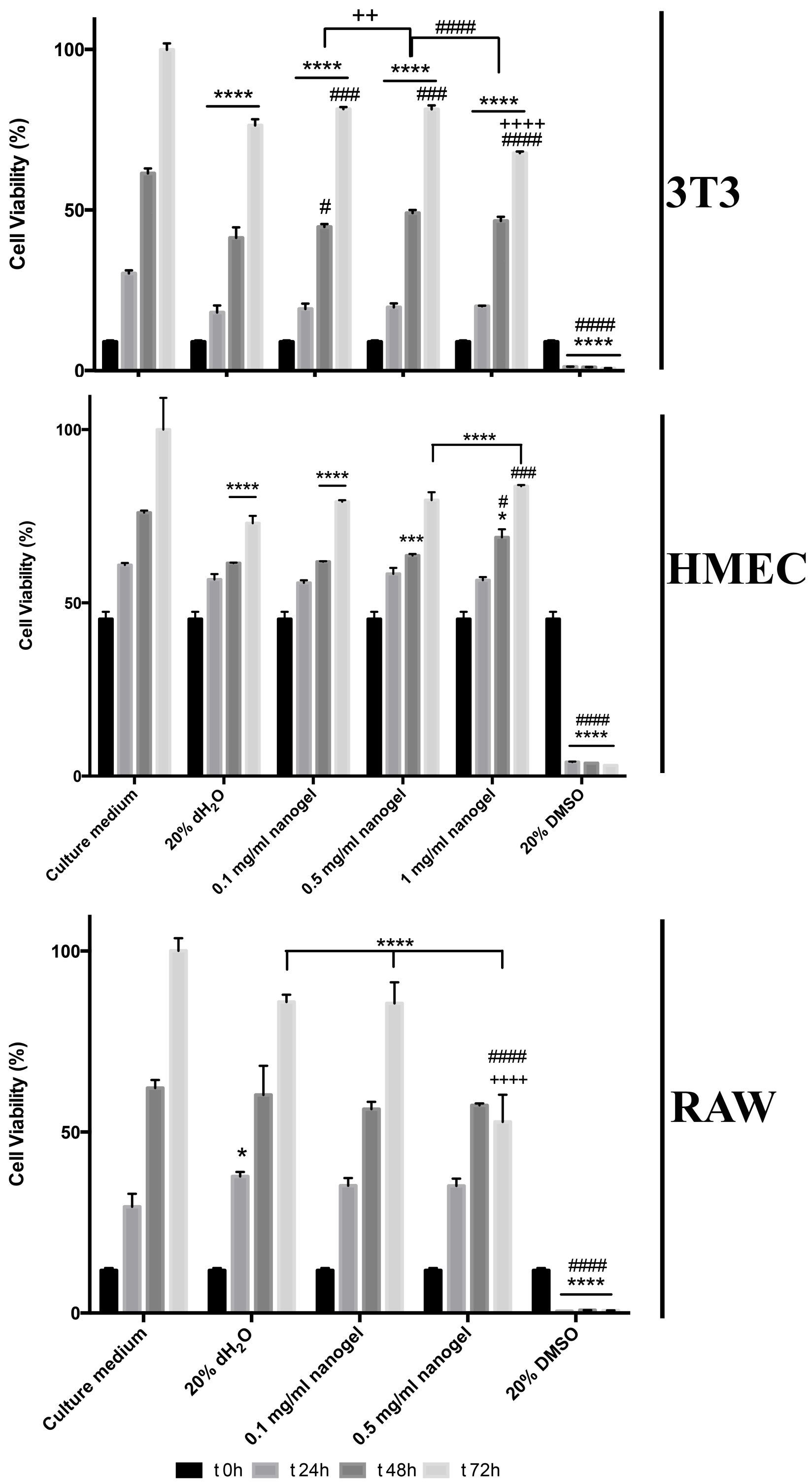

Figure 2: Cell viability of 3T3, HMEC and RAW cells determined by MTT assay as to exposure to HyA-AT nanogel at 0.1 to 1 mg/ml concentration. Non-treated cells referred to as culture medium are considered 100% cell viability at 72h. Statistical analysis was performed using a two-way ANOVA and a Tukey's

comparison test. Differences between samples and culture medium at any given time point are represented by (*); whereas differences between samples and 20% dH_2O diluted control at any given time point are represented by (#); differences between nanogel concentration are represented by (+).

3.2.2. EVALUATION OF MEMBRANE CELL INTEGRITY

The evaluation of cell membrane integrity was performed by LDH release assay. As shown in figure 3, membrane integrity was preserved at all nanogel concentrations for all cell lines. This indicates that the nanogel did not affect membrane stability in any of the cells tested – 3T3, HMEC and RAW. According to Fotakis and Timbrell [15], LDH release is not as sensitive as the MTT assay and requires higher concentration of sample or longer incubation time for the detection of cytotoxic effects. However, even at high nanogel dosage such as 1mg/ml, any effect was observed.

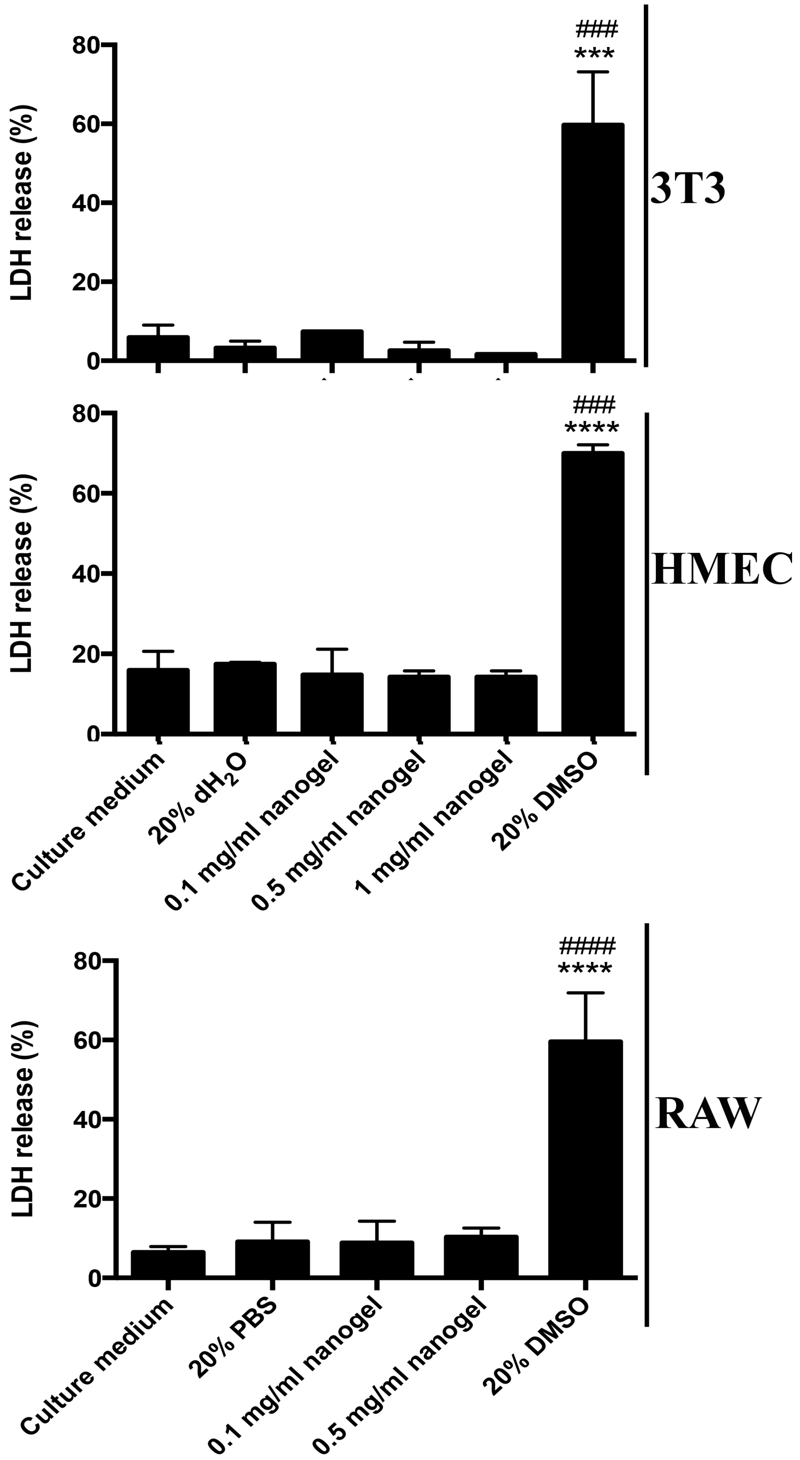

<u>Figure 3:</u> Cell membrane integrity of 3T3, HMEC and RAW cells determined by LDH release assay as to exposure to HyA-AT nanogel at 0.1 to 1 mg/ml concentration. Results are present as LDH release percentage after 24h sample incubation. Statistical analysis was performed using a t-test. Differences

between samples and culture medium are represented by (*); whereas differences among samples and 20% dH_2O control are represented by (#).

3.2.3. APOPTOSIS ASSAY

Nanogel induced apoptosis was determined by annexin V-FITC and PI double staining resorting to flow cytometry. Early apoptosis is characterized by plasma membrane reorganization (translocation of phosphatidylserine to the external surface), detected by positive staining for Annexin V-FITC. In later stage of apoptosis cells present membrane damage, therefore PI can bind to DNA in cytoplasm resulting in positive staining for both Annexin V and PI [25]. In all cell lines tested no significant effect by nanogels presence was noticed in comparison with the negative control (20% water diluted culture medium). Nanogel interaction with HMEC cells caused a slight increase in only late apoptic population (Annexin V positive) regarding control cells. The observed effect was indeed dose dependent.

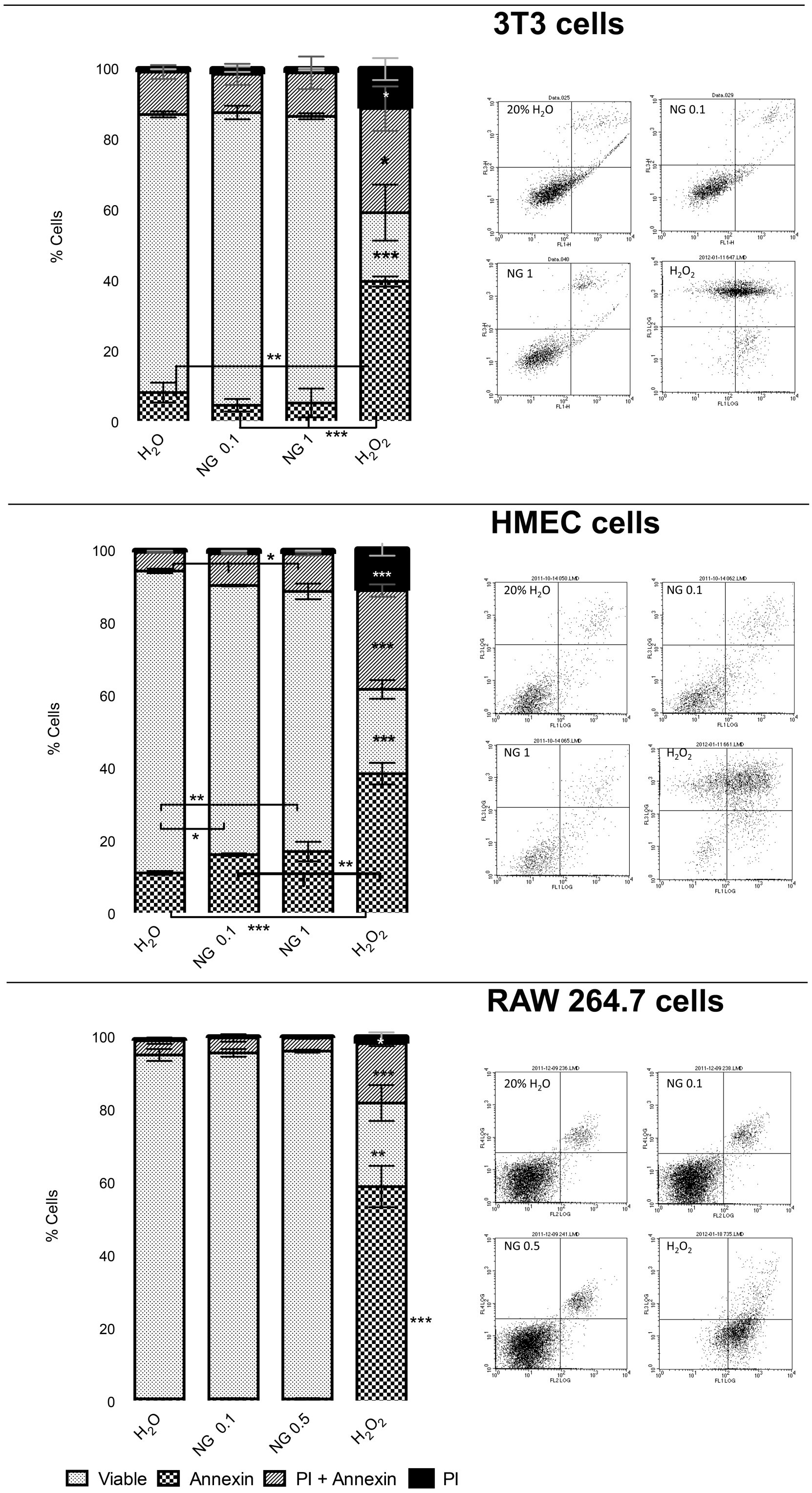

Figure 4: Flow cytometry analysis of 3T3, HMEC and RAW cell line for the presence or absence of the Annexin v-FITC and/or PI markers. Cells were previously incubated with two different nanogel concentrations for 24h. A

negative control with 1:5 distilled water-diluted culture medium and hydrogen peroxide was used as apoptosis positive control. Statistical analysis was performed using a t-test and a Tukey's comparison test. Differences between samples and culture medium are represented by (*). Dot Plots of the correspondent cell lines are presented at the right side of the image. Top left quadrants matches annexin V negative and PI positive cells (legend: PI); top right quadrants corresponds to late apoptotic cells that express annexin V and PI positive (legend: Annexin + PI); bottom right quadrants pairs with apoptotic cells that express annexin V positive and PI negative (legend: annexin); and for last, bottom left quadrants, viable cells that doesn't express neither annexin V or PI.

3.3. Complement activation

The nanogel effect on the complement cascade activation was evaluated by the cleavage of C3, which is a marker for both activation pathways. Western blot analysis for the presence of the C3 fragment was performed after incubation of the HyA-AT nanogel (at 1 mg/mL concentration) with human plasma. The results are shown in Figure 5. The upper band of 115 kDa corresponds to the intact C3 factor and the one with 43 kDa to the main degradation product. The protein degradation was quantified considering the intensity of the band at 43 kDa normalized to the value obtained with the positive control (cobra venom factor). As could be observed in Figure 5, the percentage of C3 cleavage product(s) was similar to those found in the negative control, so it may be concluded that the nanogel does not activate the complement system.

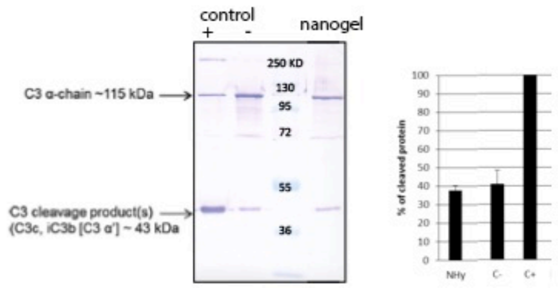

Figure 5: Analysis of HyA nanogel complement activation through C3 protein cleavage by western blot. A) Western blot membrane is presented on the left and B) graphical representation of the % of C3 protein as comparison to PBS and Cobra venon, negative and positive controls, respectively.

3.4. Murine bone marrow derived macrophages nanogel uptake

The phagocytic recognition and nanogel uptake by BMDM was investigated by confocal microscopy. Murine BMDM are extensively used as a phagocytic model due to its peculiar capacity of internalizing extracellular materials by a wide range of mechanisms and entry routes [26]. Macrophages were incubated with Dextrin-FITC labelled nanogel (Figure 6a), native HyA-Fluorescein labelled (Figure 6b), and HyA-AT-Fluorescein labelled nanogel (Figure 6c), the different formulations (used at the same concentration) presenting similar levels of fluorescence. Also, untreated cells were observed, as a control (figure 6d). Gonçalves,

C. et al. [18] have demonstrated that dextrin nanogels were extensively recognised and internalized by BMDM. Therefore, dextrin-FITC labelled nanogel was used as a positive control (Figure 6a). As it was expected, the dextrin nanogel incubated BMDM cells presented an intense green staining, demonstrating much higher internalization than the HyA-AT nanogels. Interestingly, the native HyA was slightly more internalized by BMDM than HyA-AT nanogel (Figure 6). This result suggests a promising behaviour *in vivo*, *i.e.*, the ability of the nanogel to escape blood clearance and exhibit a large circulation time in the vascular system.

a b c d

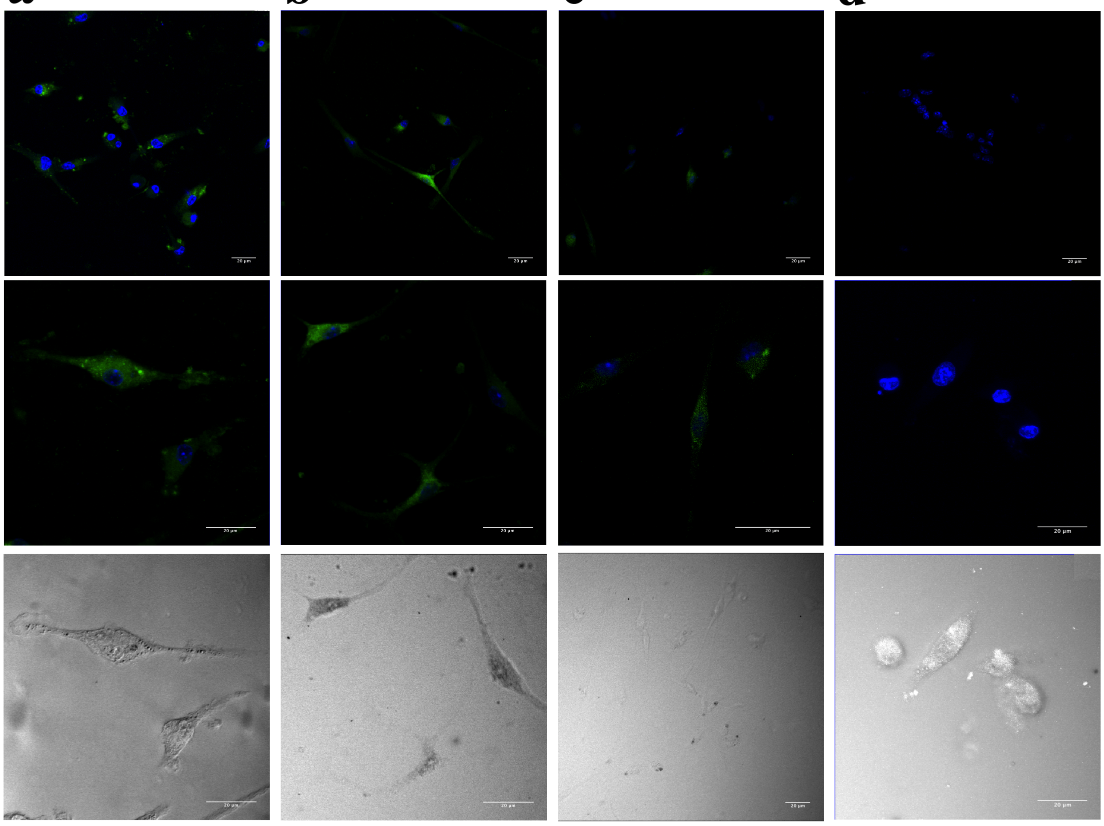

Figure 6: Fluorescence images of murine BMDM obtained by confocal microscopy, incubated for 6h 0.2 mg/ml suspension of: dextrin nanogel (a); native HyA (b); hyaluronic acid nanogel (HyA-AT) (c); and untreated cells, as a

control (d). Cells nucleus was stained blue with DAPI, 120ng/mL. The green fluorescence is due to the fluorescein labelled samples.

3.5. HEMOCOMPATIBILITY STUDY

Experiment was performed in agreement with the Standard Practice for Assessment of Haemolytic Properties of Materials from the American Society for Testing Materials (ASTM F756-00, 2000). Nanogel proved to be non-haemolytic at the concentrations tested, since the corrected haemolytic index is inferior to 5% (Figure 7). Still, as compared to the negative control, no visible haemolytic effect was observed in the presence of the nanogel.

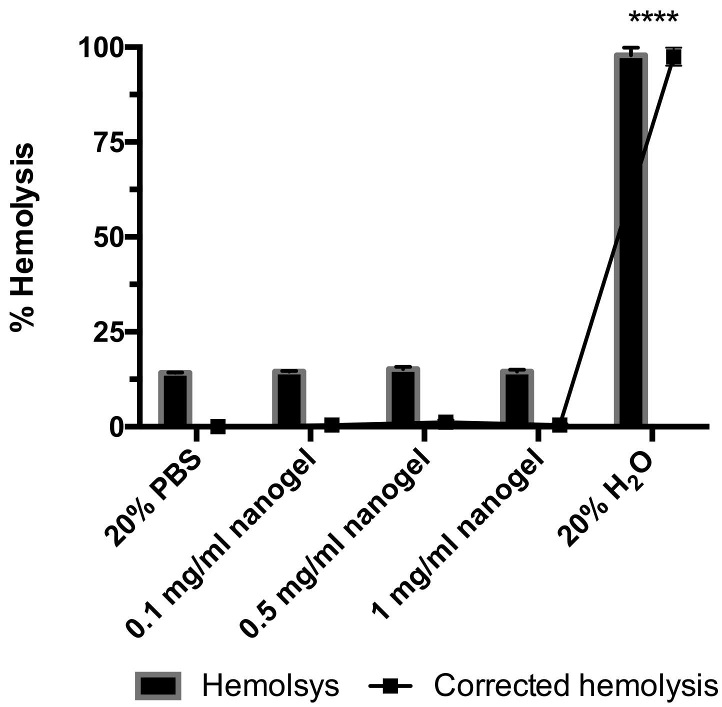

Figure 7: Blood hemolysis index of whole human blood from healthy donors after incubation with 0.1 until 1 mg/ml HyA-AT nanogel dispersions and 1:5 PBS

diluted culture medium and hydrogen peroxide as negative and positive control, respectively.

3.6. IN VIVO NANOGEL BIODISTRIBUTION PROFILE

In vivo biodistribution analysis is an important tool to assess the potential of nanocarriers as delivery systems [27]. Nude mice were intravenously injected in the tail vein (5mg/kg animal weight). Native HyA-Cy 5.5 was used as a control and administered following the same protocol.

In vivo biodistribution was monitored non-invasively as a function of time, over a period of 48h (Figure 8a). At each time point, NIRF images of the whole animal were obtained and blood samples were also collected, from every animal, by retro-orbital punction. By the analysis of the whole body images we can say that the animals treated with the nanogel seem to exhibit higher fluorescence intensity at all time points, in comparison to native HyA treated animals, as further confirmed by observing the blood-collected samples. In fact, 24h post injection, the native HyA fluorescence was almost absent from mice whole body (Figure 8a) and undetectable in the blood (Figure 8c), proving its fast clearance.

It is interesting to note that some fluorescence signal is detectable in nanogel treated animals even after 24h, indicating a fairly long half-live in the circulatory system, relevant for the development of drug delivery systems.

Each organ of the mice was withdrawn at 48 h post-injection, and *ex vivo* fluorescence images were obtained (Figure 8). For both

HyA polymer and HyA-AT nanogel strong signals were observed in the lung mostly, but also in the skin and kidney. Weak intensities were observed in heart, spleen and liver, while in the brain no fluorescence signal was detected. This result is consistent with the BMDM internalization studies, which suggest fairly poor recognition of the nanogel, and thus ability to evade the mononuclear phagocytic system. Concerning the observed nanogels accumulation in the lungs, other researchers[28-31] have also reported lung accumulation of nanoparticles, when labeled with Cy5.5 probe. We were able to further clarify the influence of NIR probe - namely Cy5.5 and Alexa Fluor 680 – on the nanogels pharmacokinetics (to be shown elsewhere) and assign the accumulation in the lungs to the probe and not to the nanogel itself.

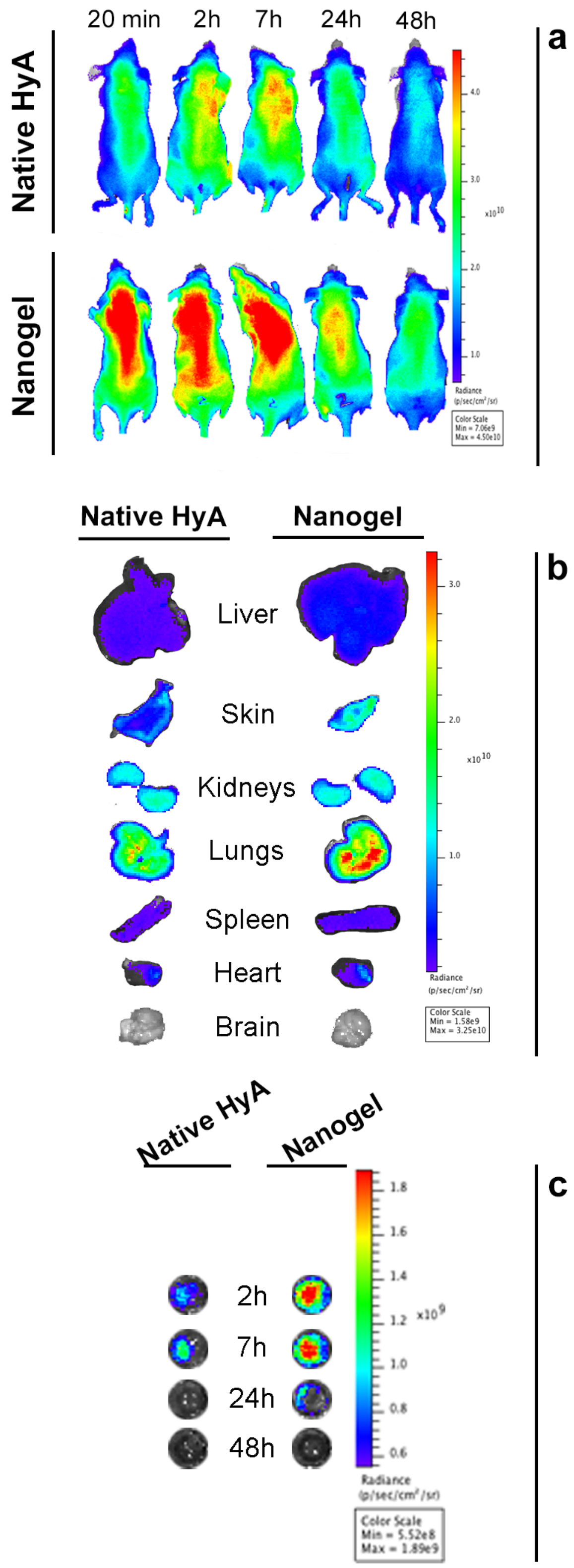

Figure 8: *In vivo* and *ex vivo* biodistribution profile of HyA-AT nanogel and native HyA. a) Whole body NIRF images of CD1-Foxn1nu mice treated with native HyA labeled with Cy5.5 hydrazide and HyA-AT nanogel also labeled with the same

fluorophore. Top row of animals were administered with native HyA and bottom row with HyA-AT nanogel. b) Ex vivo NIRF images of the organs – Liver, Skin, Kidneys, Lungs, Spleen, Heart and Brain -, 48h post sample injection. a) Blood sample collected by retro-orbital punction at established time point post sample administration, analysed in NIRF equipment.

4. Conclusion

Amphiphilic HyA-AT conjugate was successfully synthetized and self-assembled onto nanostructures with desirable features for drug delivery applications. The engineered nanogel was extensively characterized as for its biocompatibility. Mitochondrial metabolic activity measurements revealed that only for RAW cells challenged with the highest nanogel concentration at the highest incubation time (72h), a slight reduction on growth rate was observed. However, this effect was not corroborated by membrane integrity evaluation or apoptosis induction. As a matter a fact, in all the cell lines tested and at all the time points it is not perceptible any inhibitory effect. Also, HyA-AT nanogel did not induce the activation of the complement system, was poorly recognized and internalized by BMDM and did not cause hemolysis. *In vivo* biodistribution studies demonstrated the nanogel has a fairly long circulation time, and can be detected in the blood flow up to 48h. These findings suggest that the nanogel can be a promising drug delivery nanosystem.

5. ACKNOWLEDGMENTS

The authors thank the FCT Strategic Project of UID/BIO/04469/2013 unit, the project RECI/BBB-EBI/0179/2012 (FCOMP-01-0124-FEDER-027462) and the Project "BioHealth - Biotechnology and Bioengineering approaches to improve health quality", Ref. NORTE-07-0124-FEDER-000027, co-funded by the Programa Operacional Regional do Norte (ON.2 – O Novo Norte), QREN, FEDER. We would like to acknowledge also the support of FCT for the PhD grant reference SFRH/BD/61516/2009. We would also like to thank Bioimaging department on Molecular Medicine Institute (IMM) in Lisbon, namely Dr José Rino and Dr António Temudo. Also thank the animal facilities in IMM (Lisbon), specially Drª Dolores Bonaparte and Drª Joana Marques.

Finally, the authors thank Dr Africa Gonzalez and Mercedes Pelletero the performance of the studies on the activation of complement.

6. BIBLIOGRAPHY

1. Zolnik, B.S., et al., *Nanoparticles and the immune system.* Endocrinology, 2010. **151**(2): p. 458-65.
2. Pujalte, I., et al., *Cytotoxicity and oxidative stress induced by different metallic nanoparticles on human kidney cells.* Part Fibre Toxicol, 2011. **8**: p. 10.
3. Arpicco, S., et al., *Hyaluronic acid conjugates as vectors for the active targeting of drugs, genes and nanocomposites in cancer treatment.* Molecules, 2014. **19**(3): p. 3193-230.
4. Naahidi, S., et al., *Biocompatibility of engineered nanoparticles for drug delivery.* J Control Release, 2013. **166**(2): p. 182-94.
5. Pedrosa, S.S., et al., *A novel crosslinked hyaluronic acid nanogel for drug delivery.* Macromol Biosci, 2014. **14**(11): p. 1556-68.
6. Glabe, C.G., P.K. Harty, and S.D. Rosen, *Preparation and properties of fluorescent polysaccharides.* Anal Biochem, 1983. **130**(2): p. 287-94.
7. Piatnitski Chekler, E.L., H.M. Elokdah, and J. Butera, *Efficient one-pot synthesis of substituted 2-amino-1,3,4-oxadiazoles.* Tetrahedron Letters, 2008. **49**(47): p. 6709-6711.
8. Hermanson, G.T., *Bioconjugate techniques*. 2nd edition. ed. 2008, San Diego: Academic Press. xxx, 1202 pages.
9. Ahn, B., S.G. Rhee, and E.R. Stadtman, *Use of fluorescein hydrazide and fluorescein thiosemicarbazide reagents for the fluorometric determination of protein carbonyl groups and for the detection of oxidized protein on polyacrylamide gels.* Anal Biochem, 1987. **161**(2): p. 245-57.
10. Na, K., et al., *Synergistic effect of TGFbeta-3 on chondrogenic differentiation of rabbit chondrocytes in thermo-reversible hydrogel constructs blended with hyaluronic acid by in vivo test.* J Biotechnol, 2007. **128**(2): p. 412-22.
11. Luo, Y. and G.D. Prestwich, *Synthesis and selective cytotoxicity of a hyaluronic acid-antitumor bioconjugate.* Bioconjug Chem, 1999. **10**(5): p. 755-63.
12. Carvalho, V., et al., *Self-assembled dextrin nanogel as protein carrier: controlled release and biological activity of IL-10.* Biotechnol Bioeng, 2011. **108**(8): p. 1977-86.
13. Cerca, F., et al., *Staphylococcus epidermidis biofilms with higher proportions of dormant bacteria induce a lower activation of murine macrophages.* J Med Microbiol, 2011. **60**(Pt 12): p. 1717-24.
14. Mosmann, T., *Rapid colorimetric assay for cellular growth and survival: application to proliferation and cytotoxicity assays.* J Immunol Methods, 1983. **65**(1-2): p. 55-63.

15. Fotakis, G. and J.A. Timbrell, *In vitro cytotoxicity assays: comparison of LDH, neutral red, MTT and protein assay in hepatoma cell lines following exposure to cadmium chloride*. Toxicol Lett, 2006. **160**(2): p. 171-7.
16. Piao, S., Y.N. Cha, and C. Kim, *Taurine chloramine protects RAW 264.7 macrophages against hydrogen peroxide-induced apoptosis by increasing antioxidants.* J Clin Biochem Nutr, 2011. **49**(1): p. 50-6.
17. Chang, Y., et al., *In vitro toxicity evaluation of graphene oxide on A549 cells.* Toxicol Lett, 2011. **200**(3): p. 201-10.
18. Goncalves, C., et al., *Dextrin nanoparticles: studies on the interaction with murine macrophages and blood clearance.* Colloids Surf B Biointerfaces, 2010. **75**(2): p. 483-9.
19. International, A., *Practice for Assessment of Hemolytic Properties of Materials*. 2000, ASTM International.
20. Pereira, P., et al., *Biocompatibility of a self-assembled glycol chitosan nanogel.* Toxicol In Vitro, 2015. **29**(3): p. 638-46.
21. Singh, R.P. and P. Ramarao, *Cellular uptake, intracellular trafficking and cytotoxicity of silver nanoparticles.* Toxicol Lett, 2012. **213**(2): p. 249-59.
22. Sohaebuddin, S.K., et al., *Nanomaterial cytotoxicity is composition, size, and cell type dependent.* Part Fibre Toxicol, 2010. **7**: p. 22.
23. Kim, T.H., et al., *Mannosylated chitosan nanoparticle-based cytokine gene therapy suppressed cancer growth in BALB/c mice bearing CT-26 carcinoma cells.* Mol Cancer Ther, 2006. **5**(7): p. 1723-32.
24. Choi, K.Y., et al., *Smart nanocarrier based on PEGylated hyaluronic acid for cancer therapy.* ACS Nano, 2011. **5**(11): p. 8591-9.
25. Lee, M.K., S.J. Lim, and C.K. Kim, *Preparation, characterization and in vitro cytotoxicity of paclitaxel-loaded sterically stabilized solid lipid nanoparticles.* Biomaterials, 2007. **28**(12): p. 2137-46.
26. Firdessa, R., T.A. Oelschlaeger, and H. Moll, *Identification of multiple cellular uptake pathways of polystyrene nanoparticles and factors affecting the uptake: relevance for drug delivery systems.* Eur J Cell Biol, 2014. **93**(8-9): p. 323-37.
27. Choi, K.Y., et al., *Self-assembled hyaluronic acid nanoparticles for active tumor targeting.* Biomaterials, 2010. **31**(1): p. 106-14.
28. Hue, J.J., et al., *Distribution and accumulation of Cy5.5-labeled thermally cross-linked superparamagnetic iron oxide nanoparticles in the tissues of ICR mice.* J Vet Sci, 2013. **14**(4): p. 473-9.
29. Lee, C.M., et al., *Optical imaging to trace near infrared fluorescent zinc oxide nanoparticles following oral exposure.* Int J Nanomedicine, 2012. **7**: p. 3203-9.
30. Lee, H., et al., *Thermally cross-linked superparamagnetic iron oxide nanoparticles: synthesis and application as a dual imaging probe for cancer in vivo.* J Am Chem Soc, 2007. **129**(42): p. 12739-45.

31. Iqbal, U., et al., *Molecular imaging of glioblastoma multiforme using anti-insulin-like growth factor-binding protein-7 single-domain antibodies.* Br J Cancer, 2010. **103**(10): p. 1606-16.

CHAPTER IV

TARGETABILITY OF HYALURONIC ACID NANOGEL TO CANCER CELLS: IN VITRO AND IN VIVO STUDIES

Adapted from
Pedrosa, S. S.[1*], Pereira, P.[1], Correia, A.[2] and Gama, F.M[1]
Submitted work

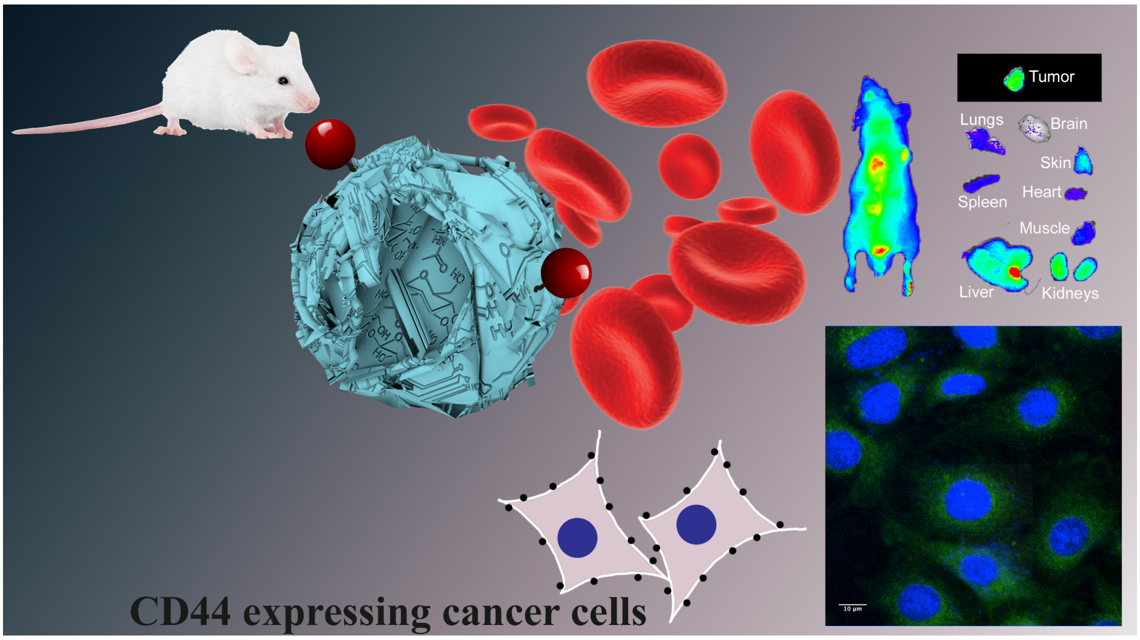

ABSTRACT

We have, in previous work developed, characterized and evaluated the biocompatibility of an engineered hyaluronic acid nanogel. Here we assess the targetability of a hyaluronic acid nanogel towards CD44 overexpressing cells, *in vitro* and *in vivo*. Results obtained by flow cytometry and confocal fluorescence microscopy shows that nanogel is internalized more effectively by CD44 overexpressing cells (A549). The biodistribution and tumour targetability of the nanogel labelled with a near-infrared (NIR) probe was performed, in mice, through a non-invasive imaging system. Results revealed nanogel high targetability towards an induced subcutaneous A549 tumour. Nanogels pharmacokinetics was evaluated also in healthy animals, and Alexa Fluor 680 labelled nanogel exhibited higher accumulation in liver, kidneys and skin. Also, a comparative biodistribution study was performed, using two NIR imaging probes, Cy5.5 and Alexa Fluor 680.

1. Introduction

Hyaluronic acid is a naturally occurring polysaccharide, ubiquitous in the human body, widely used in biomedical applications as a conjugate, hydrogel, nanogel and many other applications. Hyaluronic acid demonstrates appealing biological properties such as, biocompatibility, biodegradability and non-immunogenicity [1]. Among the most attractive features of hyaluronic acid applied to nanomaterials is its potential for active targeting [2]. The strong affinity of hyaluronic acid for cell surface receptors, namely CD44 and Receptor for Hyaluronan Mediated Motility (RHAMM), has been demonstrated [2, 3]. The CD44 receptor is a glycoprotein overexpressed in the cell membrane of numerous cancer cells and important in the metastization process [1, 2]. Therefore, we have developed a hyaluronic acid nanogel by grafting a thiolated hydrophobic chain in the polysaccharide backbone. The amphiphilic conjugate self assembles in aqueous environment onto nanostructures. The nanogel has already proven to be crosslinkable by disulfide bond and its physicochemical characterization has already been addressed [4]. Also, *in vitro* and *in vivo* biocompatibility of the engineered nanogel has also been demonstrated (in press). In this work, we intend to assess the nanogel targetability mediated by hyaluronic acid interface towards CD44 overexpressing cancer cells. Non-small cancer lung cells - A549 cell line – express high levels of CD44 receptors [1, 5] and therefore, were used as a target for nanogel uptake studies. The *in vitro* cellular uptake of nanogel by A549 cells was assessed by flow cytometry analysis and confocal fluorescence microscopy. Also, we investigated the nanogel targetability in tumor bearing mice - induced with subcutaneous A549 cells tumour. The biodistribution was analyzed in a non-invasive real time NIR imaging system, after intravenous administration of probe labeled samples. NIR probes have the advantage of high depth penetration, high fluorescence intensity and amenable selfquenching [6]. Studies have shown that changes in particle size, surface charge, texture and heterogeneity in nanoparticles formulation influence its biodistribution [7]. Therefore, we also performed a comparative study of *in vivo* pharmacokinetics of the HyA nanogel, native HyA and free probe in healthy animals, using two different NIR probes, namely Cy5.5 and Alexa Fluor 680.

2. Materials

Sodium hyaluronate (MW.7.46 kDa) was purchased from Lifecore Biomedical (USA).1-ethyl-3-[3 dimethylaminopropyl]carbodiimide hydrochloride (EDC), Cysteamine hydrochloride, trypan blue, 3-(4,5-dimethylthiazol-2-yl)-2,5-diphenyl tetrazolium bromide (MTT), hydrogen nicotinamide adenine dinucleotide (NADH) and pyruvate were purchased from Sigma-Aldrich (Italy).
Cy 5.5 hydrazide was purchased from GE Healthcare (UK). Fluorescein-5-thiosemicarbazide and Alexa Fuor 680 C_2 maleimide acquired from Thermo Fisher Scientific/Life Technologies (USA).
Cell Culture materials were purchased from Biochrom (Germany).
Animals were acquired from Charles River (Germany) and maintained in Molecular Medicine Institute (Lisbon) Rodents Facility.

3. Methods

3.1. Cell lines and cell culture

Human alveolar adenocarcinoma cells (A549) were maintained in Dulbecco's modified Eagle's media (DMEM) supplemented with 10% (v/v) of heat-inactivated foetal bovine serum (FBS), 100 IU/mL penicillin and 0.1 mg/mL streptomycin. Cystic fibrosis bronchial epithelial cells (CFBE) were cultured in Roswell Park Memorial Institute (RPMI) 1640

Medium supplemented with 10% (v/v) of heat-inactivated FBS, penicillin and streptomycin. The cells were maintained as a subconfluent monolayer in a humidified atmosphere containing 5 % CO_2 at 37 °C.

3.2. In vitro cell toxicity

Nanogel toxicity in A549 cell line was assessed through 3-[4,5-dimethylthiazol-2-yl]-2,5-diphenyl tetrazolium bromide (MTT) reduction assay [8] and lactate dehydrogenase (LDH) release assay [9].

3.2.1. Cell proliferation assay

A549 cells were seeded in 24-well cell culture plates at a density of 1×10^4 cells per well and left adhering in 0.5mL of adequate culture medium overnight. HyA-AT nanogel 0.1mg/ml, 0.5 mg/ml and 1mg/ml dispersions were suspended in adequate culture medium, resulting in a 1:5 fresh medium dilution. Untreated cells were used as control of 100% cell viability and 20% distilled water control was used to access the effect of water dilution of samples containing the nanogel. A positive control with 20% of DMSO was used in every analysis. The samples were incubated for 24, 48 and 72 hours and the cells metabolic activity is calculated due to the reduction of tetrazolium salt of MTT by mitochondrial succinate dehydrogenase enzymes of metabolically active cells. To which well, 10% (v/v) of a MTT solution (5 mg/ml in PBS) was added and it was incubated at 37°C and 5% CO_2 for a period of 4 hours. In this period of time, the tetrazolium salt is bioreduced to a formazan product that consists in is dark blue crystals that are insoluble in the culture medium. The supernatant was discarded slowly and the crystals were solubilized in dimethyl sulfoxide and quantified spectrophotometrically at 570 nm. The experiments were performed in triplicates as the results are presented as percentage in which 100% viability corresponds to the non-treated cells.

3.2.2. LDH RELEASE ASSAY

Cells were seeded in 12-well plate at a density of the $2x10^5$ cells per well and allowed to settle overnight in 0.5 mL of adequate culture medium. Then, cells were treated with nanogel dispersions with a concentration of 0.1 and 1.0 mg/ml in suitable culture medium and supplementation. Untreated cells were used as control of 100% cell viability. Another control with 20% distilled water was used to access the effect of the water dilution of the samples containing the nanogel. A control with 20% of DMSO was used in every analysis as a positive control. The samples where incubated for 24 hours and after that period each culture medium from every well was collected and centrifuged at 13000 rpm for 1min and the cell free supernatant was collected and stored on ice for further analysis – Extracellular LDH. Cells were scraped with a Tris solution (15mM) extracellular and further lysed by sonication. The resulting supernatants were used to quantify the LDH present - Intracellular LDH. An aliquot of extracellular (40 µL) or intracellular (10 µL) LDH were assigned into a microplate and 250 µL of the NADH solution 0.31 mM in phosphate buffer 0.05 M, pH7.4 added to each well. Lastly, 10 µL of an 8.96 mM piruvate solution in phosphate buffer (substrate solution) was added and immediately afterwards the variation of the absorbance at 340 nm was read in a microplate spectrophotometer system, as to determine the rate of NADH consumption (slope of the line). LDH leakage was expressed as the ratio between extracellular and total LDH, corresponding the inverse value to the cell membrane integrity. Each experiment was performed in triplicate.

3.3. IN VITRO CELLULAR UPTAKE

The cellular uptake was evaluated by flow cytometry (FCM) analysis, confocal fluorescence microscopy and Trypan Blue exclusion assays.

3.3.1. SYNTHESIS OF FLUORESCEIN LABELLED NANOGEL

Hyaluronic acid nanogel (HyA-AT) synthesis was described elsewhere [4]. HyA-AT nanogel was conjugated with Fluorescein-5-thiosemicarbazide for *in vitro* cellular studies. Thiosemicarbazide group of the probe reacted with carboxylic group of hyaluronic acid nanogel in presence of EDC as a coupling agent. The theoretical labelling degree, defined by the ratio between probe and the nanogel, was 0.25. The lack of unconjugated fluorescein was confirmed by ultrafiltration through a 2 KDa MW cut-off membrane. In filtrate and concentrate, probe emission was measured spectrophotometrically and the absence of fluorescence signal was achieved in the last filtrate [10, 11].

3.3.2. FLOW CYTOMETRY ANALYSIS

Quantitative cellular uptake of nanogel in CD44 expressing (A549) and non-expressing cells (CFBE) was conducted in a Coulter Epics XL Flow Cytometer (Beckman Coulter Inc., Miami, FL, USA). Cells were seeded in 24-well plates at 1.0×10^5 density and incubated overnight to allow attachment. Culture medium was removed and A549 cells were incubated with culture medium containing 0.2 mg/mL and 0.5 mg/mL of HyA-AT nanogel, for designated time intervals. Then, CFBE cells were processed similarly using a concentration of 0.5 mg/mL of nanogel. After 0 and 30 minutes, 1, 2, 3, 5, 7 and 24 hours, culture medium was removed and cells were rinsed with PBS. Cells were then harvested by trypsinization, collected with FBS supplemented culture medium and centrifuged at 300g for 10 minutes. Supernatant was rejected and cells were washed with PBS twice and finally ressuspended in flow cytometry staining buffer prior to analysis. Cells were gated based on size vs granularity (Forward Scattered/ Side Scattered, FSC/SSC) dot plots. The fluorescence due to nanogel internalization was evaluated in FL1 (green channel), where FL1 positive cells had internalized/adhered nanogel. Cell count was set to minimum 20,000 events. Results are expressed as mean fluorescence intensity and the frequencies (or percentage) of cells in gates of interest (n=5).

3.3.2.1. Trypan Blue exclusion assay

Trypan blue (TB) is a cell impermeable dye. The exclusion assay is based on the capability of TB to quench green fluorescence (FITC/Fluorescein) signal at the cell surface [12-14]. Therefore, TB assay allows us to distinguish between internalized and cell adhering nanogel [12, 15]. Samples, after being analysed were further incubated with 0.1% trypan blue for 1 minute. Cellular debris and aggregates were excluded by FSC/SSC gating and results were analysed in FL1/FL3 (green/red channels). Results are expressed as mean fluorescence intensity of the FL1 signal (n=5).

3.3.3. Confocal fluorescence microscopy

Cellular uptake of HyA-AT nanogel labelled with fluorescein was evaluated using $CD44^{+}$ - A549 cells [16-18] and $CD44^{-}$ cells – CFBE [19].
Cells were seeded on coverslip discs in 24 well plates at 5×10^{5} cells/well density. HyA-AT-Fluoresceín (0.2 mg/mL concentration) was incubated with cells for 7 hin adequate culture medium and atmosphere conditions. To further assess if the nanogel uptake was mediated by hyaluronic acid receptors, we performed a competitive study with free

hyaluronic acid, in A549 cells. So, we pre-incubated A549 cells with 10 mg/mL free HyA dispersed in culture medium, for 1 hour prior to nanogel addition. The culture medium was removed and replaced with 0.2 mg/mL of nanogel, and incubated for 7h. Then, medium was removed and cells were rinsed twice with PBS and fixed with a 2% para-formaldehyde solution (in PBS). After 20 minutes, cells were again washed twice with cold PBS. Cell nucleus were stained with 4',6-diamidino-2-phenylindole (DAPI, 120 ng/mL) for 3 minutes at room temperature. Cell seeded coverslips were observed in a confocal laser scanning microscope Leica SP2 AOBS SE (Leica Mycrosystems, Germany).[13, 15]

3.4. In vivo spectral imaging studies

3.4.1. Animals and treatments

All animal experiments were performed in compliance with the Portuguese General alimentary and Veterinarian Board (authorization number 006315/27/03/2014, from DGAV-Portugal) and animals were kept and used strictly in accordance with National rules and the European Communities Council Directive (86/609/EEC), for the care and handling of laboratory animals. Balb/cByJ 6-week old male mice and CD1 nude crl:CD1nude 6-week old mice were acquired from Charles River (Germany) and maintained in Molecular Medicine Institute (Lisbon) Rodents Facility. Animals were divided into groups (n=5), for different time point analysis and samples administration. The following samples were tested: nanogels HyA-AT-Cy5.5 and HyA-AT-Alexa680; native HyA-Cy5.5 and HyA-Alexa680; free Cy 5.5 and Alexa680. The labelled nanogels (HyA-AT-Cy5.5 and HyA-AT-Alexa680) were dispersed in saline solution and filtered through cellulose acetate syringe filter (pore size 0.22 μm) in aseptic conditions and its size distribution analysed by DLS. All the samples were administered intravenously through the tail vein at 5 mg/kg body weight, as described by several authors [20-22]. Samples labelling intensity was compared by UV/Vis spectroscopy at probes maximum excitation wavelength to compare their intensity.

3.4.2. Synthesis of Alexa Fluor labelled hyaluronic acid and hyaluronic acid nanogel

Alexa Fuor 680 C_2 maleimide is a thiol reactive conjugate used for NIR probing. Maleimide undergoes an alkylation reaction with sulfhydryl groups to form a thioether bond [23]. HyA-AT nanogel is a thiolated hyaluronic acid conjugate and therefore, its thiol group reacts directly with maleimide moiety of the probe. Native hyaluronic acid had to be modified to become reactive towards the maleimide reactive probe. Therefore, similarly to the nanogel synthesis [4] cysteamine hydrochloride was grafted by amide bond formation to the carboxylic acid residue of native hyaluronic acid. In brief, HyA-TBA salt was dissolved in DMSO and reacted with cysteamine hydrochloride (10:1) in presence of EDC and NHS (equimolar amounts). The solution was dialysed against a NaCl solution and then dH_2O and lyophilized. Resulting thiolated native HyA was conjugated with the probe by the same chemistry.

Hence, 10 mg of nanogel and native HyA reacted with 0.4 mg (2% theoretical labelling) of Alexa Fuor 680 C_2 maleimide in 0.1 M PBS solution (pH 7.4). Reaction was allowed to occur overnight at room temperature and protected from light. Afterwards, solutions were dialysed through a 2 KDa cutoff membrane to remove the unreacted probe. Confirmation was obtained by ultrafiltration and UV/VIS analysis of the solutions collected from the upper and lower compartments. Samples were analysed spectrophotometrically at 679 nm. [24] [10, 25, 26]

3.4.3. Synthesis of Cyanine (Cy 5.5) labelled hyaluronic acid and hyaluronic acid nanogel

HyA nanogel and native HyA were labelled with Cy 5.5 – hydrazide. Hydrazide reactive moiety was conjugated with carboxylic groups of HyA-AT nanogel [10, 27-29] in presence of EDC, as coupling agent. The molar ratio of Cy 5.5 - hydrazide to free carboxylic acid groups of HyA-AT nanogel and native HyA was 0.25. EDC was also added at an equimolar ratio to the free carboxylic acid groups of HyA-AT nanogel. The reaction was allowed to occur overnight at room temperature, in the dark. The reaction mixture was thoroughly dialysed (MW cut-off 2 000 Da) against distilled water to remove non-desired reaction products. Also, the absence of unconjugated dye was confirmed by ultrafiltration through a 2 KDa MW cut-off membrane. Samples labelling was assessed spectrophotometrically at 649 nm. Samples labelling was assessed spectrophotometrically at 649 nm. [6, 30] [31, 32]

3.4.4. Comparison of pharmacokinetics of Cy5.5 and Alexa Fluor 680

To evaluate the possible differences in biodistribution profile of nanogel when labelled with chemically different NIRF probes, two probes were analysed - Cy 5.5 and Alexa680. Therefore, HyA-AT nanogel and native HyA were labelled with Cy5.5 hydrazide or Alexa680. Free probe was also analysed to infer its *in vivo* biodistribution profile. Samples were administrated to BALB/c mice at 5 mg/Kg BW through the tail vein. At established intervals (20 minutes, 2, 7, 24 and 48 hours) mice were anesthetised with Ketamine/Medetomidine and whole body NIR fluorescence images were acquired. At the final time point (48 hours after sample administration) animals were sacrificed and major organs - liver, lung, spleen, kidney, skin, muscle, heart and brain -, and also blood samples were collected for analysis. NIRF images of dissected organs and blood were obtained and fluorescence intensity quantified by ROI measurement. *In vivo* real time NIR fluorescence images of the animas were acquired in a Xenogen's IVIS® Lumina Series and Living Image® Software. Imaging was obtained under the following settings: excitation passband of 615–665 nm and emission passband of 695–770 wavelength; exposure time was set to 1 sec, pixel binning medium and lens aperture (f/stop) 16.

All values are presented as average fluorescence intensity (p/s/cm^2/sr) +/- SD for n=5 animals.

3.4.5. STUDY OF IN VIVO NANOGEL PHARMACOKINETICS IN HEALTHY ANIMALS

We proposed to assess HyA-AT nanogel biodistribution profile in comparison to native HyA after intravenous administration, using free NIR fluorescent probe as control. BALB/c mice were injected in the tail vein with Alexa680 labelled HyA-AT nanogel (HyA-AT-Alexa680) and native HyA (HyA-Alexa680) at 5 mg/Kg BW. At established time points – 5 minutes, 1, 8, 24 and 48 hours – animals (n=5) were anesthetised to remain immobile with Ketamine 75 mg/KgBW and Medetomidine 1 mg/KgBW intraperitonealy. *In vivo* real time NIR fluorescence images of the animas were acquired in a Xenogen's IVIS® Lumina Series and Living Image® Software. After, whole blood was harvested by cardiac puncture and *ex vivo* organ collection was performed. Major organs - liver, lung, spleen, kidney, skin, muscle, heart and brain were collected and further analysed. NIRF images of dissected organs and blood were obtained, and fluorescence intensity quantified by ROI measurement. All values are presented as average fluorescence intensity (p/s/cm^2/sr) +/- SD for n=5 animals.

3.4.6. Study of nanogel targetability in tumor xenograft animals

In vivo tumour targetability of HyA-AT nanogel was assessed in CD1 nude mice with A549 subcutaneous induced tumour. With that intent, HyA-AT nanogel and also native HyA, as a control, were labelled with Alexa Fluor 680. The animal model chosen was Crl:CD1-Foxn1nu mice, due to the lack of thymus once we intended to induce a subcutaneous xenograft tumour. Approximately 5 x 10^6 A549 cells were suspended in 100 uL of saline physiological and Matrigel (BD Biosciences, CA, USA) and were subcutaneously injected into dorsa right side of mice [5, 20, 21, 33]. Tumor mass was monitored periodically with a caliper and was calculated as V =1/2 (length × $width^2$). Animals were used in experiment when tumors size reached approximately 100 mm^3. As in previous section, HyA-AT-Alexa680 and HyA-Alexa680 labelled materials were administered and at the following time points animals were analysed: 5 minutes, 1, 8, 24 and 48 hours (n=5). Prior to image acquisition animals were anesthetised with Ketamine/Medetomidine combination. After the whole body *in vivo* image acquisition, whole blood was harvested by cardiac puncture and *ex vivo* organ collection was performed. Major organs - liver, lung, spleen, kidney, skin, muscle, heart and brain -, also the tumour mass were collected and further analysed. NIRF images of dissected organs, blood and tumour were obtained and fluorescence intensity quantified by ROI measurement. All values are presented as average fluorescence intensity (p/s/cm^2/sr) +/- SD for n=5 animals.

3.4.7. Ex vivo tissue distribution

Soon after NIR fluorescence images of mice whole body were obtained, animal's whole blood was collected through cardiac puncture. After, animals were euthanized with a lethal dose of anaesthesia and major organs were collected - liver, lung, spleen, kidney, skin, muscle, heart and brain – and tumour (in tumour targetability assay). Herein, NIR fluorescence images of dissected organs and blood were obtained in the same IVIS® Lumina equipment and fluorescence intensity quantified by ROI measurement. Similar parameters were applied in this analysis as the described in prior section. All values are presented as average fluorescence intensity (p/s/cm^2/sr) +/- SD for n=5 animals.

3.5. Statistical Analysis

The results were expressed as mean ± SD of 3 independent experiments (n=5). Statistical analysis was performed with t-test or two-way ANOVA followed by Tukey's comparison test using using GraphPad Prism version 6.00 for Mac OS X, GraphPad Software, La Jolla California USA. Significance of the results is indicated according to P values with one, two, three or four of the used symbols (*, # or +) corresponding to P=0.01 to 0.05; P=0.001 to 0.01; P=0.0001 to 0.001 and P<0.0001, respectively).

4. RESULTS AND DISCUSSION

4.1. IN VITRO CELL TOXICITY

Cell proliferation assay using MTT is a colorimetric, easy, fast and safe assay that measures the mitochondrial metabolic activity of viable cells. In figure 1a, we observed that the control with 20% water dilution presented a slightly lower cell growth or activity may be due to the dilution of nutrients of the culture medium. This effect was most noticed in the longer incubation time (72 hours).

Cells metabolic activity was not overall affected by the nanogel presence in comparison to the water diluted control. However, at highest incubation time (72 hours) and nanogel concentration (1mg/ml) a significative difference was observed (figure 1a). A549 cell line is a human pulmonary adenocarcinoma cell line that overexpresses CD44 receptors - a hyaluronic acid receptor. Therefore, it may be speculated that these receptors mediate a significant nanogel uptake. However, we must mention that the highest concentration tested (1mg/ml) is very high, with the intention of really testing the limits of toxicity.

The evaluation of cell membrane integrity was performed by LDH release assay. As shown in figure 1b, membrane integrity was preserved at all nanogel concentrations.

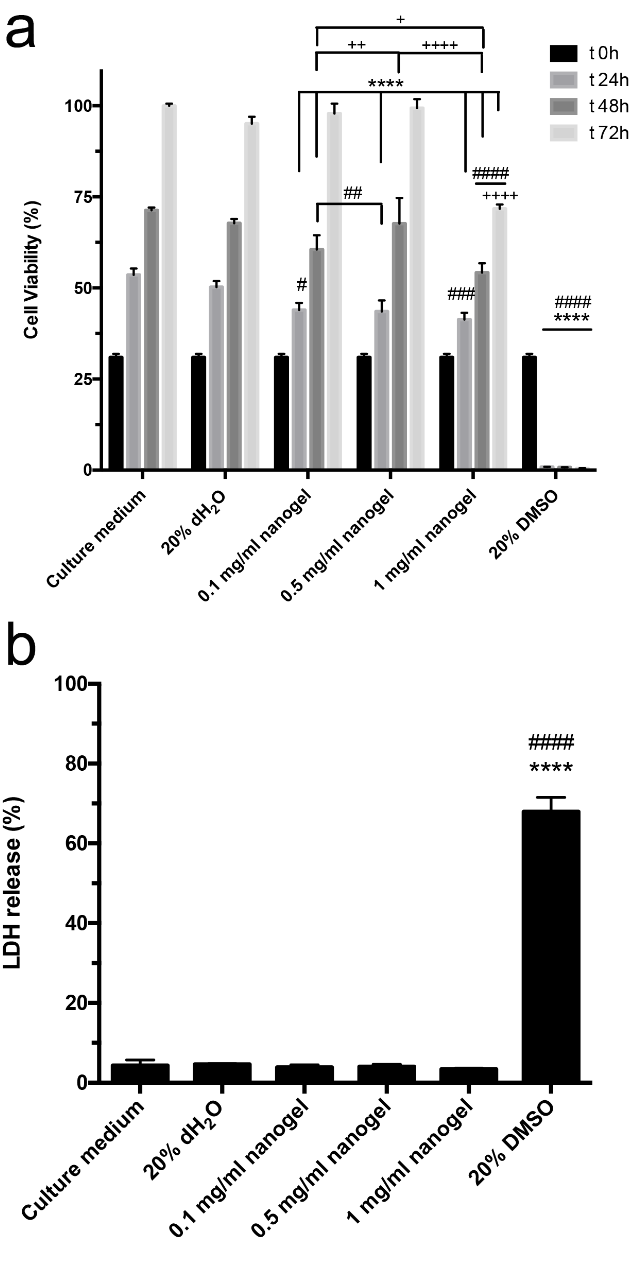

Figure 1: Nanogel cytotoxic effect on A549 cells was determined by MTT and LDH release assays. a) Cell viability was evaluated by MTT assay at 24, 48 and 72 hours and; b) cell membrane integrity by LDH release assay, at 24 hours incubation time.

4.2. IN VITRO CELLULAR UPTAKE

We aim to demonstrate HyA nanogel´s ability to actively target cell receptors such as CD44 and RHAMM, overexpressed in numerous tumour cells. [16, 20, 33-35]. Therefore, we studied the nanogel cellular uptake by A549 human non-small cancer lung cells that overexpress CD44 receptors. Also, cellular uptake was compared to CFBE cells, also obtained from pulmonary tissue (human cystic fibrosis), that do not express those receptors [19, 36].

Hence, A549 cells were treated with two nanogel concentrations (0.2 mg/mL and 0.5 mg/mL) to evaluate the dose effect on the internalization kinetics. In figure 2a, b, and d, we can see the nanogel uptake was dose dependent at almost all points, and fluorescence intensity was double.

We also analysed the nanogel uptake in CFBE cells (figure 2c). Although testing only the highest nanogel dosage we can see that MFI values were much lower than those obtained with A549 cells using similar conditions.

The TB exclusion assay makes it possible to distinguish between cell adhering and cell internalized nanogel particles. Trypan blue is a cell impermeable dye able to quench fluorescence signal originated from nanogel adhered to the cell surface [12, 13, 37]. Results of TB quenching, show that around 20-50% of the nanogel detected was not internalized (figure 2 a, b and c).

An interesting feature of the internalization process in A549 cells concerns is its kinetics. As observed after quenching of membrane adherent nanogel in A549 cells, the rate of internalization was initially slow, and then accelerated considerably. This effect was more evident at the lowest dosage of nanogel.

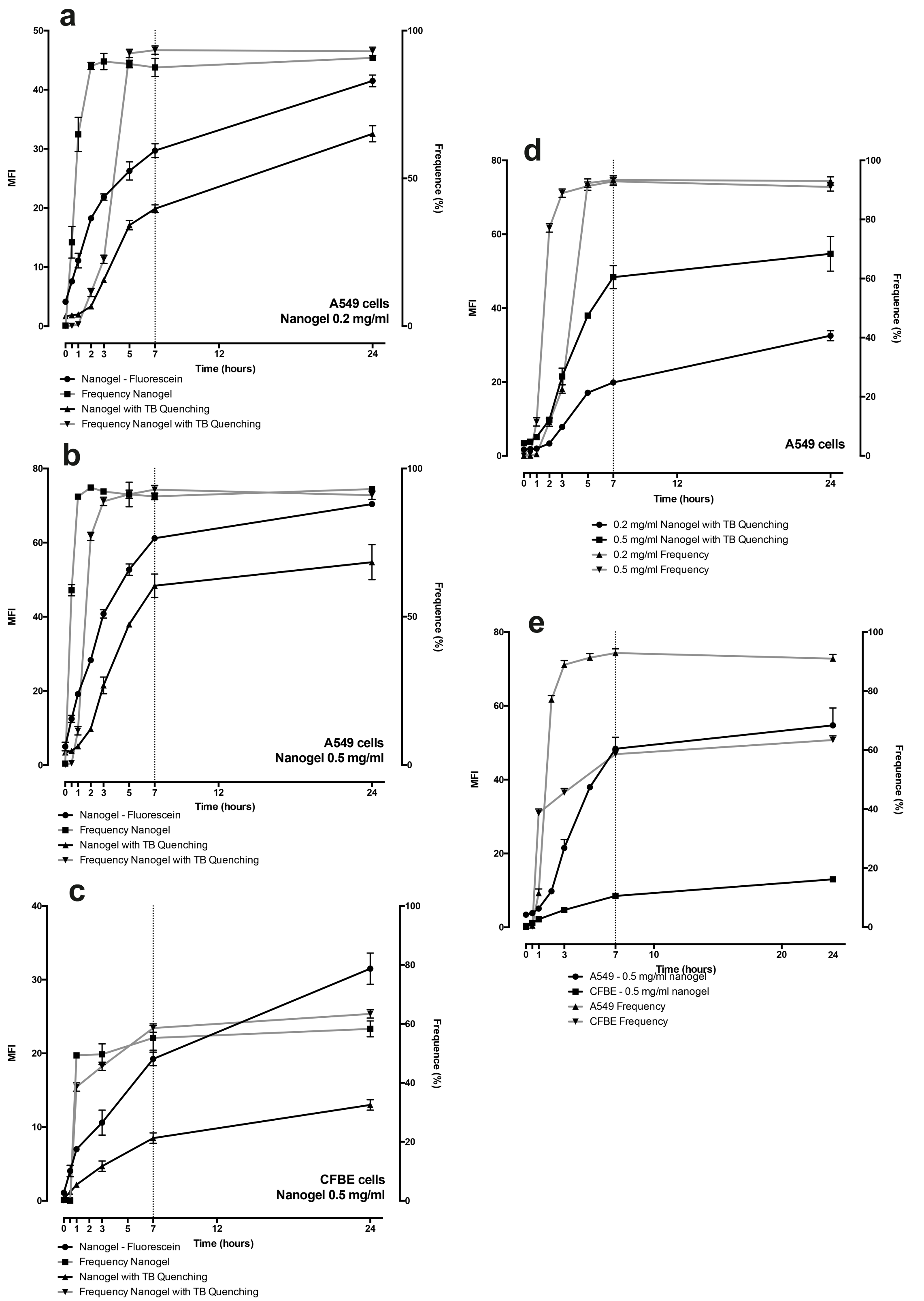

Figure 2: Flow cytometry analysis of Fluorescein labelled HyA-AT nanogel uptake a) Mean fluorescence intensity (MFI) observed on A549 cells along with the incubation time after incubation with nanogel (0.2 mg/mL), with and

without trypan blue (TB) treatment and; b) Mean fluorescence intensity (MFI) observed on A549 cells along with the incubation time after incubation with nanogel (0.5 mg/mL), with and without trypan blue (TB) treatment; c) Mean fluorescence intensity (MFI) observed on CFBE cells along with the incubation time after incubation with nanogel (0.5 mg/mL), with and without trypan blue (TB) treatment; d) Comparison of the nanogel internalization in A549 cells, using two nanogel concentrations – 0.2 mg/mL and 0.5 mg/mL - with and without TB quenching assay; e) Comparison of the nanogel internalization in A549 and CFBE cells after incubation with the same dosage of nanogel - 0.5 mg/mL – after TB treatment. Results are presented as MFI +/- SD, n=5.

Indeed, it has been reported that hyaluronic acid nanoparticles uptake by CD44 expressing cells may take 20-30 minutes [38, 39] or up to 1 hour [40].

A comparative analysis of nanogel uptake in A549 and CFBE cells, after TB quenching revealed (figure 2e) a higher nanogel uptake by CD44 expressing cells, persuading us to think that nanogel is trafficked into A549 cells via CD44 mediated endocytosis.

Confocal microscopy analysis of nanogel internalization was also performed in A549 and CFBE cells, qualitatively corroborating the FCM results. In figure 3, we can see much brighter green fluorescence signals in the cytoplasm of A549 cells than, under the same conditions, in CFBE cells. To evaluate the mechanism of cellular uptake, a competitive study in which, A549 cells were treated with an excess of free HyA, 1 hour before nanogel incubation was performed. As expected, fluorescence in HyA-treated A549 cells decreased substantially in comparison to non-treated cells. This result suggests that free HyA, by interacting with CD44 receptors, may inhibit the nanogel uptake.

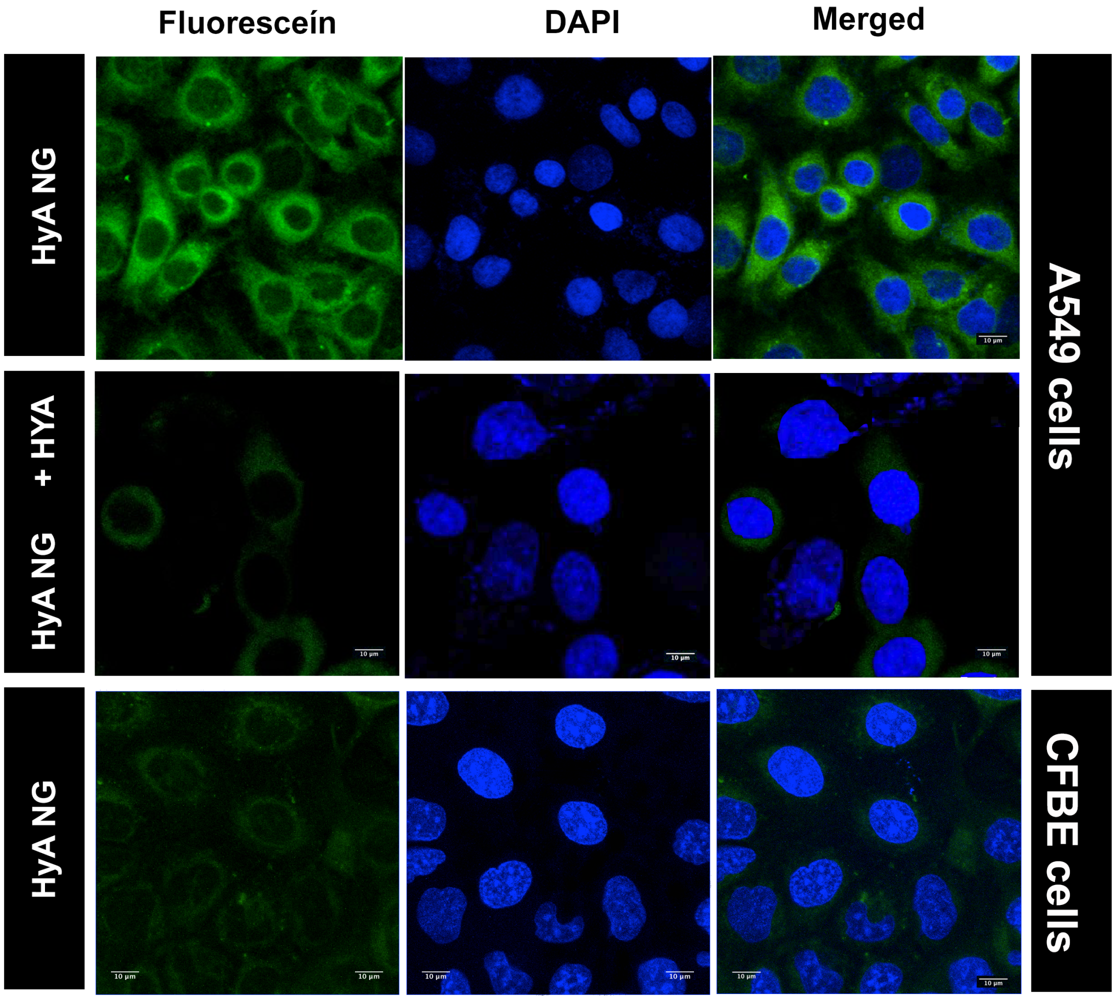

Figure 3: Confocal analysis of A549 and CFBE cells exposed to HyA-AT-Fluorescein nanogel at 0.2 mg/mL concentration. Competitive study of nanogel internalization by pre-incubating A549 cells with free HyA. Cells were stained with DAPI (blue) for the cell nucleus and Fluorescein (green) is credited to nanogel. Images are presented as a projection of all images acquired in a Z stack.

4.3. In vivo imaging studies

4.3.1. Nanogel labelling and characterization

In order to evaluate the biodistribution profile of HyA-AT nanogel, Alexa680 and Cy5.5 were chemically conjugated to nanogel and native

HyA (figure 4). Also, the biodistribution of each probe was analysed, to evaluate whether it bears specific affinity for a specific tissue. The obtained nanogel- probe conjugates were characterized regarding their size distribution profile, by DLS (figure 4). For biodistribution studies near-infrared (NIR) probes are a pertinent choice due to deep tissue penetration, high fluorescence signal and amenable self-quenching [6]. Cyanine dyes, and in particular 5.5, has shown high background fluorescence, high plasma protein binding and undesired aggregation. In turn, Alexa680 has higher excitation /emission threshold and therefore less background, being less sensitive to photobleaching [41, 42].

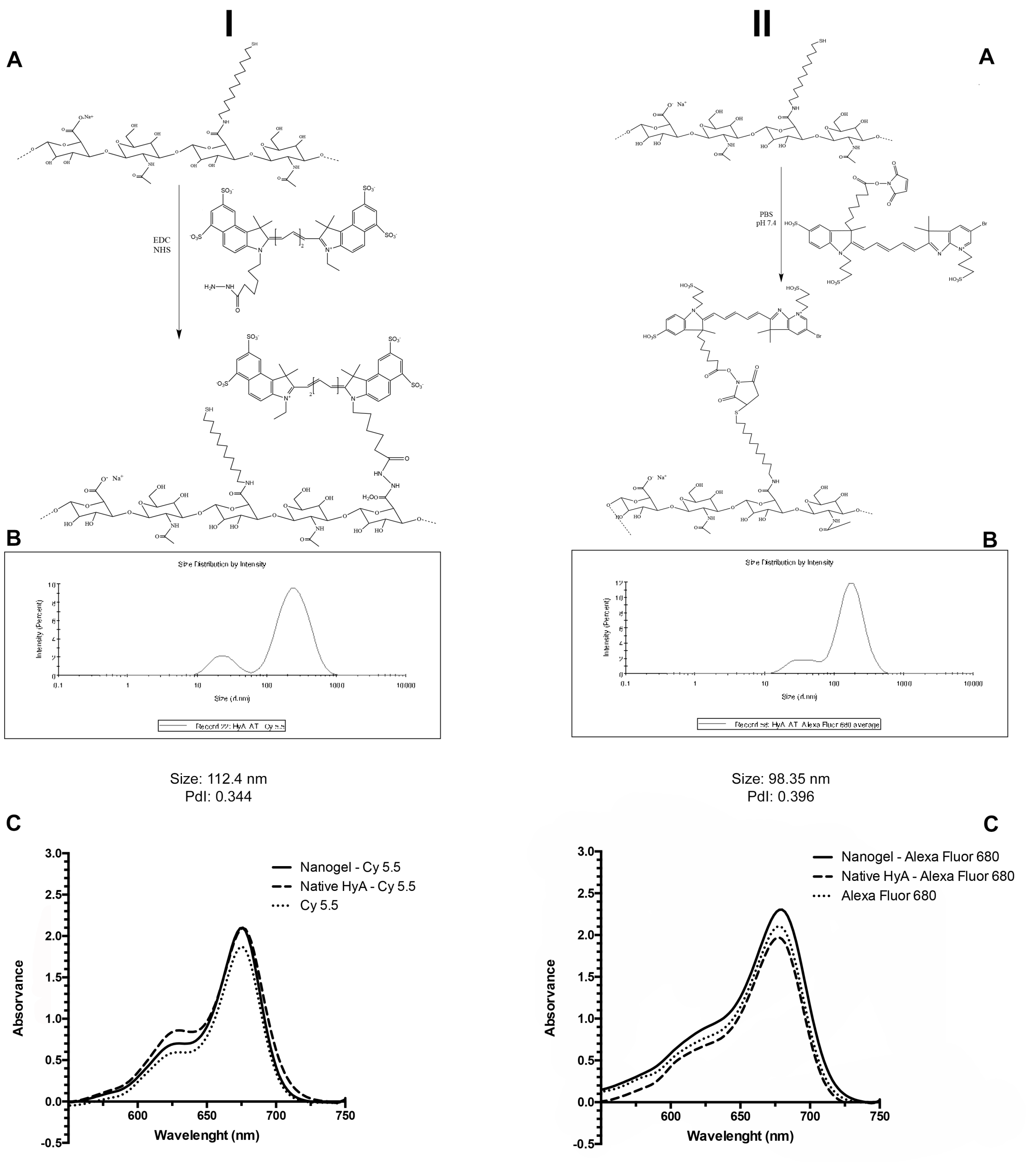

Figure 4: Schematic representation of HyA-AT nanogel labelled with Cy5.5 (IA) and Alexa680 (IIA). B) Hydrodynamic diameter of labelled nanogels was determined by DLS. C) Excitation spectra of 4x diluted HyA-AT-Cy5.5 and HyA-AT-Alexa680 samples.

4.4. Comparison of Alexa Fluor 680 and Cy 5.5 pharmacokinetics in healthy mice

Changes in size, surface charge, texture and heterogeneity in nanoparticles formulation are known to influence their biodistribution [7]. As shown in figure 4, the mean size diameter of the nanogel-probe conjugates was slightly higher in the nanogel-Cy5.5 conjugate. The zeta potential was also measured in the nanogels decorated with the probes and values of -28.7mV +/- 1.99mV (Cy5.5), and -18.9 +/- 1.87 mV (Alexa680) were obtained. The original – non-labelled - nanogel zeta potential is -19.3 +/- 1.97mV [4]. So it was not strange to see that, Cy5.5 conjugation increased somewhat the zeta potential of the nanogel, owing to its negative charge. Alexa680, on the other hand is a smaller, non-charged molecule (figure 4). The effect on the zeta potential suggest that the grafted Cy5.5 molecule, which reacts with the HyA carboxylic groups, is displayed on the nanogel surface. The Alexa680 grafting took place in the sulfhydryl residues of the hydrophobic chain of the nanogel and, also because of its lipophilicity, this probe may likely be lodged in nanogel hydrophobic domains. Since we could not find Alexa Fluor dyes reactive towards carboxylic groups, such as in the case of Cy5.5, we could not compare the two probes grafted using the same chemistry.

We studied the biodistribution of nanogel labelled with two different probes and as a control, native HyA and free probe. As can be seen in figures 5.Ia and 5.IIa, even after 48 hours there was higher NIR background signal in Cy5.5 treated animals than in Alexa680 treated animals. In the later, signal was more concentrated and not spread in the whole body as seen for Cy5.5. The *ex vivo* images (figure 5.IIb) of major organs collected 48 hours post-administration, revealed that Cy5.5 labelled samples showed a higher accumulation in lung, kidneys and skin, whereas, Alexa680 samples were mostly distributed to liver, kidneys and skin (figure 5.Ib). Adjei et al. [7] compared the biodistribution profile of large anionic as opposed to small neutral, PLGA nanoparticles. They reported that large anionic NPs showed greater accumulation in the reticuloendothelial system, such as the liver and spleen, whereas small neutral NPs, showed accumulation in highly vascularized organs, such as the lungs, the kidneys and the heart. However, the mechanism throughout this occurs is yet to be proven. It is well established that the properties of the NPs interface influence protein binding and therefore their behaviour *in vivo* [43]. One may speculate that the NIR probes can cause different protein corona *in vivo* upon entering the circulatory system and therefore affect, the organ distribution and accumulation. It has been reported that higher liver, spleen and bone marrow uptake is largely attributed to macrophages uptake. The serum proteins that compose the protein corona of nanomaterials are responsible for the recognition by the scavenger receptors of the macrophages [44]. Noteworthy is the fact that, for both probes, a low spleen accumulation was observed. Other researchers have also found a preferable lung accumulation when using Cy5.5 as NIR probe for pharmacokinetics studies. Hue et al. [45] studied the *ex vivo* kinetic of free Cy5.5, and Cy5.5 labelled thermally cross-linked superparamagnetic iron oxide nanoparticles. Cy5.5 dye fluorescence in the body was rapidly eliminated, although high fluorescence intensity was observed in the lungs, kidneys and also liver. Thermally cross-linked superparamagnetic iron oxide nanoparticles labelled with Cy5.5, had the highest fluorescence intensity in the lungs at earlier times and decreased over time, until 28 days. Other researchers [46], have found that 7 hours after administration Cy5.5 N-hydroxysuccinimide ester accumulated in the lungs and liver, and Cy5.5-conjugated ZnO nanoparticles showed strong signal in the kidneys and liver. Others researchers had encountered lung accumulation of nanoparticles when using Cy5.5 probe [47, 48]. Alexa680 biodistribution is at the moment not much studied and therefore, information regarding its pharmacokinetics is yet insufficient. Given the differential biodistribution of the nanogels labelled with the two NIR probes, it may be concluded that at least one of the probes influences the results obtained. Considering the published evidence suggesting that Cy5.5 exhibits some trend towards concentration in the lung, and the fact that in this case the probe is likely present in the surface of the particles (as opposed to the case of Alexa), we believe that the biodistribution obtained using Alexa680 is probably the more reliable one, therefore this was analysed with more detail.

Analysing figure 5.Ia, we could see that animals administered with nanogel exhibited higher fluorescence intensity at all time points, as compared to native HyA and Alexa680. In fact, 8 hours after administration, free Alexa680 has almost fully cleared from animals and native HyA has taken an abrupt reduction. To further investigate sample biodistribution, we collected mice whole blood and major organs – spleen, heart, kidneys, lungs, liver, skin, muscle and brain – which were analysed *ex vivo* by NIRF spectroscopy (figure 5.Ib), since whole body images may be misleading [20-22]

The results revealed that, 48 hours after administration, only nanogel treated mice exhibited fluorescence in all organs, including the blood.

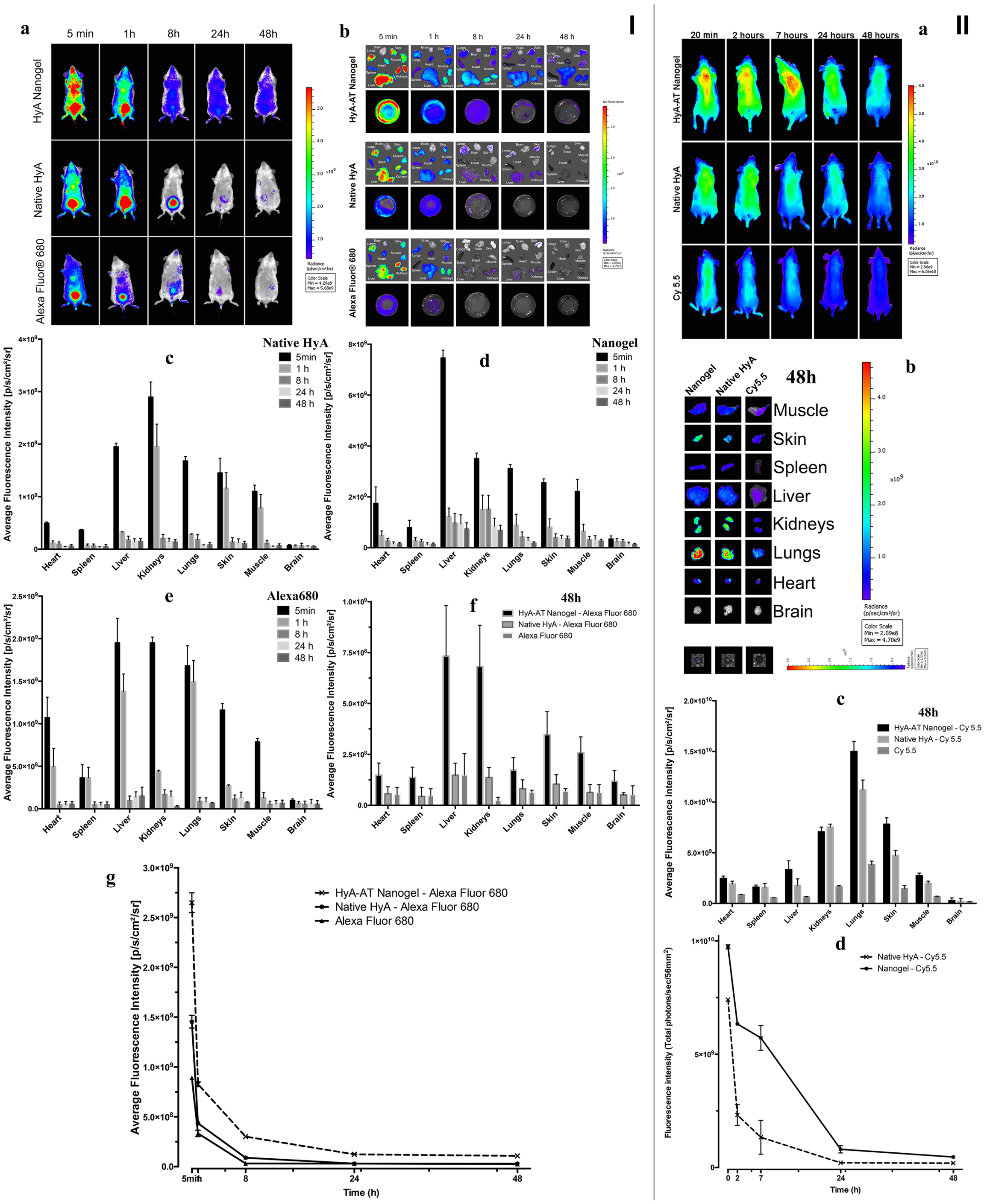

Figure 5: Section I: *In vivo* biodistribution profile of nanogel labelled with Alexa680, in healthy mice. a) Fluorescence intensity images of mice whole body. b) *ex vivo* imaging of major organs and whole blood. c) Average fluorescence intensity from excised organs of HyA treated mice. d) Average fluorescence intensity from excised organs of nanogel treated mice. e) Average fluorescence intensity from excised organs of Alexa680 treated mice.

f) Average fluorescence intensity from excised organs, 48 hours after samples administration. Comparative analysis. g) Average fluorescence intensity from whole blood, through time in all samples. Section II: *In vivo* pharmacokinetics of Cy5.5 labelled nanogel, in healthy animals. a) Fluorescence images of mice whole body after Cy5.5 labelled nanogel and HyA administration. b) *ex vivo* imaging of fluorescence intensity in major organs and blood after administration of Cy5.5 labelled samples. c) Average fluorescence intensity of excised organs, 48 hours after Cy5.5 labelled samples administration. d) Blood average fluorescence intensity through time, in Cy5.5 labelled samples. Data are shown as mean +/- SD, n=5.

As described by others [6], Alexa Fluor is a small, neutral molecule that doesn´t accumulate in any specific organ and is quickly eliminated from the body. A similar behaviour was observed in native HyA labelled samples. Indeed, after only 1 h, HyA and free Alexa680 samples were almost extinguished. Researchers [49, 50] have described that native HyA half-life ranged between 2.5 and 5.5 minutes. Also, described that its elimination predominantly by the kidneys, being the upper molecular weight limit for renal excretion, 25000 Da. In turn, nanogel was concentrated in major organs, especially in the liver and kidneys, presumably in the reticuloendothelial system. Also, It has been demonstrated that [44] smaller sized nanoparticles can be effectively cleared from body by renal excretion. Larger sized particles are processed by the reticuloendothelial system in the liver and kidneys. Nanogel has a bimodal size distribution, bearing two populations with ~30nm and ~200nm, therefore it is not surprising that the nanogel is being filtered in the kidneys and internalized by macrophages in the liver [20, 51]. In addition, being made of hyaluronic acid, the nanogel is probably also digested by hyaluronidases to some extent.

4.5. Biodistribution profile of nanogel in tumour xenograft models

Understanding the *in vivo* biodistribution of nanogel, especially in disease animal models, is essential for the design and effective biomedical application of nanomedicines [20]. Real-time NIRF images of nanogel and native HyA labelled with Alexa680, were assessed in A549 tumour-bearing mice, over the course of 48 h. *In vitro* results demonstrated higher recognition and uptake of the HyA nanogel by A549 cells, which overexpress CD44 receptors. Therefore, we evaluated the CD44 targeting in mice subcutaneously induced with A549 tumour [5, 52].

As expected, initially a strong NIR signal was observed throughout the body (figure 6.I), in the major organs and blood (figure 6.II) after administration of both nanogel and native HyA samples. As expected, and as observed in the case of the healthy animals, liver was the major clearance organ. Only 5 minutes after administration, NIR images revealed similar distribution for nanogel and HyA, namely in tumour tissue. In turn, 1 hour post-administration, the free polymer signal decreased noticeably in all organs and largely in the tumour, while the nanogel concentrated over the first hour at tumour site (figure 6.V). Around 8 hours post-administration it was noticeable that almost all traces of HyA were eliminated. However, at that time point, the nanogel remained detectable in the tumour, exhibiting a strong signal. This effect may be due to a combination of two factors; receptor mediated targeting through CD44 and enhanced permeation and retention (EPR) [5, 35, 53-55]. Also, the fact that nanogel continued to be detected in circulation up to 48 hours (figure 6.II and 6.IV) it is expected to allow higher tumour targetability. The increased blood circulation half-life, as well as the longer residence time in the tumour tissue as compared to the native hyaluronic acid, is probably due to the lower degradability owing to the chemical modification.

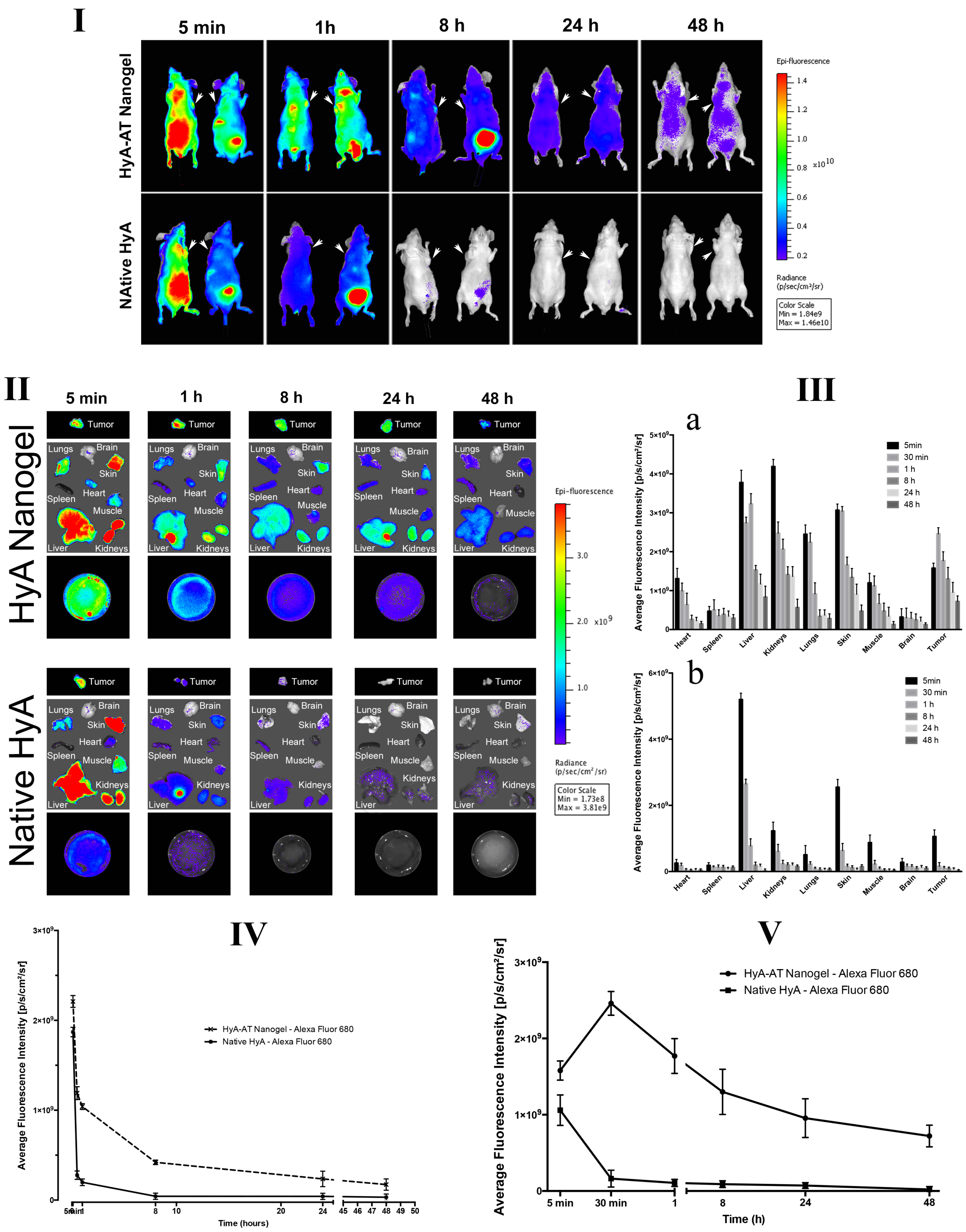

Figure 6: *In vivo* biodistribution profile of HyA-AT nanogel in A549 tumor bearing mice. I) Fluorescence intensity images of mice whole body. Arrows indicate the tumour mass localization. Images were acquired with mice in dorsal (left) and ventral position (right). II) *ex vivo* imaging of major organs, tumour mass and whole blood. IIIa) Average fluorescence intensity from excised organs of nanogel treated mice. IIIb) Average fluorescence intensity from excised organs of HyA treated mice. IV) Average fluorescence intensity from whole blood over

time in all samples. V) Average fluorescence intensity in tumour mass over time in all samples. Data are shown as mean +/- SD, n=5.

Ganesh et al., also described *in vivo* high tumour targetability in A549 cell lines [5], using cisplatin loaded CD44 targeted hyaluronic acid nanoparticles. Photo-crosslinked hyaluronic acid nanoparticles [22] and hyaluronic acid nanoparticles [20] also demonstrated hyaluronic acid targetability to SCC7 cancer cells, also CD44 overexpressing cells.

5. Conclusion

Hyaluronic acid nanogel has proven *in vitro* and *in vivo* targetability towards CD44 overexpressing cells. *In vitro* studies revealed higher cellular uptake by CD44 overexpressing lung cancer cells. Also, *in vivo* reports showed selective targeting towards tumour tissue, probably due to both passive accumulation through EPR effect and active targeting by high CD44 affinity. It is described that nanomaterials behaviour *in vivo*, namely its pharmacokinetics, is influenced by size, shape and surface characteristics; in this work we wanted to observe the influence of the NIR probe used for biodistribution studies. The most studied probe in NIR imaging is Cy5.5. Therefore we wanted to compare the pharmacokinetics profile of nanogel labelled with Cy5.5 and Alexa680 with similar excitation and emission wavelength. Our results showed that organ accumulation was different in nanogel labelled with Cy5.5 and Alexa680. Further work, regarding the protein corona of labelled nanogel is necessary to understand the differences in pharmacokinetics profiles. In conclusion, results show that HyA-AT nanogel can be used for active tumour targeting, as a drug delivery system, optical imaging agent and others.

6. Acknowledgments

The authors thank the FCT Strategic Project of UID/BIO/04469/2013 unit, the project RECI/BBB-EBI/0179/2012 (FCOMP-01-0124-FEDER-027462) and the Project "BioHealth - Biotechnology and Bioengineering approaches to improve health quality", Ref. NORTE-07-0124-FEDER-000027, co-funded by the Programa Operacional Regional do Norte (ON.2 – O Novo Norte), QREN, FEDER. We would like to acknowledge also the support of FCT for the PhD grant reference SFRH/BD/61516/2009. We would also like to thank Bioimaging department on Molecular Medicine Institute (IMM) in Lisbon, namely Dr José Rino and Dr António Temudo. Also thank the animal facilities in IMM (Lisbon), specially Drª Dolores Bonaparte and Drª Joana Marques.

7. BIBLIOGRAPHY

1. Arpicco, S., et al., *Hyaluronic acid conjugates as vectors for the active targeting of drugs, genes and nanocomposites in cancer treatment.* Molecules, 2014. **19**(3): p. 3193-230.
2. Goodarzi, N., et al., *A review of polysaccharide cytotoxic drug conjugates for cancer therapy.* Carbohydr Polym, 2013. **92**(2): p. 1280-93.
3. Platt, V.M. and F.C. Szoka, Jr., *Anticancer therapeutics: targeting macromolecules and nanocarriers to hyaluronan or CD44, a hyaluronan receptor.* Mol Pharm, 2008. **5**(4): p. 474-86.
4. Pedrosa, S.S., et al., *A novel crosslinked hyaluronic acid nanogel for drug delivery.* Macromol Biosci, 2014. **14**(11): p. 1556-68.
5. Ganesh, S., et al., *In vivo biodistribution of siRNA and cisplatin administered using CD44-targeted hyaluronic acid nanoparticles.* J Control Release, 2013. **172**(3): p. 699-706.
6. Ogawa, M., et al., *In vivo target-specific activatable near-infrared optical labeling of humanized monoclonal antibodies.* Mol Cancer Ther, 2009. **8**(1): p. 232-9.
7. Adjei, I.M., C. Peetla, and V. Labhasetwar, *Heterogeneity in nanoparticles influences biodistribution and targeting.* Nanomedicine (Lond), 2014. **9**(2): p. 267-78.
8. Hermanson, G.T., *Bioconjugate techniques*. 2nd edition. ed. 2008, San Diego: Academic Press. xxx, 1202 pages.
9. Tanzer, M.L., D. Monroe, and J. Gross, *Inhibition of collagen intermolecular cross-linking by thiosemicarbazide.* Biochemistry, 1966. **5**(6): p. 1919-26.
10. Vranic, S., et al., *Deciphering the mechanisms of cellular uptake of engineered nanoparticles by accurate evaluation of internalization using imaging flow cytometry.* Part Fibre Toxicol, 2013. **10**: p. 2.
11. Avelar-Freitas, B.A., et al., *Trypan blue exclusion assay by flow cytometry.* Braz J Med Biol Res, 2014. **47**(4): p. 307-15.
12. Keogh, M.J., et al., *Simultaneous measurement of phagocytosis and respiratory burst of leukocytes in whole blood from bottlenose dolphins (Tursiops truncatus) utilizing flow cytometry.* Vet Immunol Immunopathol, 2011. **144**(3-4): p. 468-75.
13. Gratton, S.E., et al., *The effect of particle design on cellular internalization pathways.* Proc Natl Acad Sci U S A, 2008. **105**(33): p. 11613-8.
14. McDonald, B., et al., *Interaction of CD44 and hyaluronan is the dominant mechanism for neutrophil sequestration in inflamed liver sinusoids.* J Exp Med, 2008. **205**(4): p. 915-27.

15. Roudi, R., et al., *CD44 and CD24 cannot act as cancer stem cell markers in human lung adenocarcinoma cell line A549.* Cell Mol Biol Lett, 2014. **19**(1): p. 23-36.
16. Zhang, H.Z., et al., *The study of the tumor stem cell properties of CD133+CD44+ cells in the human lung adenocarcinoma cell line A549.* Cell Mol Biol (Noisy-le-grand), 2010. **56 Suppl**: p. OL1350-8.
17. Zabner, J., et al., *Development of cystic fibrosis and noncystic fibrosis airway cell lines.* Am J Physiol Lung Cell Mol Physiol, 2003. **284**(5): p. L844-54.
18. Choi, K.Y., et al., *Self-assembled hyaluronic acid nanoparticles for active tumor targeting.* Biomaterials, 2010. **31**(1): p. 106-14.
19. Choi, K.Y., et al., *Smart nanocarrier based on PEGylated hyaluronic acid for cancer therapy.* ACS Nano, 2011. **5**(11): p. 8591-9.
20. Yoon, H.Y., et al., *Photo-crosslinked hyaluronic acid nanoparticles with improved stability for in vivo tumor-targeted drug delivery.* Biomaterials, 2013. **34**(21): p. 5273-80.
21. Nobs, L., et al., *Surface modification of poly(lactic acid) nanoparticles by covalent attachment of thiol groups by means of three methods.* Int J Pharm, 2003. **250**(2): p. 327-37.
22. Gruber, H.J., et al., *Anomalous fluorescence enhancement of Cy3 and cy3.5 versus anomalous fluorescence loss of Cy5 and Cy7 upon covalent linking to IgG and noncovalent binding to avidin.* Bioconjug Chem, 2000. **11**(5): p. 696-704.
23. Bae, K.H., et al., *Intracellular delivery of heparin complexed with chitosan-g-poly(ethylene glycol) for inducing apoptosis.* Pharm Res, 2009. **26**(1): p. 93-100.
24. Bae, K.H., H. Mok, and T.G. Park, *Synthesis, characterization, and intracellular delivery of reducible heparin nanogels for apoptotic cell death.* Biomaterials, 2008. **29**(23): p. 3376-83.
25. Ahn, B., S.G. Rhee, and E.R. Stadtman, *Use of fluorescein hydrazide and fluorescein thiosemicarbazide reagents for the fluorometric determination of protein carbonyl groups and for the detection of oxidized protein on polyacrylamide gels.* Anal Biochem, 1987. **161**(2): p. 245-57.
26. Na, K., et al., *Synergistic effect of TGFbeta-3 on chondrogenic differentiation of rabbit chondrocytes in thermo-reversible hydrogel constructs blended with hyaluronic acid by in vivo test.* J Biotechnol, 2007. **128**(2): p. 412-22.
27. Luo, Y. and G.D. Prestwich, *Synthesis and selective cytotoxicity of a hyaluronic acid-antitumor bioconjugate.* Bioconjug Chem, 1999. **10**(5): p. 755-63.
28. Berlier, J.E., et al., *Quantitative comparison of long-wavelength Alexa Fluor dyes to Cy dyes: fluorescence of the dyes and their bioconjugates.* J Histochem Cytochem, 2003. **51**(12): p. 1699-712.

29. Ilgin, P., et al., *Colloidal drug carries from (sub)micron hyaluronic acid hydrogel particles with tunable properties for biomedical applications.* Carbohydrate Polymers, 2010. **82**(3): p. 997-1003.
30. Kadi, S., et al., *Alkylamino hydrazide derivatives of hyaluronic acid: synthesis, characterization in semidilute aqueous solutions, and assembly into thin multilayer films.* Biomacromolecules, 2009. **10**(10): p. 2875-84.
31. Abbad, S., et al., *Preparation, in vitro and in vivo evaluation of polymeric nanoparticles based on hyaluronic acid-poly(butyl cyanoacrylate) and D-alpha-tocopheryl polyethylene glycol 1000 succinate for tumor-targeted delivery of morin hydrate.* Int J Nanomedicine, 2015. **10**: p. 305-20.
32. Li, J., et al., *Hyaluronic acid-modified hydrothermally synthesized iron oxide nanoparticles for targeted tumor MR imaging.* Biomaterials, 2014. **35**(11): p. 3666-77.
33. Leung, E.L., et al., *Non-small cell lung cancer cells expressing CD44 are enriched for stem cell-like properties.* PLoS One, 2010. **5**(11): p. e14062.
34. Graczyk, H., et al., *Physicochemical characterization of nebulized superparamagnetic iron oxide nanoparticles (SPIONs).* J Aerosol Med Pulm Drug Deliv, 2015. **28**(1): p. 43-51.
35. Van Amersfoort, E.S. and J.A. Van Strijp, *Evaluation of a flow cytometric fluorescence quenching assay of phagocytosis of sensitized sheep erythrocytes by polymorphonuclear leukocytes.* Cytometry, 1994. **17**(4): p. 294-301.
36. Schuldt, A., *Nature reviews. Molecular cell biology*. 2000, Nature Pub. Group: London, UK. p. v.
37. Scarselli, M. and J.G. Donaldson, *Constitutive internalization of G protein-coupled receptors and G proteins via clathrin-independent endocytosis.* J Biol Chem, 2009. **284**(6): p. 3577-85.
38. Zaki, N.M., A. Nasti, and N. Tirelli, *Nanocarriers for cytoplasmic delivery: cellular uptake and intracellular fate of chitosan and hyaluronic acid-coated chitosan nanoparticles in a phagocytic cell model.* Macromol Biosci, 2011. **11**(12): p. 1747-60.
39. Luo, S., et al., *A review of NIR dyes in cancer targeting and imaging.* Biomaterials, 2011. **32**(29): p. 7127-38.
40. Yang, X., et al., *Near IR heptamethine cyanine dye-mediated cancer imaging.* Clin Cancer Res, 2010. **16**(10): p. 2833-44.
41. Gref, R., et al., *'Stealth' corona-core nanoparticles surface modified by polyethylene glycol (PEG): influences of the corona (PEG chain length and surface density) and of the core composition on phagocytic uptake and plasma protein adsorption.* Colloids Surf B Biointerfaces, 2000. **18**(3-4): p. 301-313.
42. Kumar, R., et al., *In vivo biodistribution and clearance studies using multimodal organically modified silica nanoparticles.* ACS Nano, 2010. **4**(2): p. 699-708.

43. Hue, J.J., et al., *Distribution and accumulation of Cy5.5-labeled thermally cross-linked superparamagnetic iron oxide nanoparticles in the tissues of ICR mice.* J Vet Sci, 2013. **14**(4): p. 473-9.
44. Lee, C.M., et al., *Optical imaging to trace near infrared fluorescent zinc oxide nanoparticles following oral exposure.* Int J Nanomedicine, 2012. **7**: p. 3203-9.
45. Lee, H., et al., *Thermally cross-linked superparamagnetic iron oxide nanoparticles: synthesis and application as a dual imaging probe for cancer in vivo.* J Am Chem Soc, 2007. **129**(42): p. 12739-45.
46. Iqbal, U., et al., *Molecular imaging of glioblastoma multiforme using anti-insulin-like growth factor-binding protein-7 single-domain antibodies.* Br J Cancer, 2010. **103**(10): p. 1606-16.
47. Fraser, J.R., et al., *Elimination of hyaluronic acid from the blood stream in the human.* Clin Exp Pharmacol Physiol, 1984. **11**(1): p. 17-25.
48. Necas, J., et al., *Hyaluronic acid (hyaluronan): a review.* Veterinarni medicina, 2008. **53**(8): p. 397-411.
49. Arami, H., et al., *In vivo delivery, pharmacokinetics, biodistribution and toxicity of iron oxide nanoparticles.* Chem Soc Rev, 2015.
50. Hwang, H.Y., et al., *Tumor targetability and antitumor effect of docetaxel-loaded hydrophobically modified glycol chitosan nanoparticles.* J Control Release, 2008. **128**(1): p. 23-31.
51. Whitmire, R.E., et al., *Self-assembling nanoparticles for intra-articular delivery of anti-inflammatory proteins.* Biomaterials, 2012. **33**(30): p. 7665-75.
52. Bartlett, D.W., et al., *Impact of tumor-specific targeting on the biodistribution and efficacy of siRNA nanoparticles measured by multimodality in vivo imaging.* Proc Natl Acad Sci U S A, 2007. **104**(39): p. 15549-54.
53. Yhee, J.Y., S. Lee, and K. Kim, *Advances in targeting strategies for nanoparticles in cancer imaging and therapy.* Nanoscale, 2014. **6**(22): p. 13383-90.

CHAPTER V

HYALURONIC ACID NANOGEL: CELL UPTAKE AND EXPLORATORY INTRACELLULAR DRUG DELIVERY

Adapted from

Pedrosa, S.S., Silva, J.P.; Pereira, P.; Correia, A.; Appelberg, R.; Castro, AG.; Pedrosa, J.; Wymant, J.M.; Sayers, E.; Jones, A; Gama, FM

Submitted work

ABSTRACT

Hyaluronic acid (HyA) is a natural occurring polysaccharide that is used widely in biomedical applications. The cellular uptake of a previously developed hyaluronic acid nanogel by the HeLa cervical cancer cell line was evaluated: quantitatively by flow cytometry analysis and qualitatively by confocal microscopy. Results showed that the nanogel uptake was dose and time dependent and relied on active membrane transport mechanisms. To further understand the uptake mechanism, selective siRNA depletion of key proteins regulating specific endocytic pathways was performed. Results showed that hyaluronic acid nanogel internalization occurs mainly via clathrin and caveolae-mediated endocytosis. The HyA-AT nanogel was subsequently tested as drug carrier for the intracellular delivery of antimicrobials to mycobacteria-infected macrophages. Targeting host-residing mycobacteria is usually difficult to achieve. However, here we showed that the nanogel loaded with rifampicin or an antimicrobial peptide could significantly reduce the mycobacterial burden within macrophages. Our data collectively suggest that HyA-AT nanogel may have considerable potential for intracellular delivery of therapeutic cargo via endocytosis.

1. INTRODUCTION

The importance of effective intracellular delivery and targeting in the therapeutic efficacy of nanomedicines cannot be overstated. Interactions between nanocarriers and the plasma membrane determine nanocarrier uptake and further affect intracellular transport and fate. Cellular uptake may occur through simple physical proximity and diffusion or by active endocytic processes [1, 2]. Endocytosis is characterized by the formation of intracellular vesicles from plasma membrane. However, a number of different endocytic processes and pathways exist. Endocytosis can be grossly classified as either phagocytosis or pinocytosis. The former describes the uptake of large, solid or solid-like bodies, such as bacteria while pinocytosis refers to the uptake of fluid containing dispersed/soluble materials. Pinocytosis can be further subdivided into macropinocytosis, clathrin-mediated endocytosis (CME), caveolae-mediated endocytosis (CvME) and clathrin- and caveolae-independent endocytosis. Macropinocytosis is a mechanism of endocytosis that can be constitutive or induced by growth factor (e.g. EGF) stimulation. It is a non-specific process, by which membrane protrusions are formed in areas where cell membrane is highly ruffled. Macropinosomes ingest portions of extracellular fluids containing soluble or dispersed material and their vesicles go up to low micrometer in size (0.5-5 μm) and through a so far unknown mechanism, fuse back with cell membrane. It is known that p21-activated kinase (Pak-1) is associated with growth factor-induced macropinosome [2-5].
Remaining pinocytic mechanisms are associated with the uptake of small volumes of extracellular fluid and include: CvME, CME and clathrin and caveolae independent endocytosis. Clathrin- and caveolae-independent pathways also include: Flotillin-dependent endocytosis, cdc42-dependent uptake, RhoA-dependent uptake and Arf6 (ADP-ribosylation factor 6)-dependent uptake [2].

Clathrin-mediated endocytosis (CME) is the most well-studied endocytic pathway, known to be regulated by several proteins, including clathrin heavy chain (CHC) [3, 4]. Examples of receptors that adopt this mechanism of internalization are: transferrin, low-density lipoprotein (LDL) receptor and the epidermal growth factor receptor (EGFR) [2]. CME is a classical endocytic pathway, by which agents are internalized by cells and travel through early endosomes and then are delivered to other organelles, such as lysosomes, or go back to cell surface through recycling endosomes [4, 6].

Caveolae mediated endocytosis (CvME) is the most common clathrin-independent mechanism of receptor mediated endocytosis. Caveolins are the proteins associated with caveolae and are often bound to lipid rafts. Caveolae are flask-shaped invaginations in plasma membrane, with size ranging between 50-100 nm [2, 4]. Caveolin-1 (CAV-1) is not found only in caveolae, but is often associated with lipid rafts. Caveolae pit formation occurs in both endoplasmatic reticulum and Golgi. Then caveolae reaches cell membrane, achieving complete maturation. Caveolae is then detached from cell membrane and fused with early endosomes and with caveosomes, where they don't undergo acidification [2, 4].

Also, we studied clathrin and caveolin independent endocytosis, the endocytic mechanisms most recently discovered. Flotillin-dependent endocytosis is probably the most significant one. Flottilin-1 and -2 are two inter-dependent membrane proteins, associated to lipid rafts and therefore, this mechanism has analogies to CvME. Flotilins associated with lipid rafts are capable of originating cell membrane microdomais. Several receptors including folic acid belong to this class [2].

Hyaluronic acid (HyA) is a naturally occurring polysaccharide, which has a number of attractive features for biomedical applications, such as biocompatibility, biodegradability and targetability for specific cellular receptors [7-9]. It has demonstrated high affinity for CD44 and Receptor for Hyaluronan Mediated Motility (RHAMM), both overexpressed in numerous tumors and associated with metastasis [7, 10, 11]. The HeLa cervical adenocarcinoma cell line is known to overexpress the RHAMM receptor and also, to a lesser extent, CD44 [12, 13]. In this study we investigated the cell trafficking of an engineered hyaluronic acid nanogel [14] in HeLa cells. Although pharmacological inhibition is a common approach to analyse cellular uptake of materials, the efficacy and specificity of many endocytic inhibitors has been questioned [6, 15]. Studies have shown that small interfering RNA (siRNA) induced silencing of endocytic proteins may be a more selective and accurate approach [15]. Therefore, siRNA depletion was used in this work to target key proteins regulating endocytic pathways: clathrin heavy chain (si-CHC), caveolin-1 (si-Cav-1), p21-activated kinase 1 (si-Pak-1) and Flotillin-1 (si-Flot-1). After siRNA depletion of pathway-specific endocytic proteins, cells were incubated with HyA-AT nanogel and uptake of the nanogel was analysed by flow cytometry. We subsequently investigated the potential of the HyA-AT nanogel as a vector to facilitate the intracellular delivery of hydrophobic drugs targeting mycobacteria on a preliminary tuberculosis model. This model shows great relevance, since tuberculosis has been recently recognized by the World Health Organization (WHO) as one of the deadliest infectious diseases, with 9.6 million cases reported in 2014 [16]. Standard chemotherapy, which consists of a long-lasting (6-24 months), multiple drug regimen, often fails in controlling the disease. The high therapy costs, associated with low patient compliance and reports of toxicity issues represent major drawbacks [17, 18]. Moreover, the drugs commonly used in tuberculosis therapy are rapidly degraded or excreted, show poor bioavailability when administered via specific routes and are distributed systemically rather than targeting the main sites of infection [19, 20]. A proper delivery system, like HyA-AT nanogel, could help overcome such obstacles, improving the efficiency of anti-tuberculosis therapy. Additionally, infected macrophages are known to overexpress the CD44 receptor as part of their initial inflammatory response to infection and the ready uptake of hyaluronan by CD44-positive macrophages has already been reported [21, 22]. To this end, we evaluated mycobacterial infection levels within macrophages treated with the HyA-AT nanogel loaded with either the antimycobacterial rifampicin or an antimicrobial peptide.

2. Materials and methods

2.1. Reagents

1-Ethyl-3-[3-dimethylaminopropyl]carbodiimide hydrochloride (EDC), Opti-MEM, oligofectamine, Alexa Fluor 633 - Transferrin (Alexa633-Transferrin), Alexa Fluor ® 488 Cadaverine were bought from Invitrogen (Carlsbad, CA, USA). Complete mini protease inhibitor cocktail tablets were from Roche Diagnostics (Mannheim, Germany). Single siRNA sequences of 21-23 residues were acquired from Europhins MWG Operon (Ebesburg, Germany) as previously described [3, 4].

2.2. Cell culture

Human cervical adenocarcinoma cells (HeLa) were maintained in complete media comprising: Dulbecco's modified Eagle's media (DMEM) supplemented with 10% (v/v) of heat-inactivated foetal bovine serum (FBS), 100 IU/ml penicillin and 0.1 mg/ml streptomycin. HeLa cells [23] were kindly provided by Dr Jorge Pedrosa, at Life and Health Sciences Research Institute (ICVS, University of Minho). Cells were grown as a subconfluent monolayer in a humidified atmosphere containing 5 % CO_2 at 37 °C.

Bone marrow-derived cells (BMMΦ) were isolated, under aseptic conditions, from femurs and tibias of C57BL/6 female mice aged 6 weeks, as previously described [24]. The animals, purchased from Charles River Laboratories, Inc. (Barcelona, Spain), were housed at the ICVS vivarium in a room with controlled temperature and humidity (22ºC +/- 3ºC and 50-60% humidity), and supplied with standard chow and water *ad libitum*. Animal experiments were performed according to the European Union Directive 86/609/EEC and were approved by the Portuguese Veterinary authorities (Direção Geral de Veterinária). Following bone removal, these were flushed with 5 ml of DMEM supplemented with 10 % FBS and passed through a cell strainer. Cells were then centrifuged at 1200 rpm, 6 min, at 4 °C and the pellet resuspended in 10 ml DMEM containing 20 % L-cell conditioned medium (LCCM). Differentiation into macrophages was achieved after a 7-day culture in 100 mm diameter Petri dishes. At day 4, additional 10 ml DMEM supplemented with 20 % LCCM were added to the cells.

2.3. Mycobacterial strains

The strains used in this study showed distinct degrees of pathogenicity. The opportunistic *Mycobacterium avium* strain 2447, which forms smooth transparent (SmT) colonies was obtained from the American Type Culture Collection (Manassas, VA, USA). *M. avium 2447* was grown at 37 °C in Middlebrook 7H9 medium (Difco, Sparks, MD) supplemented with Middlebrook Albumin, Dextrose, Catalase (ADC) Supplement (Sigma-Aldrich, Barcelona, Spain) and 0.04 % Tween 80. *M. tuberculosis* H37Rv was obtained from the Trudeau Institute Mycobacterial Collection. For CFU counting, mycobacteria were plated in solid Middlebrook 7H10 (*M. avium*) or 7H11 (*M. tuberculosis*) medium supplemented with Middlebrook Oleic acid, Albumin, Dextrose, Catalase (OADC) Supplement (Sigma-Aldrich, Barcelona, Spain) and 0.5 % glycerol.

2.4. SYNTHESIS OF FLUORESCEIN LABELLED NANOGEL

Hyaluronic acid nanogel (HyA-AT) synthesis was described elsewhere [14]. HyA-AT nanogel was conjugated with Fluorescein-5-thiosemicarbazide for *in vitro* cellular studies. Thiosemicarbazide groups of fluorescin reacted with carboxylic group of hyaluronic acid nanogel in presence of EDC coupling agent. The theoretical labelling degree, defined by the ratio between probe and the nanogel, was 4:1 (HyA dissacharide: thiosemicarbazide group). The lack of unconjugated fluorescein was confirmed by ultrafiltration through a 2 KDa MW cut-off membrane. In filtrate and concentrate, probe emission was measured spectrophotometrically and the absence of fluorescence signal was achieved in the last filtrate [25, 26].

2.5. NANOGEL ENCAPSULATION OF HYDROPHOBIC DRUGS

Encapsulation of relevant bioactive molecules was performed by mixing 0.5 mg/ml of the HyA-AT nanogel (dissolved in Phosphate Buffered Saline - PBS) with either 7.5 mg/ml rifampicin or 100 μM of the antimicrobial peptide (AMP) KIWWWWRKRC (Schafer-N, Denmark), under mild rotation in a wheel, for 24 h at room temperature. The concentration of rifampicin tested has been previously reported as effective against three different mycobacterial strains [27]. The referred AMP contains an additional C-terminal cysteine relatively to the sequence firstly described by Ramon-Garcia and co-workers as having high antimycobacterial activity [28]. The presence of a C-terminal cysteine has been previously described as increasing the antimicrobial activity of AMPs [29].

Unloaded molecules were removed by centrifuging the solutions (470 rcf, 2 min) in Amicon® Ultra-centrifugal filter units (Millipore) with a molecular weight cut-off of 100 KDa. The original volume in the concentrated solution containing the loaded nanogel was then restored and the solution further filtered with a 0.22 µm polyethersulphone (PES) syringe filter.

2.6. Synthesis of Alexa Fluor ® 488 Cadaverine

Alexa Fuor 488 cadaverine (Alexa488) is a carboxylate reactive probe with a diamine group. The coupling occurs by amide bond formation at a pH range of 4.5–7.5 in presence of EDC as coupling agent [25]. For the nanogel labelling, 10 mg of HyA-AT was dispersed in 0.1 M PBS solution (pH 7.4) and Alexa 488 was solubilized in a minimum amount of DMSO. The molar ratio of cadaverine group to free carboxylic acid groups was 0.1. Nanogel dispersion, Alexa488 and EDC (equimolar amount to free carboxylic acid groups) were mixed, and the reaction was allowed to proceed overnight, at room temperature, protected from light. The mixture was subsequently dialysed extensively against distilled water through a 2 KDa MW cut-off membrane. Purification of the nanogel-Alexa488 conjugate sample was confirmed by ultrafiltration and spectrophotometric analysis at 490 nm - probe maximum absorbance wavelength.

2.7. Nanogel cellular uptake by flow cytometry

2.7.1. Flow cytometry analysis

Quantitative cellular uptake of nanogel in HeLa cells was conducted in a Coulter Epics XL Flow Cytometer (Beckman Coulter Inc., Miami, FL, USA). Cells were seeded in 24-well plates at 2.0 x 10^5 density and incubated overnight. Culture medium was then removed and cells were treated with culture medium containing 0.2 mg/ml or 0.5 mg/ml fluorescein labelled nanogel. After 0 and 30 min, 1, 2, 3, 5, 7 and 24h, culture medium was removed and cells were rinsed with PBS. Cells were collected by trypsinization, resuspended in complete medium and centrifuged at 300 x g for 10 min. Cells were then rinsed with PBS twice and finally ressuspended in flow cytometry staining buffer (0.01M PBS, 0.1M sodium azide and 1% albumin) prior to analysis. Cells were gated based on size vs granularity (Forward Scattered/ Side Scattered, FSC/SSC) dot plots. The fluorescence due to nanogel internalization was evaluated in FL1 (green channel), where FL1 positive cells had internalized/adhered nanogel. Afterwards, to assess cell viability, each sample was incubated with 5 µL of a 10 µg/mL propidium iodide (PI) solution (in PBS). Cells were incubated for 1 min in the dark. Then, PI fluorescence was measured in FL 3 (red channel). Cell count was set to 20,000 events minimum. Results are expressed as mean fluorescence intensity (MFI) and the frequencies (or percentage) of cells (data results from three independent experiments performed in triplicates).

2.7.2. Trypan Blue exclusion assay

Trypan blue (TB) is a cell impermeable dye that is able to quench green fluorescence (FITC/Fluorescein) at the cell surface [15, 30, 31]. After the nanogel-fluorescein content of cells was analysed, samples were further incubated with 0.1% TB, for 1 min. Cellular debris and aggregates were excluded from the analysis by FSC/SSC gating and results were analysed in FL1/FL3 (green/red channels). Results are expressed as MFI of the FL1 signal and the frequency (or percentage) of cells (performed in triplicates, in three independent experiments).

2.7.3. MTS reduction test

BMMΦ were scraped from Petri dishes, seeded at 5×10^4 cells/well in 96-well plates and allowed to adhere overnight. Cell culture medium was then replaced by vehicle control, unloaded HyA-AT nanogel and either rifampicin or AMP-loaded nanogel solutions. These were prepared in DMEM to a final volume of 200 µl, and cells were incubated for 24 h at 37°C, 5% CO_2. The metabolic activity of the BMMΦ was then determined using the MTS (3-(4,5-dimethyl-2-yl)-5-(3-carboxy-methoxyphenyl)-2-(4-sulfophenyl)-2H tetrazolium) reduction assay (CellTiter 96® Aqueous One Solution Cell Proliferation Assay, Promega). The MTS assay is based on the formation of formazan crystals upon reduction of the tetrazolium salt MTS by metabolically active cells. As such, 20 µl of MTS solution were added per well and the plate was incubated for 2 h at 37 °C, 5 % CO_2, protected from light. Metabolic activity was measured spectrophotometrically at 490 nm in a Synergy HT (BioTek, Winooski, VT, USA) microplate reader. Results were expressed as the percentage of metabolic activity relatively to the control, for at least three independent experiments, performed in duplicates.

2.8. Nanogel cellular uptake by Confocal Fluorescence microscopy

2.8.1. Confocal fluorescence microscopy

HeLa cells were seeded in glass-bottomed 35 mm culture dishes from MatTek at 3 x 105 cells density/mL, and were left to adhere overnight. HyA-AT nanogel labelled with Alexa488 (0.2 mg/ml concentration) was added to cells and incubated for 7 h in complete culture medium at 37°C, 5% CO2. Where indicated, cell nuclei were also stained with a 300 nM DAPI solution. Then, cells were washed thrice with PBS and covered with 1.0 ml of live cell imaging solution (Phenol red free RPMI and 20mM HEPES). Samples were immediately imaged as live cells and differential interference contrast (DIC) by confocal microscopy at 37 °C on a Leica SP5 system objective (40X, 63X) numerical aperature (1.4NA for 40X or

63X), Laser Argon 30%, scan speed 700Hz, emission wavelength 515-572nm[4, 32].

2.8.2. THE EFFECT OF TEMPERATURE AND ENERGY ON NAOGEL UPTAKE

Cells were seeded in glass-bottomed 35 mm culture dishes at 3 x 10^5 cells/ml density, and were left to adhere overnight.
In order to determine uptake mechanism was energy dependent, cells were preincubated at 4 °C for 30 min, and then nanogel (0.2 mg/ml) dispersed in refrigerated culture medium was incubated for 30 min at approximately 4 °C (on ice). Then, cells were washed with PBS and visualized in live cell imaging solution by confocal microscopy [32]. A parallel assay was performed at 37 °C with same incubation time, as a physiological temperature control for cellular uptake. Cells were washed tree times with ice cold PBS and imaged with live cell imaging solution by confocal microscopy.

2.9. SIRNA TRANSFECTIONS

The endocytic mechanisms of nanogel internalization mechanism were studied via siRNA silencing, with a procedure described elsewhere [3, 4]. Briefly, cells were seeded in antibiotic-free FBS supplemented culture medium at 1.6x10^5 cells/well density in a 6-well plate. Cells were incubated overnight, reaching ≈60% confluency at the time of transfection. Transfection protocol was performed as follows (volumes are per well): 1.2 µL of 50 µM of siRNA stock solution was diluted in 214.7 µL of Opti-MEM. Also, 4.8 µL of Oligofectamine was gently mixed with 19.2 µL of Opti-MEM. The diluted siRNA and oligofectamine were then gently mixed together and incubated at room temperature for 30 min. Culture medium was removed from each well and replaced with 960 μL of Opti-MEM. The siRNA-oligofectamine complex solution was added to each well dropwise and incubated for 4 h at 37°C, 5% CO_2. Finally, 600 μL of Opti-MEM supplemented with FBS (30%) was added to each well and cells were incubated for 48 h before downstream analysis [3, 4].

2.9.1. NANOGEL INTERNALIZATION IN TRANSFECTED CELLS

After being transfected with siRNA sequences, cells were incubated with nanogel and the obtained fluorescence was evaluated by flow cytometry. siRNA-transfected cells in 6-well plates were further incubated with nanogel-Alexa488 (0.2 mg/ml) for 7 h at 37°C and 5% CO_2 atmosphere. Cells were then washed three time with PBS and harvested by trypsinization (trypsin/EDTA 0.25%/0.02%). Complete medium was added and the cell suspension was centrifuged at 300 xg for 10 min. Finally, cells were washed with PBS ressuspended in flow cytometry staining buffer (0.01M PBS, 0.1M sodium azide and 1% albumin) and fluorescence was measured in a Coulter Epics XL Flow Cytometer (Beckman Coulter Inc., Miami, FL, USA).

2.10. INTRACELLULAR DELIVERY OF BIOACTIVE AGENTS TO INFECTED MACROPHAGES

The ability of the HyA-AT nanogel to deliver bioactive molecules with antimicrobial activity into infected macrophages was assessed in mycobateria-infected BMMΦ. The macrophages were infected with one of two mycobacterial strains of distinct virulence: the opportunistic *M. avium* 2447, which only affects immunocompromised individuals, or the highly human pathogenic *M. tuberculosis* H37Rv. BMMΦ were seeded at 5×10^5 cells/ml in 24-well plates and allowed to adhere overnight. Cells were then infected with either mycobacteria strain at a multiplicity of infection of 2 for 4 h, which allowed mycobacteria internalization. Following the removal of non-internalized mycobacteria (by washing the wells 4 times in pre-warmed DMEM), the blank and antimicrobial-loaded nanogels were added to the BMMΦ at the concentrations mentioned in section 2.4. A PBS solution was added to the control group. Intracellular growth of mycobacteria was measured after 7 days (*M. avium*) or 4 days (*M. tuberculosis*).

After 7 days (*M. avium*) or 4 days (*M. tuberculosis*), BMMΦ were permeabilised with 10 % saponin, for 10 min, at room temperature. Differences in incubation periods relate to the different survival rates of macrophages in the presence of each mycobacterial strain. Although 7 days has been described as the adequate timepoint to measure *M. avium* CFUs [33], the higher virulence of *M. tuberculosis* results in the earlier killing of infected macrophages, thus requiring CFUs to be counted at an early timepoint. Serial dilutions (1:10, 1:100, 1:1000, 1:10000) of mycobacteria were then plated on 7H10 or 7H11 agar plates and cultured at 37 °C, 5 % CO_2. Mycobacterial survival was evaluated by CFU counting after 2 weeks of culture). The initial intracellular mycobacterial load was assessed identically at day 0.

2.11. Statistical analysis

The results were expressed as mean ± SD of 3 independent experiments (n=3). Statistical analysis was performed with one-way ANOVA followed by Tukey's comparison test using using GraphPad Prism version 6.00, GraphPad Software, La Jolla California USA. Significance of the results is indicated according to P values corresponding to P=0.01 to 0.05 (*); P=0.001 to 0.01 (**); P=0.0001 to 0.001 (***) and P<0.0001 (****), respectively.

3. Results and discussion

Hyaluronic acid (HyA) nanogel was produced by the grafting of a thiolated hydrophobic chain to a HyA backbone resulting in an amphiphilic molecule capable of self-assembling into nanostructures in aqueous solution. The particles produced were spherical with a bimodal size distribution and a mean diameter of 80.2 +/- 0.4 nm (n=5) [14]. Production, characterization and crosslinkability of the nanogel through redox sensitive linkage were assessed in our previous work [14].

3.1. Nanogel cellular uptake by flow cytometry

We studied the HyA-AT nanogel's ability to target hyaluronan cell receptors such as CD44 and RHAMM, which are overexpressed in several tumours [34-38]. We conducted cellular uptake experiments of the nangel in the HeLa cell line, which overexpresses RHAMM and (to a lesser degree) CD44 [12, 13]. HeLa cells were treated using two concentrations of fluorescein labelled nanogel (0.2 and 0.5 mg/ml) to evaluate dose effect on internalization kinetics by flow cytometry. Nanogel cytotoxicity and dependency on concentration was evaluated at all time points with PI assay (Figure 1a and supplementary information S2). PI can bind to cytoplasmic DNA when cell membrane is damaged, resulting in positive PI staining [39]. Our results showed that only at the longest incubation times (24 h), with the highest nanogel concentration (0.5mg/ml), a significant difference in PI positivity in the cells treated (approximately 30%) was detected.

In Figure 1b we compare uptake of the nanogel at different concentrations over a time course up to 24 h. The results and statistical analysis demonstrate that the MFI was the double at approximately all time points for the higher nanogel dosage (e.g. at 2h MFI for 0.2 mg/ml was 241.5 and at highest dosage, 423.5). Frequence results show that for the lowest concentration (0.2 mg/ml) only about 50% of cells exhibit fluorescence signal, due to nanogel presence. Trypan blue exclusion assay was employed to help us distinguish between cell adhering fluorescence and cell-internalized nanogel particles. Trypan blue quenches fluorescent nanogel signal when at cell surface and therefore, not internalized [15, 30, 40]. Results of TB quenching show that around 20% of the nanogel detected was not internalized (supplementary information S1). Dot blots and histograms analysis of nanogel samples throughout time are presented as Supplementary information (S2). Results show that for the 0.5 mg/ml nanogel, and after 7 h of incubation, nanogel uptake seem to reach a plateau. This effect is not observed at lowest nanogel dosage.

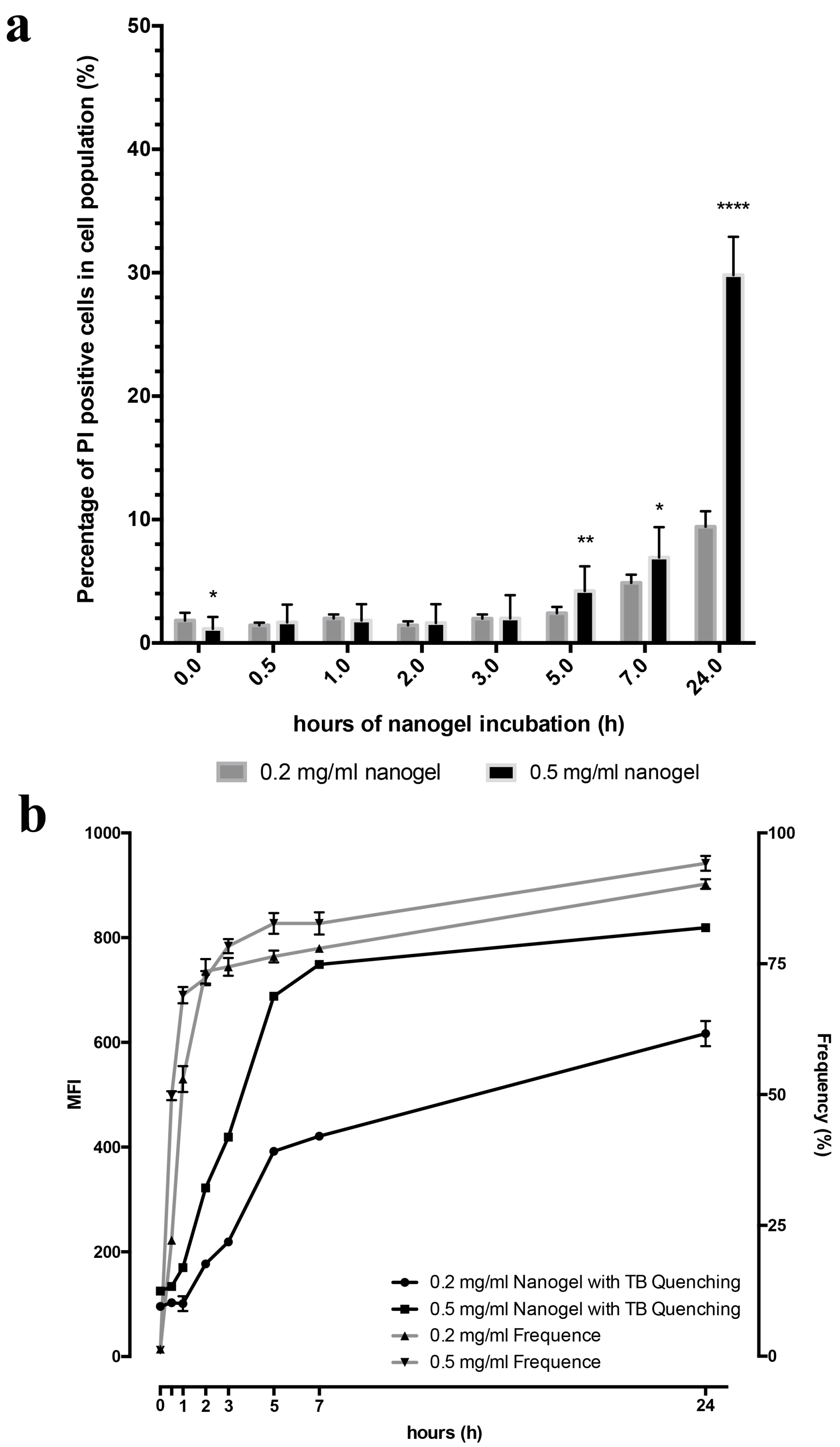

Figure 1: Flow cytometry analysis of Fluorescein labelled HyA-AT nanogel uptake a) Percentage of cells with positive propidium iodide (PI) staining at low and high nanogel doses (0.2 and 0.5 mg/ml respectively) over a time course

from 0 to 24 h. b) Comparison between MFI of HeLa cells up to 24 h incubation with 0.2 mg/ml or 0.5 mg/ml fluorescein labelled nanogel. Cells were treated with TB and membrane adherent nanogel fluorescence was quenched. Frequency of cells are displayed. Results are presented as MFI +/- SD, for experiment performed in triplicates.

Nanogel internalization by HeLa cells was also assessed by confocal microscopy. Confocal data support flow cytometry results, and demonstrate a bright green fluorescence signal in cell cytoplasm assigned to the nanogel (figure 2a). Careful examination of images in figure 2a reveals a bright fluorescence signal throughout cell cytoplasm, apparently not inside endosomes and in some areas displaying filamentous localisation.

To further understand if internalization depends an active or passive process, we performed studies in which cell energy was impaired by lowering incubation temperature or by chemical inhibition [3, 32, 41]. Results showed (figure 2b) that cells incubated for 30 min at 37ºC exhibits a low amount of nanogel (confirmed through z scanning to be present inside cells), while for cells incubated at 4ºC (figure 2c), some nanogel aggregates were detected only at the cell surface. These results seem to indicate that nanogel internalization takes advantage of energy dependent pathways. The active transport of nanomedicine is dependent on endocytosis and therefore, energy-dependent mechanisms.

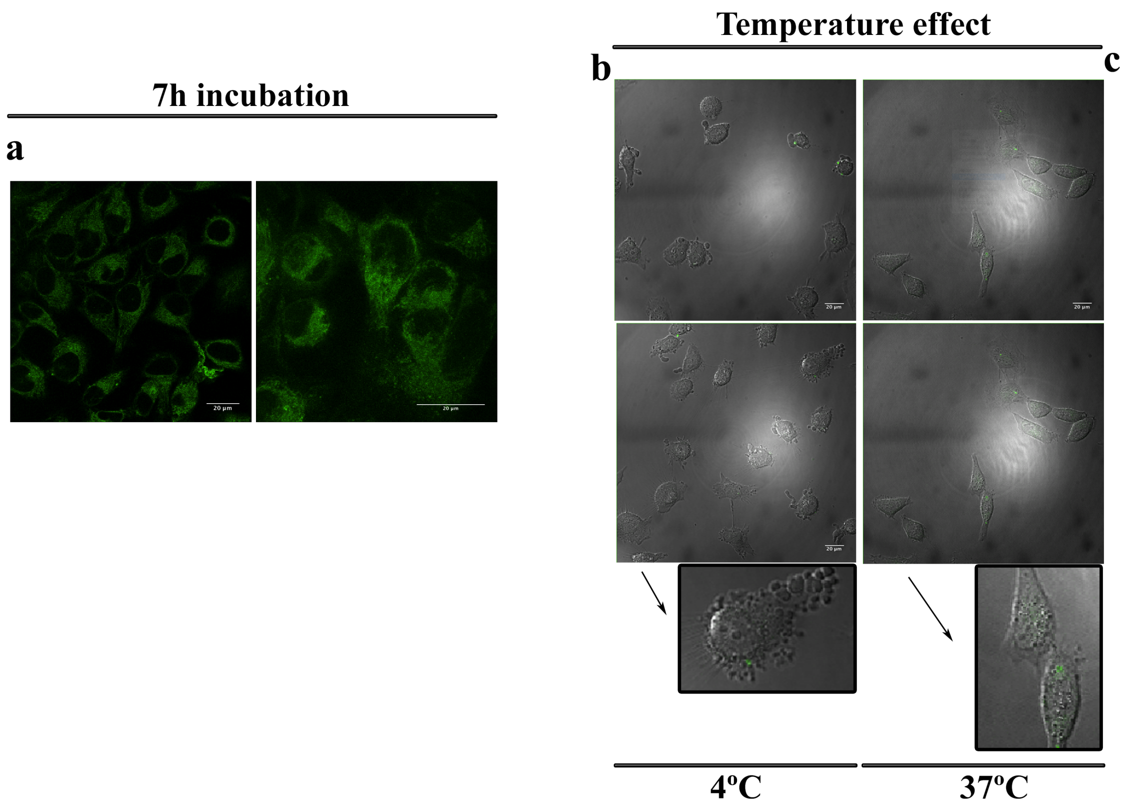

Figure 2: Confocal microscopy analysis of HeLa cells incubated with 0.2 mg/ml HyA-AT-Alexa488 labelled nanogel. a) Cellular uptake of Alexa488-nanogel in HeLa cells after 7 h incubation period under standard cell culture conditions. Images (a) presented correspond to single channel capture of nanogel labelled with fluorescein (green). b) Nanogel cellular uptake in HeLA cells at 4°C after 30 min incubation period. c) Nanogel cellular uptake at 37°C after 30 min incubation time. Superimposition of images *b* and *c* on the differential interference contrast (DIC) images show cells condition and green fluorescence is attributed to nanogel signal.

3.2. Nanogel internalization in transfected cells

To study nanogel internalization pathway in HeLA cells we used single siRNA sequences that reduce endocytic protein expression and therefore inhibit specific endocytic pathways. Although pharmacological inhibitors are a common approach their efficacy has been largely questioned [6, 15]. Studies have shown that siRNA induced silencing of endocytic proteins is a much more selective and a more accurate approach [15].

It is known that cytotoxicity associated with siRNA transfection depends on the reagents used and on the nature of cells [32]. So in previous work [4] we studied the cell proliferation and metabolic activity of HeLA cells transfected with the same siRNA and transfection protocol used in these studies. The results showed that siRNA transfection didn't compromise cell viability.

HeLA cells were transfected with siRNA sequences that inhibit key proteins of macropynocytosis (p21-activated kinase 1), clathrin (clathrin heavy chain), caveolin (caveolin-1) and flotlin (Flotillin-1) mediated endocytosis pathways. Non-transfected cells, oligofectamine-treated cells and cells transfected with siRNA-GFP were used as negative controls. Transfected cells were incubated with the nanogel for 7 h and fluorescence intensity was measured by flow cytometry analysis. Results shown in figure 3a, suggest that nanogel uptake by HeLA cells occurs by a combination of caveolae- and and clathrin-mediated endocytosis. This is indicated by the reductions in MFI in the CAV-1 (63%) and CHC (42%) siRNA depleted cells compared with the GFP-siRNA transfected control; depletion of other endocytic pathways (via PAK-1 and Flot1A) did not significantly alter nanogel uptake.

Other published studies with pharmacological endocytosis inhibitors demonstrated that cellular uptake of hyaluronic acid poly(l-histidine) micelle was also mediated by CME and CvME [42]. Yin et al. [1], also used pharmacological inhibitors to demonstrate that hyaluronic acid-paclitaxel conjugated micelles were internalized by CvME (54.6%) and CME (31.2%). Hyaluronic acid–spermine conjugates (HHSCs) also proved to be preferentially taken up by CvME [43]. Finally, Contreras-Ruiz et al. also demonstrated hyaluronic acid (HA)-chitosan oligomer (CSO)-based nanoparticles uptake was mediated by hyaluronic acid receptors through CvME [5]. It is reported that chemical endocytosis inhibitors are associated with problems related to toxicity and low specificity [6].

HeLa cells are known to overexpress RHAMM receptors and in smaller amount CD44 receptors that are known to be associated with CvME [44-46]. Also, CvME is known to be associated with both endoplasmic reticulum (ER) and Golgi. It is believed that non-degradative pathway of caveolae-ligand ensemble are transported and delivered to ER and Golgi [3, 6, 32]. So, this seem to corroborate our findings that nanogel was distributed throughout the cytoplasm in an almost linear pattern and therefore, hypothetically, its association with those organelles.

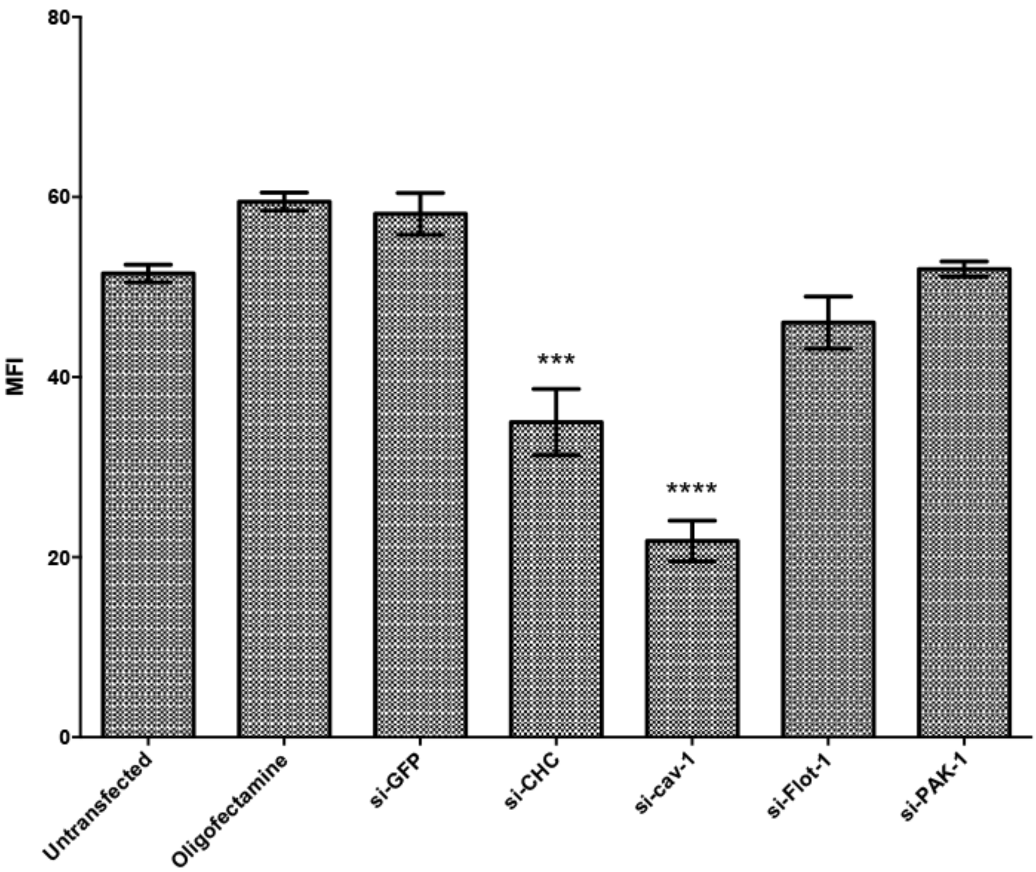

Figure 3: MFI of the HyA-AT nanogel labeled with Alexa488 internalization by HeLa cells transfected with si-CHC, si-Cav-1, si-Pak-1 and si-Flot-1, measured by flow cytometry. Untreated cells, cells incubated with oligofectamine alone or transfected with oligofectamine/si-GFP were tested as negative controls.

P=0.0001 to 0.001 (***) and P<0.0001 (****) represent statistical significance of differences between samples. Error bars represent S.D.

3.3. HyA-AT nanogel as a drug carrier for intracellular delivery

Finally, we assessed the potential of the HyA-AT nanogel as a broader drug-targeting tool, by widening its scope to the delivery of antimicrobials into mycobacteria-infected macrophages. This is a relevant model of infection taking into account the global burden of tuberculosis, currently one of the deadliest infectious diseases [16]. Moreover, activated macrophages overexpress the CD44 receptor in response to infection, thus being able to uptake hyaluronan [21, 22]. Here, we explored the ability of HyA-AT nanogel to deliver hydrophobic anti-tuberculosis drugs to infected macrophages and target them into mycobacteria residing within the host macrophages. Two different antimicrobials of known efficacy were loaded into the HyA-AT nanogel: rifampicin, a standard antibiotic used as part of a multi-drug cocktail in the treatment of tuberculosis and whose *in vitro* efficacy has been described [27]; and an antimicrobial peptide (AMP), with the following amino acid sequence: KIWWWWRKRC. A C-terminal cysteine was added to the peptide KIWWWWRKR – which displayed a low Minimal Inhibitory Concentration (MIC = 4.1 μM) against *M. tuberculosis* [28] - to further increase the peptide's antimicrobial activity. Indeed, Wiradharma and co-workers [29] have reported the significant enhancement of AMP antimicrobial activity against both Gram-positive and Gram-negative bacteria by incorporating cysteine(s) - a polar uncharged residue – at the terminal ends of antimicrobial peptides.

The ability of HyA-AT nanogel to internalise macrophages and deliver hydrophobic anti-tuberculosis drugs was assessed by adding the blank or drug-loaded nanogel to mycobacteria-infected macrophages. Figure

4a shows that, infected macrophages are able to internalise the HyA-AT nanogel, which is found within punctate intracellular vesicles after 24 h, unlike what is observed in loaded HeLa cells, where a more broad intracellular distribution of the nanogel was observed. It is thus reasonable to suspect that the pathway of internalisation differs in infected macrophages, where we can speculated that phagocytosis plays a more relevant role, compared to HeLa cells.

Figure 4b demonstrates that the nanogel significantly prevented the decrease in metabolic activity, indicated by the enzymatic reduction of MTS, that occurred in the presence of high concentrations of free (non-loaded) antimicrobials (Fig. 4b). These are important features, since some of the major drawbacks associated with the elimination of mycobacteria by antimicrobials include: the drugs inability to target intracellular compartments where the mycobacteria reside; cytotoxicity at therapeutically relevant concentrations, and intracellular degradability [47, 48].

Loading of rifampicin into the HyA-AT nanogel and treatment of infected macrophages allowed a significant reduction (~1.2 log) in *M. avium* 2447 load (Fig. 4c). The nanogel loaded with an antimicrobial peptide also demonstrated strong activity against *M. tuberculosis:* ~1.7 log reduction in the intracellular infection levels of this highly virulent strain (Fig. 4d. As such, the HyA-AT nanogel not only allows the use of therapeutically relevant concentrations of antimicrobials, but also provides a mechanism to target these molecules towards mycobacteria residing in the phagosomes of host cells. These results thus confirm the potential of the HyA-AT nanogel as a drug delivery approach of therapeutically relevant hydrophobic molecules for at least two relevant biomedical applications, since its effect is not limited to cancer cells.

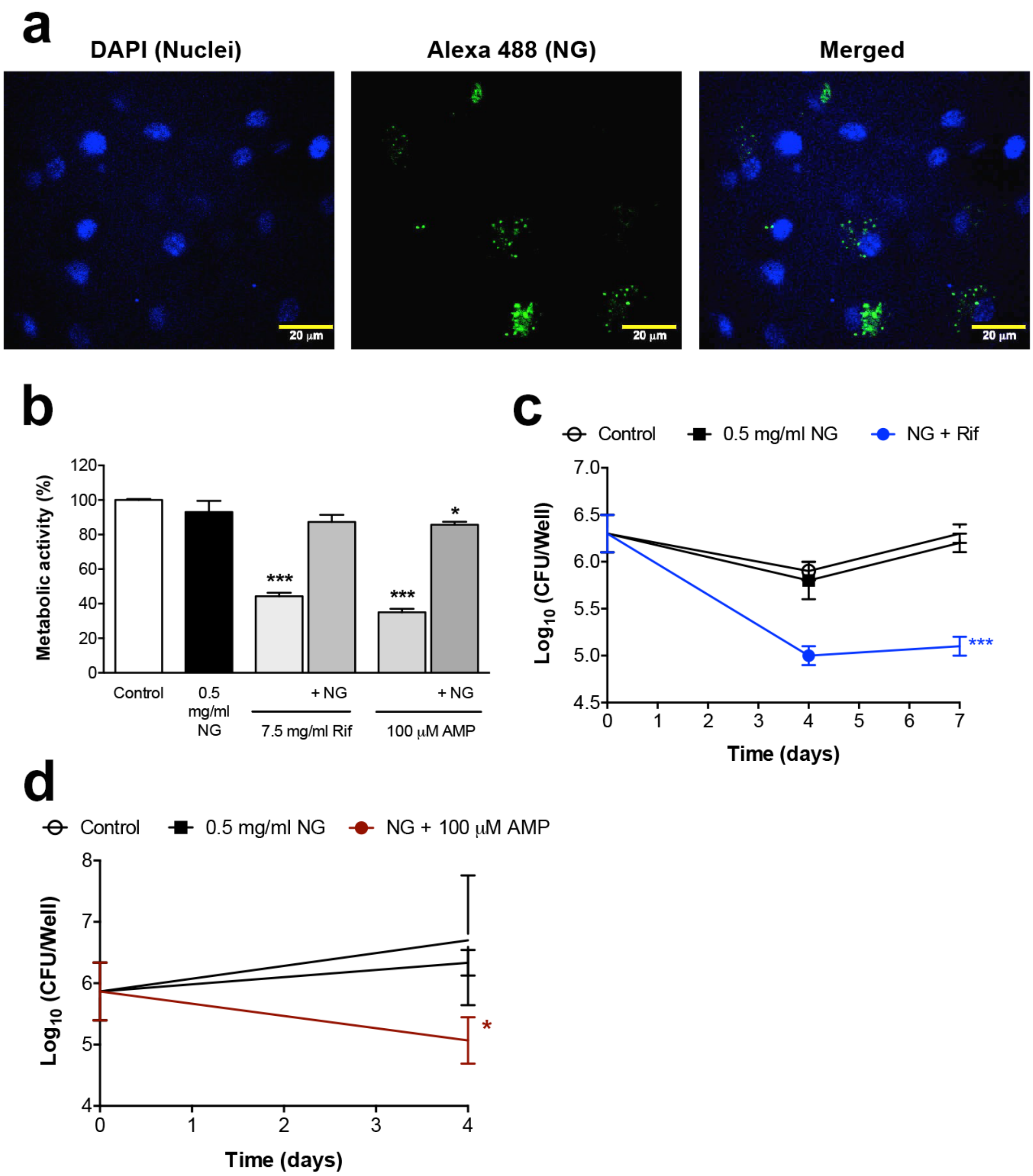

Figure 4: Intracellular delivery of therapeutic drugs by HyA-AT nanogel loaded into macrophages(a) BMMΦ were incubated with Alexa Fluor 488-labeled HyA-AT nanogel (green) for 24 h and the internalisation of the nanogel was imaged through confocal microscopy. BMMΦ nuclei were stained with DAPI (blue). (b) Quantification of BMMΦ's metabolic activity, using the MTS reduction test, following a 24 h incubation in the presence of the different formulations. (c) Blank and rifampicin-loaded nanogel was added to M. avium 2447-infected BMMΦ. After 7 days, macrophages were lysed and the number of M. avium CFUs counted. Data represents the mean ± SEM, for at least 3 independent experiments performed in triplicates. *** $p < 0.001$, compared to control. (d)

HyA-AT nanogel containing or not the antimicrobial peptide (AMP) KIWWWWRKRC were added to M. tuberculosis-infected BMMΦ. After 4 days, cells were lysed and the number of mycobacteria CFUs counted. Data represents the mean ± SEM, for at least 3 independent experiments performed in triplicates. * $p < 0.05$, compared to control

4. Conclusion

Nanogel internalization by HeLa cells proved to be dose, time and energy dependent. Further studies with selective inhibition of endocytic pathways proteins via siRNA transfection gave us further information about the nanogel endocytosis process. Results showed that essentially caveolae mediated endocytosis and also clathrin mediated endocytosis were the primary mechanisms by which the nanogel entered cells.

We also demonstrated the broader potential usage of the HyA-AT nanogel in biomedicine extending our studies to a model of mycobacterial infection. The HyA-AT nanogel proved to be able to perform as a carrier of different kinds of drug (small and slightly water-soluble rifampicin and cationic antimicrobial peptides), thus showing as a promising drug delivery system.

5. Acknowledgments

The authors thank the FCT Strategic Project of UID/BIO/04469/2013 unit, the project RECI/BBB-EBI/0179/2012 (FCOMP-01-0124-FEDER-027462) and the Project “BioHealth - Biotechnology and Bioengineering approaches to improve health quality", Ref. NORTE-07-0124-FEDER-000027, co-funded by the Programa Operacional Regional do Norte (ON.2 – O Novo Norte), QREN, FEDER. We would like to acknowledge also the support of FCT for the PhD grant reference SFRH/BD/61516/2009.

6. References

1. Yin, S., et al., *Intracellular delivery and antitumor effects of a redox-responsive polymeric paclitaxel conjugate based on hyaluronic acid.* Acta Biomater, 2015. **26**: p. 274-85.
2. Zaki, N.M., A. Nasti, and N. Tirelli, *Nanocarriers for cytoplasmic delivery: cellular uptake and intracellular fate of chitosan and hyaluronic acid-coated chitosan nanoparticles in a phagocytic cell model.* Macromol Biosci, 2011. **11**(12): p. 1747-60.
3. Al-Soraj, M.H., et al., *siRNA versus pharmacological inhibition of endocytic pathways for studying cellular uptake of cell penetrating peptides.* J Control Release, 2010. **148**(1): p. e86-7.
4. Pereira, P., et al., *siRNA Inhibition of Endocytic Pathways to Characterize the Cellular Uptake Mechanisms of Folate-Functionalized Glycol Chitosan Nanogels.* Mol Pharm, 2015. **12**(6): p. 1970-9.
5. Contreras-Ruiz, L., et al., *Intracellular trafficking of hyaluronic acid-chitosan oligomer-based nanoparticles in cultured human ocular surface cells.* Mol Vis, 2011. **17**: p. 279-90.
6. Vercauteren, D., et al., *The use of inhibitors to study endocytic pathways of gene carriers: optimization and pitfalls.* Mol Ther, 2010. **18**(3): p. 561-9.
7. Arpicco, S., et al., *Hyaluronic acid conjugates as vectors for the active targeting of drugs, genes and nanocomposites in cancer treatment.* Molecules, 2014. **19**(3): p. 3193-230.
8. Goodarzi, N., et al., *A review of polysaccharide cytotoxic drug conjugates for cancer therapy.* Carbohydr Polym, 2013. **92**(2): p. 1280-93.
9. Platt, V.M. and F.C. Szoka, Jr., *Anticancer therapeutics: targeting macromolecules and nanocarriers to hyaluronan or CD44, a hyaluronan receptor.* Mol Pharm, 2008. **5**(4): p. 474-86.
10. Ahrens, T., et al., *CD44 is the principal mediator of hyaluronic-acid-induced melanoma cell proliferation.* J Invest Dermatol, 2001. **116**(1): p. 93-101.
11. Necas, J., et al., *Hyaluronic acid (hyaluronan): a review.* Veterinarni medicina, 2008. **53**(8): p. 397-411.
12. Gu, W., et al., *Silencing oncogene expression in cervical cancer stem-like cells inhibits their cell growth and self-renewal ability.* Cancer Gene Ther, 2011. **18**(12): p. 897-905.
13. Maxwell, C.A., et al., *RHAMM is a centrosomal protein that interacts with dynein and maintains spindle pole stability.* Mol Biol Cell, 2003. **14**(6): p. 2262-76.
14. Pedrosa, S.S., et al., *A novel crosslinked hyaluronic Acid nanogel for drug delivery.* Macromol Biosci, 2014. **14**(11): p. 1556-68.

15. Vranic, S., et al., *Deciphering the mechanisms of cellular uptake of engineered nanoparticles by accurate evaluation of internalization using imaging flow cytometry*. Part Fibre Toxicol, 2013. **10**: p. 2.
16. (WHO), W.H.O., *Global Tuberculosis Report 2015*. 2015.
17. ACCESS, M., *DR-TB DRUGS UNDER THE MICROSCOPE*. 2012.
18. Sosnik, A., et al., *New old challenges in tuberculosis: Potentially effective nanotechnologies in drug delivery*. Advanced Drug Delivery Reviews, 2010. **62**(4–5): p. 547-559.
19. Zumla, A., P. Nahid, and S.T. Cole, *Advances in the development of new tuberculosis drugs and treatment regimens*. Nat Rev Drug Discov, 2013. **12**(5): p. 388-404.
20. Alsaad, N., et al., *Potential antimicrobial agents for the treatment of multidrug-resistant tuberculosis*. Eur Respir J, 2014. **43**(3): p. 884-97.
21. Sladek, Z. and D. Rysanek, *Expression of macrophage CD44 receptor in the course of experimental inflammatory response of bovine mammary gland induced by lipopolysaccharide and muramyl dipeptide*. Research in Veterinary Science, 2009. **86**(2): p. 235-240.
22. Underhill, C.B., et al., *Cd44 Positive Macrophages Take up Hyaluronan during Lung Development*. Developmental Biology, 1993. **155**(2): p. 324-336.
23. Chen, T.R., *Re-evaluation of HeLa, HeLa S3, and HEp-2 karyotypes*. Cytogenet Cell Genet, 1988. **48**(1): p. 19-24.
24. Torrado, E., et al., *IFN-gamma-Dependent Activation of Macrophages during Experimental Infections by Mycobacterium ulcerans Is Impaired by the Toxin Mycolactone*. Journal of Immunology, 2010. **184**(2): p. 947-955.
25. Hermanson, G.T., *Bioconjugate techniques*. 2nd edition. ed. 2008, San Diego: Academic Press. xxx, 1202 pages.
26. Tanzer, M.L., D. Monroe, and J. Gross, *Inhibition of collagen intermolecular cross-linking by thiosemicarbazide*. Biochemistry, 1966. **5**(6): p. 1919-26.
27. Khara, J.S., et al., *Anti-mycobacterial activities of synthetic cationic α-helical peptides and their synergism with rifampicin*. Biomaterials, 2014. **35**(6): p. 2032-2038.
28. Ramon-Garcia, S., et al., *Targeting Mycobacterium tuberculosis and Other Microbial Pathogens Using Improved Synthetic Antibacterial Peptides*. Antimicrobial Agents and Chemotherapy, 2013. **57**(5): p. 2295-2303.
29. Wiradharma, N., et al., *The effect of thiol functional group incorporation into cationic helical peptides on antimicrobial activities and spectra*. Biomaterials, 2011. **32**(34): p. 9100-9108.
30. Avelar-Freitas, B.A., et al., *Trypan blue exclusion assay by flow cytometry*. Braz J Med Biol Res, 2014. **47**(4): p. 307-15.

31. Keogh, M.J., et al., *Simultaneous measurement of phagocytosis and respiratory burst of leukocytes in whole blood from bottlenose dolphins (Tursiops truncatus) utilizing flow cytometry.* Vet Immunol Immunopathol, 2011. **144**(3-4): p. 468-75.
32. Jones, A.T., *Gateways and tools for drug delivery: endocytic pathways and the cellular dynamics of cell penetrating peptides.* Int J Pharm, 2008. **354**(1-2): p. 34-8.
33. Santos, J.C., et al., *Endogenous cathelicidin production limits inflammation and protective immunity to Mycobacterium avium in mice.* Immunity, Inflammation and Disease, 2014. **2**(1): p. 1-12.
34. Abbad, S., et al., *Preparation, in vitro and in vivo evaluation of polymeric nanoparticles based on hyaluronic acid-poly(butyl cyanoacrylate) and D-alpha-tocopheryl polyethylene glycol 1000 succinate for tumor-targeted delivery of morin hydrate.* Int J Nanomedicine, 2015. **10**: p. 305-20.
35. Choi, K.Y., et al., *Self-assembled hyaluronic acid nanoparticles for active tumor targeting.* Biomaterials, 2010. **31**(1): p. 106-14.
36. Leung, E.L., et al., *Non-small cell lung cancer cells expressing CD44 are enriched for stem cell-like properties.* PLoS One, 2010. **5**(11): p. e14062.
37. Li, J., et al., *Hyaluronic acid-modified hydrothermally synthesized iron oxide nanoparticles for targeted tumor MR imaging.* Biomaterials, 2014. **35**(11): p. 3666-77.
38. McDonald, B., et al., *Interaction of CD44 and hyaluronan is the dominant mechanism for neutrophil sequestration in inflamed liver sinusoids.* J Exp Med, 2008. **205**(4): p. 915-27.
39. Lee, M.K., S.J. Lim, and C.K. Kim, *Preparation, characterization and in vitro cytotoxicity of paclitaxel-loaded sterically stabilized solid lipid nanoparticles.* Biomaterials, 2007. **28**(12): p. 2137-46.
40. Van Amersfoort, E.S. and J.A. Van Strijp, *Evaluation of a flow cytometric fluorescence quenching assay of phagocytosis of sensitized sheep erythrocytes by polymorphonuclear leukocytes.* Cytometry, 1994. **17**(4): p. 294-301.
41. Kandimalla, K.K., et al., *Mechanism of neuronal versus endothelial cell uptake of Alzheimer's disease amyloid beta protein.* PLoS One, 2009. **4**(2): p. e4627.
42. Qiu, L., et al., *Self-assembled pH-responsive hyaluronic acid-g-poly((L)-histidine) copolymer micelles for targeted intracellular delivery of doxorubicin.* Acta Biomater, 2014. **10**(5): p. 2024-35.
43. Shen, Y., et al., *A novel tumor-targeted delivery system with hydrophobized hyaluronic acid-spermine conjugates (HHSCs) for efficient receptor-mediated siRNA delivery.* Int J Pharm, 2011. **414**(1-2): p. 233-43.
44. Chen, H., et al., *Spatial regulation of Aurora A activity during mitotic spindle assembly requires RHAMM to correctly localize TPX2.* Cell Cycle, 2014. **13**(14): p. 2248-61.

45. Nikitovic, D., et al., *The roles of hyaluronan/RHAMM/CD44 and their respective interactions along the insidious pathways of fibrosarcoma progression.* Biomed Res Int, 2013. **2013**: p. 929531.
46. Parent, R.A., *Comparative biology of the normal lung*. Second edition. ed. 2015, Amsterdam ; Boston: Elsevier/AP, Academic Press is an imprint of Elsevier. xvii, 815 pages.
47. Petkar, K.C., et al., *Nanostructured materials in drug and gene delivery: a review of the state of the art.* Crit Rev Ther Drug Carrier Syst, 2011. **28**(2): p. 101-64.
48. Appelberg, R., *Pathogenesis of Mycobacterium avium infection: typical responses to an atypical mycobacterium?* Immunologic Research, 2006. **35**(3): p. 179-190.

7. SUPPLEMENTARY INFORMATION

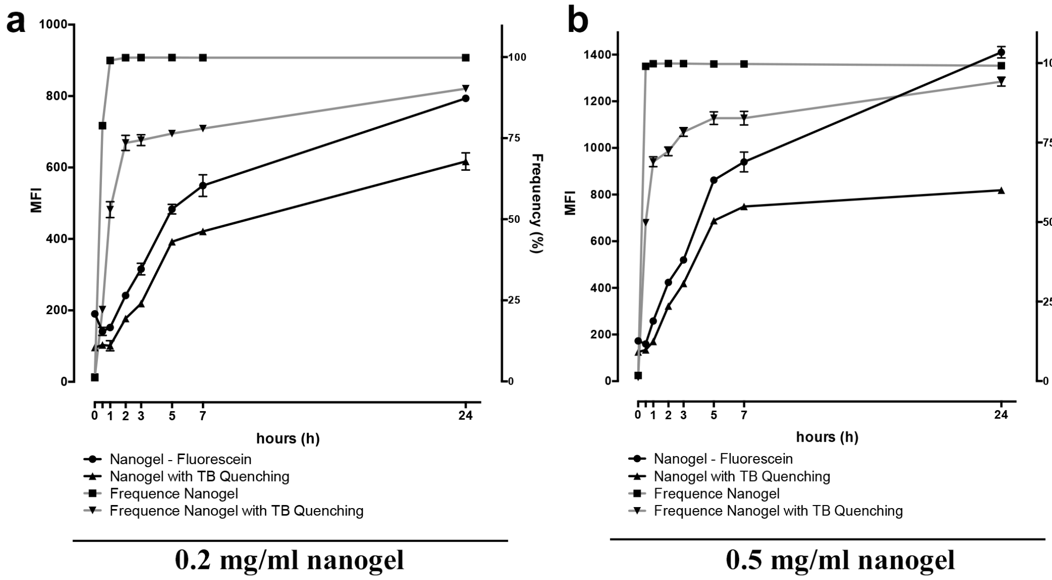

S1: Flow cytometry analysis of Fluorescein labelled HyA-AT nanogel uptake a) Mean fluorescence intensity (MFI) of HeLa cells up to 24h incubation with 0.2 mg/ml fluorescein labelled naogel. Also, comparison before and after trypan blue (TB) exclusion assay. Frequencies (or percentage) of cells in gates of interest are also presented; b) Mean fluorescence intensity (MFI) of HeLa cells when incubated with 0.5mg/ml fluorescein labelled nanogel through time, before and after trypan blue (TB) treatment. Also, frequencies of cells are presented.

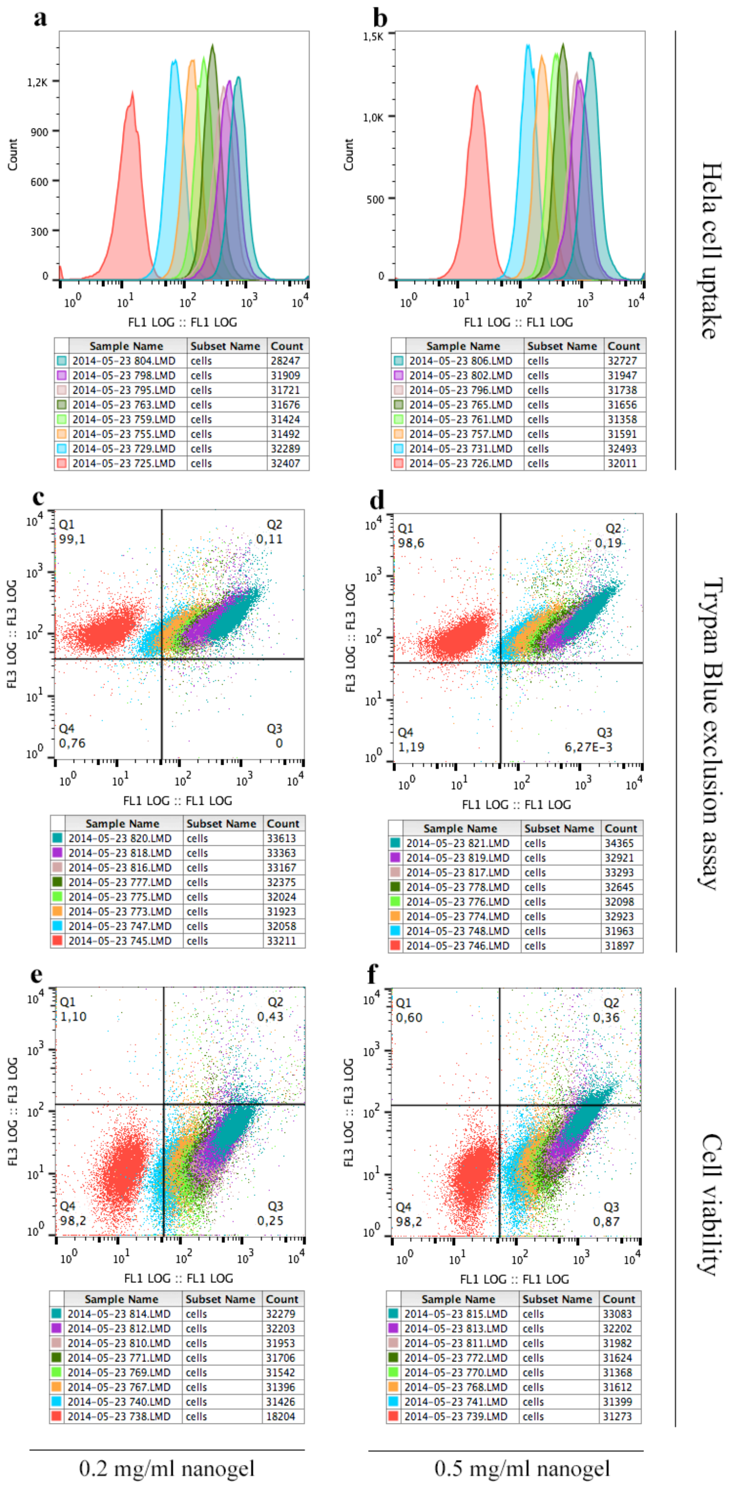

S2: Histogramas and dot blot analysis of nanogel samples through time. Histogram representation in FL1 channel of HelLa cells through time incubated with 0.2 mg/ml (a) and 0.5 mg/ml (b) of nanogel. Dot blot analysis in FL1 and FL3 of Hela cells incubated with 0.2 mg/ml (c) or 0.5 mg/ml (d) of nanogel, after TB exclusion assay. Dot blots of Hela cells through time incubation with 0.2 mg/ml (e) or 0.5 mg/ml (f) of nanogel, and with PI staining.

CHAPTER VI

CONCLUSION AND FUTURE PERSPECTIVES

In the present work we had set ourselves to produce a hyaluronic acid nanogel for the targeting of non-small cancer lung cells.

Hyaluronic acid nanogel was successfully produced by self-assembly method in a simple, quick and reproductive manner. Hyaluronic acid was conjugated by amide bond formation with 11-amino-undecanethiol (AT) resulting in an amphiphilic thiolated material capable of self-assembling into nanosized structures in aqueous environment. When dispersed in water at 1.0 mg/ml concentration, HyA-AT nanogel shows a bimodal size distribution with a smaller population around 20nm and another with about 150 nm, corresponding to a mean size diameter of 80.2+/-0.4nm (n=5). The zeta potential obtained for the nanogel was – 19.3 +/- 1.97mV (n=5) in average. Sulfhydryl groups at the end of the hydrophobic chains allowed us to further reticulate the nanogel with redox sensitive bonds. With that purpose, a homobifunctional sulfhydryl-reactive crosslinker-1,4-Bis(3-[2 pyridyldithio]propionamido)butane) (DPDPB) was conjugated with HyA-AT resulting in a 14-atom spacer of approximately 16 A° in length. Validation of the crosslinking was obtained by ^{1}HNMR analysis and identification of peaks assigned to the methyl groups of DPDPB; by UV-Vis spectroscopy due to the release of the two pyridine-2-thione during the conjugation reaction, redox Sensitive Characterization and others. Results corroborated the successful reticulation of the HyA-AT nanogel. Drug entrapment efficiency of HyA-AT nanogel and crosslinked nanogel (HyA-AT-DPDPB) were determined using Curcumin and simvastatin as model hydrophobic drugs. Results showed both HyA-AT and HyA-AT-DPDPB nanogels had high drug loading capacity and an entrapment efficiency around 50%. Also, reticulated nanogel exhibited higher size stability but didn't increase significatively the drug loading capacity.

Nanoparticles and other nanostructures offer promising solutions for future therapeutics but its safety is a primary concern regarding this new vehicles. Therefore we performed a comprehensive study of our engineered nanogel biocompatibility *in vitro* and *in vivo*. Cytotoxicity studies were performed in four different cellular lines: 3T3, HMEC, A549 and RAW 264.7. As we know materials cytotoxicity depends not only on the dosage and characteristics of the materials but also on the cell nature. This cell collection allowed us to infer the toxicological effect of nanogel in relevant tissues and in the vasculature. Nanogels metabolic activity evaluated by MTT assay was not, overall, evidently affected but nanogel incubation. Evaluation of membrane integrity by LDH leakage showed that membrane integrity was preserved at all nanogel concentrations for all cell lines. Nanogel induced apoptosis was determined by annexin V-FITC and PI double staining resorting to flow citometry in all cell lines tested and a significant effect was not detectedit was not detected in comparison with the negative control (20% water diluted culture medium). Complement cascade activation assessed by C3 cleavage upon nanogel incubation with human plasma revealed nanogel had low immunogenicity. Also, we investigated nanogel phagocytic recognition and uptake by bone marrow derived macrophages, used as a phagocytic model due to its peculiar capacity of internalizing extracellular materials by a wide range of mechanisms and entry routes. Results showed dextrin nanoparticles and native HyA showed much higher internalization than HyA-AT nanogel. In agreement with the Standard Practice for Assessment of Haemolytic Properties of Materials from the American Society for Testing Materials (ASTM F756-00, 2000) nanogel proved to be non-haemolytic at the concentrations tested.

Hyaluronic acid nanogel demonstrated appealing fico-chemical and biological properties, biocompatibility, biodegradability and non-immunogenicity. However, among the most attractive features of hyaluronic acid applied to nanomaterials is the potential for active targeting due to its strong affinity of hyaluronic acid for cell surface receptors, namely CD44 and Receptor for Hyaluronan Mediated Motility (RHAMM). Therefore, we investigated nanogel targetability mediated by hyaluronic acid interface towards CD44 overexpressing cancer cells. Non-small cancer lung cells - A549 cell line – express high levels of CD44 receptors and therefore were used as a target for nanogel uptake studies. The *in vitro* cellular uptake of nanogel by A549 cells was assessed by flow cytometry analysis and confocal fluorescence microscopy and showed the nanogel was most internalized in CD44 over-expressing cells. Also, nanogel uptake was dose and time dependent and a competitive study in which, A549 cells were treated with an excess of free HyA, 1h before nanogel incubation suggested that nanogel uptake was affected by the free HyA interaction with receptors.

Also, we investigated the nanogel targetability in tumor bearing mice induced with subcutaneous A549 cell injection. The biodistribution was analyzed in a non-invasive real time NIR imaging system, after intravenous administration of probe labeled samples. Results showed that nanogel had long circulation time – up to 48h – and long residency in tumour site as compared to native HyA. Tumour accumulation might be due to a combination of two factors; receptor mediated targeting through CD44 and enhanced permeation and retention (EPR). We also studied the effect of the NIR probe in materials biodistribution. As we know changes in particle size, surface charge, texture and heterogeneity in nanoparticles formulation influence its biodistribution, so their decoration with NIR should be accessed. We also performed a comparative study of *in vivo* pharmacokinetics of the HyA nanogel, native HyA and free probe in healthy animals, using two different NIR probes - Cy5.5 and Alexa Fluor 680. Our results showed that actually, organ accumulation was different in nanogel labelled with Cy5.5 and Alexa680.

Interactions between nanocarriers and cellular membrane determine nanogels cellular uptake and further affect its intracellular transport and fate. Therefore, we investigated the cell trafficking of Hya-AT nanogel in Human cervical adenocarcinoma cells (HeLa). HeLa cells are known to overexpress RHAMM receptors and also, in fewer number CD44 receptors. With that purpose, siRNA machinery was used to regulate expression of key proteins of endocytic pathways: clathrin heavy chain (si-CHC), caveolin-1 (si-Cav-1), p21-activated kinase 1 (si-Pak-1) and Flotillin-1 (si-Flot-1). Cells transfected with these siRNA cells were then incubated with HyA-AT nanogel and its uptake was analysed by flow cytometry. Results suggested that nanogel uptake by HeLA cells occurs mainly by caveolae mediated endocytosis and also by clathrin mediated endocytosis. Caveollae mediated endocytosis is the mechanism that is believed to not be associated with acidic cellular compartments and commonly associated with CD44 receptor mediated endocytosis.

Lastly, hyaluronic acid nanogel demonstrated attractive features as drug delivery system, crosslinkable through redox sensitive bond. Moreover demonstrated great biocompatibility, immunocompatibility and hemocompatibility, *in vitro* and in vivo. Furthermore demonstrated high targetability towards hyaluronic acid receptors both *in vitro* and *in vivo*.

Needless to say that work is yet to be done in several areas and we intend to continue working in the development and improvement of this hyaluronic acid nanogel, further comprehend its interactions with biological environment and broaden horizons as to its application. Here are some of the proposed tasks:

- Study the nanogel interaction with proteins in a biological environment and the protein corona formed aroun the nanogel. The composition of protein corona influence nanogels biocompatibility and pharmacokinetics and interaction with other blood proteins and cell receptors. Therefore, it would give us full insight of the behaviour of nanogel *in vivo* and when in contact with biological receptors.

- Further transfection studies need to be performed in other cell lines, namely A549 cells and with siRNA-CD44 and siRNA-RHAMM to further understand nanogels endocytic pathway. As its known, materials endocytic pathway varies from cell to cell.

- Nanogel crooslinking ability associated with drug loading and delivery needs to be further investigated *in vitro* and *in vivo*.

- Preliminary studies have revealed the nanogel has great potential as Superparamagnetic iron oxide nanoparticles (SPIONs) and further studies will be made in this area. Nanogel has already revealed efficient loading of iron oxide nanoparticles and superparamagnetic behavior and high stability.